Secure Stochastic Unit Commitment in Low Rotational Inertia Power Systems With The Inclusion of Frequency Stability Constraints

CARLOS JESUS FERRANDON-CERVANTES

Secure Stochastic Unit Commitment in Low Rotational Inertia Power Systems With The Inclusion of Frequency Stability Constraints

Carlos Jesús Ferrandon Cervantes

A Thesis presented for the degree of
Doctor of Philosophy

Durham Energy Institute
Department of Engineering
University of Durham
England, United Kingdom

September 2021

Dedicated to

Mom y Costi

My supervisors Behzad and Matthias, for their infinite patience

Abstract

This thesis work studies the Unit Commitment (UC) problem from a low-rotational inertia power system perspective. The novel framework used to approximate the non-linear term of the Frequency Nadir into a linear form is the separable programming technique. It has been manifested that using auxiliary variables that guarantee an special order set 2 (SOS2) condition, we can approximate into linear such non-linear term into the UC problem. Furthermore, we have included a fast-screening contingency ranking algorithm that takes into account the reliability data of the power system. This modelling is known as the Reliability Performance Index (RPI). This index can serve in addition to the implementation of Optimal Power Flow (OPF) studies of simple load flow studies using the scheduling results of the UC. The strength of this index is that it encapsulates the probabilistic behaviour of a contingency, and the severity of it at the same time, yielding a different contingency ranking when it is compared with traditional contingency ranking approaches. The uncertainty that renewable energy sources (RES) bring into the power system operations planning analysis, specifically the UC problem, is addresed via a technique known as stratified sampling. With this approach, we generate the scenarios to include into a stochastic framework of UC. Moreover, we modelled the traditional deterministic UC into a stochastic framework, specifically following a two-stage stochastic unit commitment approach (TSSUC). Under this practice, we ensure that the frequency stability constraints were enforced into a stochastic framework as well. The results indicate that it is possible to use a stochastic modelling of the frequency stability constraints using separable programming for the first time, without the need to perform pre-processing activities to include them into the UC modelling. The concept of value of information is included in this stochastic UC analysis. The results indicate the cost of the available information when making a commitment decision regarding the generation fleet in the power system. It was seen as well that it is possible to include a virtual inertia response in the scheduling, and this helps to alleviate a potential loss of largest in-feed in the system.

Declaration

The work in this thesis is based on research carried out at the Power Systems Research Group, the Department of Engineering and the Department of Mathematical Sciences, Durham University, England, United Kingdom. No part of this thesis has been submitted elsewhere for any other degree or qualification and it is all my own work unless referenced to the contrary in the text.

Acknowledgements

I would like to start thanking my mom. This work would not have been possible without her motivation and constant love, even in a different time-zone of the world. Her support words were the best words I could have had in my darkest hours. Gracias mami.

A la Costi, perché semplicemente io non sarei qui senza di te. Tutte le tue parole e il tuo sostegno significano il mondo per me. Tu hai creduto in me, perché siamo tim. Grazie mia lodestar.

A mis hermanitas Mariana y Daniela, porque las extraño a la distancia, y ojalá las pudiera ver pronto a las dos. A mis primos Lalo y Coco, Omar y Osw. Mi tía Isis, por siempre acordarse de mí. A Lola mi perrita, por no haberse olvidad de mí. To my dad, for being that rearview mirror that I try to learn from it.

A mi hermano Abraham. Por haber creído en mí cuando emprendimos esta aventura, aun cuando sabíamos de los riesgos de dejar nuestra vida en MX. Gracias carnal. A Jonathan, por su apoyo al final de la tesis!

To my supervisors. Dr Behzad, for helping me shape my understanding of the power system into a more refined manner. Dr Matthias, for teaching me maths and teaching me to love maths, in the end. For supporting me at each time point of this journey.

A mis queridos amigos en ambos lados del mundo. En MX a Rafa, Oscar, Victor, Cri, Allan, David, Doom, Hector. A ustedes, muchas gracias por no haberme olvidado, así en la distancia geográfica y de vida. son mi ejemplo.

To all the beautiful people I met in this side of the world, either in the academic department or the everyday life of Ustinov College (or any college). Every single one of you changed me, and I thank you for that.

Al Centro Nacional de Control de Energía, que sin haber iniciado la chispa de estudiar la inercia del sistema eléctrico de potencia, tal vez yo no habría tenido la visión con la que llegué a estudiar aquí. Gracias especiales al Ingeniero Gabriel García Rojas-Vasallo, por sus palabras que nunca olvidaré en mi último día de trabajo en la sala de operación. Al inge Harry por su ejemplo de liderazgo. Al inge Chepe por su increíble templanza mientras operaba el Sistema Eléctrico Nacional. Al inge Godo, por sus palabras y conocimiento. Al inge Solorio por los buenos ratos en la sala de operación. A todos mis amigos de CENACE, Edgar, Oso, Peter, Omar, Gio, Paquito, Isma, Lalito, Manuel, Dogui, Zaid, mi sensei Armenta, Nacho, el inge Celes, el inge Portillo, el inge Lujambio, el inge Carreon, y en especial a mi maestro, el inge Agus. No los olvido. Siempre los pongo de ejemplo como los mejores operadores del sistema eléctrico de potencia del mundo. El que opera el SEP en México, opera donde sea.

A mis amigos de la Sección de Estudios de Posgrado e Investigación (SEPI) ESIME-Zacatenco. A Chucho Cortés, que ahora se encuentra siguiend su sueno en Leeds, a Omar Romay por ser mi ejemplo a seguir, a Vivi por su apoyo en la maestría, a Flor por los mamuts, a Max por su fuerza. A todo el cuerpo docente de la SEPI, en especial a mi maestro y asesor, el Doctor David Romero Romero, al Doctor Daniel Olguín Salinas, al Doctor Daniel Ruiz Vega, y al director del Centro Nacional de Control de Energía, el Doctor Ricardo Mota Palomino. A ustedes gracias, por haberme dado las bases para hacer un doctorado en Ingeniería Eléctrica.

A mis amigos de CFE distribución. Con especial dedicatoria al inge Erik Bárcenas, Xavier (J68), el inge Nich, el inge Herlindo, el inge Tavo, el inge Perea, la inge Angélica, el Inge Fernando Segura Barradas, y en especial al inge Victor Manuel López Ortiz (de paso a Dani también!). El inge Mizraim, y el Inge Gil Valenzuela Mar. Ustedes empezaron este viaje conmigo, ya fuera en la brecha o haciendo estudios de distribución o medición. Muchas gracias. A los linieros de la CFE que se suben al poste y a las torres. Gracias por enseñarme lo que no se aprende en la escuela.

Al Consejo Nacional de Ciencia y Tecnología (CONACyT), por haberme apoyado económicamente en mis estudios.

To God.

Contents

List of Figures

List of Tables

List of Acronyms

AR auto regressive

CDF cumulative distribution function

CIG converter-interfaced generation technologies

DCPF Direct Current Power Flow

DG Distributed Generation

ED Economic Dispatch

FFR Fast Frequency Response

GBD Generalised Bender Decomposition

IP Integer Programming

LOLE Loss of Load Expectation

LP Linear Programming

MILP Mixed Integer Linear Programming

MINLP Mixed Integer Non Linear Programming

MISOCP Mixed Integer Second Order Cone Programming

MOST Matpower Optimal Scheduling Tool

MSSUC multi-stage stochastic unit commitment

MTTF mean time to failure

MTTR mean time to repair

NLP Nonlinear Programming

NREL National Renewable Energy Laboratory

ODE Ordinary Differential Equation

OPF Optimal Power Flow

PDF probability density function

PFR Primary Frequency Response

PI Performance Index

PU Per Unit

PVG Photovoltaic Generator

QSS quasi-steady state

RAS Remedial Action Schemes

RES Renewable Energy Source

RoCoF Rate of Change of Frequency

RoCoF Rate of Change of Frequency

RPI Reliability Performance Index

RTS Reliability Test System

SCUC Security-Constrained Unit Commitment

SG Synchronous Generators

SI Synthetic Inertia

SOS2 special order set 2

SP Stochastic Programming

SSCUC stochastic security-constrained unit commitment

SUC Stochastic Unit Commitment

TSO Transmission System Operator

TSSP two-stage stochastic programming

TSSUC two-Stage Stochastic Unit Commitment

UC Unit Commitment

WTG Wind Turbine Generator

Chapter 1

Introduction

1.1 Problem Statement

In recent years, Power Systems have been evolving at a rapid pace due to the constantly increasing levels of Renewable Energy Sources (RESs), such as wind and solar. Rising levels of integration of these so-called converter-interfaced generation technologiess (CIGs) are having a real impact on the operation of modern power systems. Transmission System Operators (TSOs) are therefore facing a new set of challenges to maintain balance between generation and demand in systems with higher levels of CIGs. More specifically, a growing level of integration of RESs across all voltage levels and their inherent variability is bringing about new challenges for TSOs both at the distribution voltage level, through distributed generation, and at the transmission voltage level, with large-scale off-shore wind farms.

This thesis focuses on studying the energy injection from RESs into a modern power system such as the UK grid [1, 2] and how the inherent variations of power output from RESs would impact the operations planning landscape, especially when considering system operational security and specifically frequency stability. It thus takes into account the fact that large-scale integration of inherently variable RESs, which are often converter-interfaced and therefore do not automatically add inertia, coupled with the displacement of conventional resources required to keep with the existing environmental targets, [3], will inevitably lead to a reduction in system total inertia, which would introduce additional challenges to maintaining frequency

stability [2, 4]. Since this concept is key throughout this thesis, we will first cover the definition of *frequency stability* in the context of this work. The latest definition according to the latest update on the Definition and classification of power system stability [5], states:

Definition 1 *Frequency stability refers to the ability of a power system to maintain steady frequency following a severe system upset resulting in a significant imbalance between generation and load.*

As the energy transition into adopting more RESs progresses, modern power systems, like the British grid, will be more prone to larger frequency excursions in the event of large disturbances due to a sustained reduction in inertia [6]. In the UK the TSO (National Grid ESO), projects that this vulnerability will increase substantially in the near future, foreseeing inertia to decrease to 60% lower than its current value in the next 10 years [7], decreasing to values down to 110 $\mathrm{GVA \cdot s}$ in the 2030[8]. As a reference, the current level of inertia sits around 200 $\mathrm{GVA \cdot s}$. Such a prediction is easily understood when considering the process by which conventional power systems amass inertia and the effects that the integration of RESs generation has on such process.

In power systems, inertia is stored as kinetic energy, a force that is propelled by rotating synchronous generators. In conventional generation plants, large rotating machines that are synchronised to the grid add the required kinetic energy that damps the effect of a sudden loss of generation, avoiding large frequency excursions in the system [9, 10]. Fossil fuelled generation facilities are indeed directly electrically coupled to the grid and their rotational inertia is the first line of defence to restore frequency after a generation outage. By contrast, RESs generation technologies often do not feed directly to the grid as they are electrically decoupled. This means that they interface first with a converter and they do not follow the conventional electrical speed of the system, i.e. its frequency, thus lacking conventional inertia.

As this thesis will show, the amount of inertia in the system determines the immediate frequency response after a generation and demand imbalance. Therefore, it is fundamental for TSOs to account for decreasing inertia in power systems.

Moreover, even though TSOs are required to plan for a scenario of a minimum level of inertia, this value on its own is not necessarily enough to safeguard against a frequency excursion, especially in low inertia systems. This is exemplified by the 9 August 2019 Power Outage [11], a contingency which will be briefly discussed below and will serve to introduce another great challenge implied by low inertia systems populated by RESs: low PFR capability.

On August 9th, 2019 two power plants in the UK, in particular a wind farm and a combined-cycle power plant, experienced a simultaneous outage due to a lightening storm, which was then followed by the outage of smaller distributed generation facilities. This amounted to an N-2 event (i.e., outage of two power plants at the same time), a contingency that caused the system not to have the energy necessary to provide sufficient PFR to recover the frequency to its safe operational region in a timely manner. PFR is part of a suite of frequency response service provisions devised by the UK TSOs, National Grid ESO. According to National Grid's official definition, PFR is a "response provided within 10 seconds of an event, which can be sustained for a further 20 seconds" [12]. It serves to bring back the frequency to a secure operating point by injecting more power to the grid via generators. Unless they are coupled with storage facilities, RES generation technologies are not set up to provide PFR because they do not operate under an upward and downward reserve system. This means that all the energy they produce is fed immediately to the grid, and no amount is reserved to be used for frequency control.

Events like the 9th August 2019 Power Outage show that TSOs require further resources from operational planning experts to respond effectively to the large frequency excursions implied by RES-heavy low inertia systems. And providing such resources is fundamental considering that setting a minimum value of inertia and PFR is part of the frequency stability studies required by the System Operator Guideline (SOGL) European Network Code[13].

What the system needs to confront the low inertia and low PFR capability inherent to the increasingly RES-populated generation landscape is greater flexibility and greater hedging against frequency excursions. [4] defines flexibility as "the ability of a power system to respond to change in demand and supply". As enumerated in

[14], the characteristics that flexibility covers from a system operability perspective are: synchronisation and desynchronisation, ramp rates, operational range, reactive support and controllability. Some of these characteristics are embedded in the generation fleet, and some are covered by ancillary services. As more RESs are expected to connect to the grid, these features will be required to respond faster than ever before to power imbalances, because frequency drops faster when less inertia is connected to the system, a fact that is further verified by studies outlined in this thesis.

Considering National Grid's goal to operate in a carbon neutral scenario by 2025 [2], operations and planning experts need to ensure RESs themselves can optimally contribute to providing the necessary level of flexibility to the system. In the UK, one of the responses taken so far to ensure this is the case is a new product that National Grid has launched concomitantly with the writing of this thesis, called "Dynamic Containment", which is now part of their balancing services. Via this specific service, they are hedging against frequency excursions by allocating more reserve to deal with future contingencies, aiming to reduce the delivery time through faster-acting frequency response services [15]. This type of response works on a very short time frame of 1 to 3 seconds, thus attending to transient stability as well as frequency stability, but its efficacy depends also on the inertia allocated to the system. Operations planning therefore needs to optimise the number of plants synchronised to the grid to secure the minimum amount of inertia and of PFR, be it plants fossil-fuelled or RESs.

This thesis aims to do just so by addressing the frequency stability constraints and investigating ways to optimally schedule generators that provide inertia to the power system. Working from the operations and planning layer, specifically on the day and week ahead scheduling of generators in the power system, this study focuses particularly on a scenario of widespread proliferation of inverter-based RESs, mostly Wind Turbine Generators (WTGs) and Photovoltaic Generators (PVGs). It will include security restrictions in the system, such as an N-1 reliability criterion. Reliability indices will also be included in the analysis, aiming to rank contingencies not only on their severity, but also on the probability of such an event occurring.

This work will also look to address what will be called from now on the *stochasticity* of RESs, i.e. the uncertainty of their output, and how this behaviour affects the power system dispatch.

Such an investigation takes inspiration from research in Power Systems Economics, Operations Planning and Power Systems Risk Analysis. This is a constantly evolving field, from which new research continues to emerge to deal with the challenges and opportunities created by increasingly decentralized power systems. For this reason, the next section will review the state of the art to situate this thesis in continuity with emerging research as well as to show gaps in the literature that this work aims to fill. In doing so, it will amount to a delineation of a research scope.

1.2 State of the Art

The problem of low rotational inertia in the power system can be tackled from different planning horizons. In line with the research questions to be addressed, this thesis will be looking at a day-ahead to week-ahead horizon. Hence, the Unit Commitment (UC) optimisation will be the point of entry into the analysis. For this reason, this chapter will begin with section 1.2.1 reviewing literature on UC optimisation approaches that tackle the problem of low rotational inertia in the power system. This will encompass works both from the planning perspective and the risk and security analysis perspective.

The following section 1.2.2 will cover power systems contingency analysis, which is paramount to maintain security and reliability in power systems. This review will help shed a light on the reasons to focus on quantifying risks using reliability analysis in light of possible contingencies in power systems.

Both sections will elaborate on what has been previously termed *stochasticity*, that is the uncertainty that a power system increasingly penetrated by RESs inherently works with. The uncertainty in this context is inherent in the fact that there is always an error between what we forecast as the output of RES and what it will be in reality and this essentially propagates into our decision-making processes, including operational planning in a day-ahead/week-ahead timescale.

1.2.1 Low rotational inertia scheduling in power systems - state of the art

With growing proliferation of RESs like wind and solar generation in modern power systems, including in the UK grid, conventional inertia is continuously decreasing, thus creating frequency stability problems [16]. In contrast to just a few years ago, the UK now counts 2,576 onshore wind operational projects, totalling a 13.745 GW capacity and 39 offshore wind operational projects, for a 10.415 GW capacity [17]. As for solar energy, as of January 2021, there is a total of 13.472 GW of solar capacity across 1,064,148 installations [18]. Therefore, there is a need to investigate this relatively new operating point in large power systems, where a significant penetration of RESs is present.

Following is a review of previous research that addresses this problem from the day-ahead planning horizon, i.e. the so-called UC [19], and that includes frequency stability constraints in the optimisation problem in order to confront the issues of low rotational inertia.

The history of UC dates back to the end of the 1940s [20]. As the size of power systems was increasing, the decision process involved in the synchronisation and de-synchronisation of power plants was becoming more complex to manage. What in the beginning was a problem solved by a simple heuristic or merit order priority list methods, later became a difficult question only solvable through the optimisation of an objective function involving variable and fixed costs of power plants. It is indeed in the UC problem that the optimal scheduling of power plants is solved. This is done by considering the plants' physical and inter-temporal ramping constraints and allocating enough spinning reserve to handle the deviation from the forecast load. This all happens over a time horizon that can range from hours to weeks or even months.

The results of UC are the entry input of further processes, such as the OPF [21, 22], which is one of the most used tools in modern TSOs optimisation suites. For solving an OPF problem, one must know which power plants are committed, and this information comes from UC, which is thus evidently fundamental.

A good entry point to the the UC problem in large power systems is [23]. The authors there delve into the solution of the UC problem, but before doing so they highlight something crucial to the understanding of the UC problem as it appears today: the benefits of solving it within large-scale power systems with non-heuristic methods. Indeed, they point to the fact that non-linear programs such as the one they used take advantage of the fact that computational requirements grow linearly with the number of units in the system. The algorithm behaves better with large-scale power systems, converging much faster than with smaller systems, like predictably other similarly non-heuristic methods would do.

Although the UC problem has been considered solved ever since the implementation of linear programming in the 1960s, mathematically it is a difficult problem [24], consisting of optimising an economic criterion that involves fixed and variable costs, under these physical constraints [25, 26, 27, 28]. With the recent adoption of RESs generation to the system, committing units to the grid has become all the more complex because it now needs to include provisions to hedge against large frequency excursions. Since the work of [23], research on the UC problem has thus moved towards an investigation of the effects of further constraints to generation scheduling brought about by the ever growing levels of adoption of RESs.

In the work of O'Malley et al. [29], the authors, inspired by their experience with the Irish grid, which was increasingly penetrated by wind generation, look to quantify what was becoming a new requirement for the system: ensuring a surge of power system reserve for frequency response. This was either primary, secondary or tertiary frequency response, each one with a different time horizon activation. Such a provision was the predecessor of the tool of PFR to handle frequency stability as we know it. At the time of the publication, the authors did not consider yet that any amount of frequency response could be scheduled to come from non-dispatchable RESs. They were among the first to deal with an incipient line of study: the need to ensure higher reserve for frequency stability in the system.

Working on this same field of inquiry, the authors of [30] look at smaller systems, specifically islanded grids, to devise a short-term scheduling that allocates enough reserve to maintain a pre-defined system frequency minimum. They thus work with

the UC problem from a short term perspective, something that allowed them to be pioneers in the elaboration of responses that operate in the time frame of seconds. They were expecting such rapid frequency response to come from conventional thermal units, whereas nowadays so is expected more from converters. Such work was then further elaborated in the work of [31] where the authors consider the impacts of wind power on thermal generation UC.

At the time of publication of [31], the main problem in the UC for wind power and conventional generation was the deployment of reserve to maintain the frequency balance. This was mainly due to ramping restrictions and minimum load conditions of the generators, which caused a certain amount of wind spillage. Still, no fast frequency response from wind power is modelled in this work. Although their study shows that the limited predictability of wind has little effect on the UC and Economic Dispatch (ED), the authors of [31] emphasise the need for better ways to predict the behaviour of wind power. Indeed, their results about the effects on the UC and ED are entirely determined by the specific level of wind power penetration in the Dutch power system at the time.

Further working on the issue of frequency stability, which was gaining traction not only in academia but also among power system operators, the authors in [32] start to add a maximum allowable frequency deviation in the system, by incorporating more integer variables [33] to the UC. This maximum allowable frequency deviation is determined upfront, but based only on the worst contingency in the system. No inertia value is included in this analysis. At this time, a response to frequency excursions was expected to come from conventional units, just as in [31]'s paper. This work is produced for two relatively small test systems: one with 4 generators, and the other with 17 units.

It is in the work of [34] where a UC with large wind penetration is investigated for the All-Island Irish power system, which is handled by Eirgrid [35]. In this work, through a stochastic optimisation schedule, they allocate reserve to handle the uncertainty of wind input via scenarios. Yet no inertia is scheduled in this approach, and the frequency balance is only covered via the reserves. This shows that at the time, the RoCoF was yet to be considered as a constraint to the UC.

The consideration of such a constraint, which today is integral to the UC problem in power systems largely penetrated by RESs, appears in the work of [36]. Such an investigation into the RoCoF is once again inspired by the All-Island Irish power system, which already has a large level of wind penetration. The authors here involve security analysis in low rotational inertia scenarios via a time-based dynamic simulation. They use a time series sampling methodology to assess the impact of RES generation, specifically observing "N-1" state scenarios, which refer to the state of generation loss. This is done by observing two indices of the system: the maximum RoCoF and the minimum value of frequency after an event namely, the nadir. Both of these values are central to the work of this thesis, and will therefore be further explained in subsequent chapters. It is in [36] that the kinetic energy stored in the blades of the WTG is first considered as an alternative to the rotational inertia of conventional generators.

Furthermore, the work of [37] develops a Stochastic Unit Commitment (SUC) and uses a quantile-based scenario tree structure to model the transitions between time points. Basically, it creates a multi-stage [38] SUC that follows a "here and now" optimisation, where for each node of the scenario tree structure, it optimises for the amount of reserve needed in the system. This approach is modelled for a one-year simulation and it allows to include the stochasticity of wind in the original UC problem. Still, no frequency constraint is included in the problem, nor is frequency response from generators (conventional ones or non-synchronous). In the very same year, 2012, authors of [39] publish a paper acknowledging the effects of operating a low inertia power system and how such low inertia affects frequency regulation.

These almost concomitant works show that both operations planning scholars and power system dynamics experts were at this point approaching the frequency stability problem but doing so from separate time scales: the first by the day-ahead horizon via generation scheduling, and the seconds from the control perspective via dynamic simulation analyses spanning seconds. There was thus an incipient intersection between these fields of study.

From the operations planning perspective, the work of [40] presents an approach to add the frequency stability constraints into the UC. In this work they consider

Security-Constrained Unit Commitment (SCUC) by acknowledging the control parameters from the governor's generator. The authors made a sensitivity analysis of these parameters, proving which ones have more impact over the minimum frequency value (nadir). This approach allowed them to assume equal responses from the delivery time of the governors. Then, to tackle the non-linearity of the frequency, they establish minimum and maximum values of droop, gain, and reserve, setting the inertia constant to find these values. After that, they linearise the frequency nadir function following a piecewise linear approximation. They obtain the minimum inertia from the RoCoF value upfront, hence when they perform the piecewise linear approximation, the inertia is a known value. For this piecewise linearisation, they add integer variables to the problem, in order to find each corresponding section of the function that maps the possible values of droop, gain and reserve. No uncertainty effect from RESs is included in this work. Moreover, setting the minimum value of inertia, without allocating it itself in the optimisation, reduces a degree of freedom of the problem. This allows the authors to deterministically maintain a fixed value of inertia.

On the power system stability and frequency dynamics side, [41] instead demonstrates that inertia in RES scenarios is a time variant variable. This is due to the probabilistic behaviour of RESs and to the flexibility that is expected from future generators (conventional and non-synchronous ones), such as more frequent connection and disconnection events, and fast frequency response provision. The authors of this paper work on stability in a multi area system, using the swing equation modelling. An important conclusion is that rotational inertia becomes heterogeneous, thus the inertia becomes a local variable for each area of the power system. This is key for grids that are not electrically meshed and strong, such as for example the Mexican one, because large transfers of power inter-area can occur, thus prompting inter-area oscillation modes, which can exacerbate stability problems beyond frequency stability [42, 43].

For the purpose of this thesis, the key finding from this study is that in large power systems the amount of inertia becomes heterogeneous and that this implies that different RoCoF values can arise when a contingency occurs. This is significant

because it shows that in order to keep the frequency stability secure, the operator needs to not only keep a global amount of inertia, but also to maintain a share of it in each power system area that can respond before a generation outage. This finding enforces the argument of securing the right amount of inertia in the power system, and this starts from the operations planning phase, specifically the UC. Following the UC problem with frequency stability constraints, in [44], the authors take into account the inherent uncertainties that RESs bring and the generation outages by an optimal schedule of the energy with a SUC technique. In this work, the concept of synthetic inertia, which is the Fast Frequency Response (FFR) coming from RES, is assessed in order to get its economic value. Assessing the economic value of inertia emulation is also covered in [45]. In the work of [44], the transmission network constraints are not considered in the optimisation of the UC. Including these constraints would make the problem non-linear, as it is shown in the work of [46], complicating the convergence of the problem further. For this reason, in this thesis I will work on the results of the UC, making sure the network constraints are covered from a security standpoint in the power system.

Further research on UC that aims to tackle the problem of frequency stability from the operations planning perspective is presented in [47]. The authors include the frequency stability constraints in the UC optimisation by extracting a priori the bounds of the variables that have an influence in the constraints, transforming the problem into a linear form. The bound extraction time is considered to be a previous task to perform before solving the UC. The minimum level of inertia is a known value, hence when they solve for the bound extraction problem, it reduces the degree of freedom of the problem. Although this method runs faster than a piece-wise linearisation of the non-linear constraints of frequency stability, its solution is limited to the size of the system. In the cited work, this approach is run on a 20 synchronous generators system and it is solved under a stochastic environment.

In summary, this section has reviewed the state of the art on the resolution of the UC problem. It has shown how scheduling generation capacity has been approached linearly until the proliferation of RESs into power systems, which have then forced scholars to devise non-heuristic tools to deal with the issue of low rotational inertia,

low reserve capacity and stochasticity. These works summarised here take into account such constraints into the UC problem, and they do it differently depending on the approach they choose and on the time frame they work with.

While this section presented the state of the art from the planning side, the next section will cover works that address the risk and security side by devising contingency ranking algorithms and risk quantification criteria. Contingency ranking algorithms and risk quantification activities are performed in the power system to protect the grid against disturbances. These information presented as a ranking list can work in hand with the results of a UC problem, giving the control room operator another layer of security when analysing and operating the grid.

1.2.2 Contingency Analysis and Risk Quantification

Nowadays in power system analysis, contingency ranking algorithms are implemented in functions that are under constant operation in the control room [48, 49]. TSOs even have departments that work solely on contingency analysis and Remedial Action Schemess (RASs).

Already in 1972, Peterson et al. published a paper [50] that addresses contingency analysis. Since the beginning of the load flow studies [51], computing time was one of the most pressing issues to address. They proposed the iterative linear power flow to make a fast screening of contingencies that cause certain violations that meet a criteria specified. This iterative approach helped saving computational time.

Moreover trying to shorten computational time, Irisarri et al. [52] propose a Direct Current Power Flow (DCPF) approach, which converges in one single iteration. The drawback of this approach, however, is that voltages are assumed to be 1 Per Unit (PU), neglecting bus voltage violations.

The DCPF algorithm is used by Mikollinas et al. in [53], which tackles the problem of the masking effect in contingency ranking. This issue happens when a disturbance that produces no overload ends up higher in the ranking than one that produces a slight overload. This work is particularly significant for this thesis because I too will be addressing the masking effect problem in following chapters.

In [54], the authors propose system performance indices for the steady state analysis (static security). Based on the percentage of overload in each branch after a contingency, these outages are ranked via states, where every state of the system can be previously defined, under a N-1 security criterion. They propose two indices: one that measures how the outage of a branch can affect the transmission line thermal limit of the rest of the branches connected, and one that measures the impact on bus voltages or violations of physical capabilities of generators.

In [55], the authors perform a reliability assessment based on Markov Models of system components and identification methods of events that cause unreliability in the system. Including reliability data from the system, they use contingency ranking and adequacy approach to determine if the system can meet with the loadability requirements after a disturbance happens. Importantly for this thesis, they also define the concept of the state of the system, which I use for my own analysis.

Authors in [56] compute a voltage stability index. Voltage instability is more of a concern in systems that are heavily loaded because the grid needs more reactive support on long transmission lines. A heavily loaded system is thus one where the generation sources are very far from the load, electrically and geographically speaking, and where systems are not meshed enough. The particularity of contingencies in such systems is that they occur as a cascade failure mode, which starts with the weakest nodes in the system and then propagates outward.

Dobson et al. discuss such cascading outages disturbances in [57]. They define a cascade as a top-down modelling from a random initial disturbance followed by the propagation of more failures. To do this, they use the approach of branching processes to simulate the many outages that happen in a blackout, thus differing from the N-1, where only one element of the system is out. In this way, they estimate the probability distribution of blackout size.

In [58], authors plug 9 years of observed data from an electric power system in the branching process before mentioned. It should be noted that this approach requires to have historical data from many years. They show how to quantify the propagation of cascading failures from this observed data and predict the effect of the propagation on the risk cascade.

In the work of [59], authors use a different index to rank the contingency severity. They include the probability of the state and the severity, capturing the risk of a certain event to happen. This was tested with the 24 bus Reliability Test System (RTS)[60], but not with the three area version of it.

There are different approaches to tackle the problem of contingency analysis, ranging from the deterministic N-1 criterion to risk quantification methods based on cascading failures in the power system. The aim of contingency ranking is to determine the worst scenarios that can happen when a disturbance occurs and their consequences for the power system. These consequences can be violations of transmission lines thermal limits, bus voltage drop or even stability problems [61]. In this thesis, we will be investigating how the contingency ranking algorithms can be a continuation of the operations planning results of the UC, analysing each single one of their time points.

1.3 Aims and objectives of the research

This thesis aims to investigate the impact of large-scale RESs penetration on the frequency stability of electric power systems from the day-ahead scheduling perspective. Specifically it will attempt to devise techniques to incorporate the so-called frequency stability constraints into the process of day-ahead scheduling. The technique to achieving this belongs to the area of Separable Programming. To the knowledge of the author, no such technique has been used for the handling of the constraints of the UC problem. In addition, in the second half of this thesis, the problem of variability of RESs are addressed by formulating a stochastic UC problem for purposes of day-ahead to week-ahead scheduling simulations. This approach will take into account the random behaviour of RESs generation output, its *stochasticity*, as well as the demand variations over time. In addition, via reliability rates of the power system elements, we will incorporate reliability management metrics to identify the most severe contingencies in the system. In this thesis, our intention is to establish a link between the results of a secure UC that considers the largest in-feed in the power system, with the a security analysis via contingency ranking

algorithms applied to the scheduling points generated by the UC results.

1.4 Research questions to be addressed

The three prominent research questions which this work will assess are:

1. To determine a secure operating floor of inertia in the power system for the day-ahead to week-ahead planning horizon that includes frequency stability constraints, as well as PFR from the available plants. The foundations of this problem is covered in chapter 2, whereas an analysis and implementation of the frequency stability constraints is done in chapter 3.

2. To quantify a reliability metric index that indicates the severity of a contingency in the power system. This analysis is explored in chapter 4.

3. To include the stochasticity of RESs in the ahead to real time (day-ahead to week ahead) planning horizon. This is done in chapter 5.

The next section covers the past and current publications coming from this thesis.

1.5 Publications

Section 1.5 covers the current publications that are a product of this thesis. Some of them are chapters in this thesis, and some are in publication process.

Table 1.1: List of Publications

Publication	Status
[62] C. J. F. Cervantes, B. Kazemtabrizi, and M. C. M. Troffaes, "Contingency Ranking in Power Systems via Reliability Rates", in *2018 IEEE International Conference on Environment and Electrical Engineering and 2018 IEEE Industrial and Commercial Power Systems Europe (EEEIC / I CPS Europe)*, June 2018, pp. 1–6.	published
C. J. F. Cervantes, B. Kazemtabrizi, and M. C. M. Troffaes, "Inclusion of Frequency Stability Constraints in Unit Commitment Using Separable Programming," in *2021 Electric Power Systems Research Journal*, September 2021.	under minor review
Two-stage stochastic unit commitment paper	under development

Chapter 2

Literature Review and Methodology

This chapter of the thesis will cover the theoretical foundations and mathematical modelling underpinning this research. The motivation, as discussed in the previous chapter, is to analyse the security-constrained day-ahead to week-ahead operations planning interval, and mathematically devise the necessary constraints to maintain the frequency stability in the system. These added constraints increase the security and reliability of the power system, specially those systems where low-rotational inertia is a concern. To this end, the foundations of the operations planning studies will be covered in this chapter. Furthermore, the underlying methods to ensure system operational security will also be included here, in the form of a probabilistic contingency analysis given a specific reliability criterion. The whole approach will yield a coherent workflow between the two research paths.

2.1 Mathematical programming in power systems

Mathematical programming is a branch of mathematics [63] which is different from computing programming, in the sense that mathematical programming aims to "plan", based on a set of constraints and an *objective function*, to search for the best possible outcome of a problem, either to get a maximum or a minimum output. This is known as mathematical optimisation, and it is based on how a problem

is interpreted via a model. Mathematical programming and mathematical optimisation are interchangeable terms. This branch of mathematics is applied in a wide range of purposes in real-life world problems; ranging from economics, management, chemistry, physics, and engineering. The branch of mathematical programming that will be applied in this thesis is Linear Programming (LP), and its variation Mixed Integer Linear Programming (MILP), both of which will be explained in further detail throughout this chapter.

2.1.1 Linear Programming introduction

It is of interest of this thesis to showcase the foundations of the techniques used to solve the optimal allocation of generators within a specific planning time horizon of the power system. The first tool to explain here is a LP problem. In a LP problem, what we are looking for is to either maximise or minimise a linear objective function subject to a group of linear constraints of such problem. This objective function can represent the revenue sought after in a process (to maximise the objective function), or it could also represent the cost of running a process (which one usually would look to minimise). In the case of this study, our aim is to minimise the cost of running the power system, over a specific planning time horizon (typically ranging between day-ahead to week-ahead). We can start by showing a very simple example where LP is applied, taken from [64]. The first step of an optimisation via LP is to understand the process that is under analysis. We have the data in table 2.1:

Table 2.1: Factory's production data example*

optimisation of factory's production

product	ingredient x_1	ingredient x_2	prod. available
A	2	2	25
B	1	2	19

*Cost per ingredient: $45x_1$ and $80x_2$

The data presented in the table represent the following: it takes 2 units of ingredient x_1 and 2 units of ingredient x_2 to produce a unit of the product A. The

factory can produce up to 25 units in total, of product A. A similar treatment can be given to the product B. It also indicates that each ingredient x_1 costs 45£, and one ingredient x_2 costs 80£. The sum of both can be interpreted as our objective function. If the goal of the problem is to get the highest revenue in the factory, then we are looking to maximise the objective function. These ingredients can only be non-negative, and for the sake of simplicity of the problem, they can attain any real value. The formal representation of the problem is given below:

$$\begin{aligned} \text{maximise} \quad & z = 45x_1 + 80x_2 \\ & \text{subject to} \\ & 2x_1 + 2x_2 \leq 25 \\ & x_1 + 2x_2 \leq 19 \\ & x_1, x_2 \geq 0,\ x_1, x_2 \in \mathbb{R} \end{aligned}$$

And a generalised form of understanding how an LP is modelled, is shown in the following equations:

$$\text{maximise (minimise)} \quad \sum_{i \in N} c_i x_i \tag{2.1.1}$$

$$\text{subject to}$$

$$\sum_{i \in N} a_{ij} x_i \leq b_j, \qquad \forall j \in \{1, 2, \ldots, J\} \tag{2.1.2}$$

$$\text{for a LP formulation } x_i \in \mathbb{R}$$

To summarise, the prerequisites and elements of the LP model are:

- Objective function: the aim is to either minimise or maximise a result,
- Constraints: they represent the amount of resources available to include in the model,
- Variables: The variables are the ones to find out, in order to satisfy the objective function,

- Set of indices: they represent the number of variables in the problem, and the number of constraints associated to them,
- Parameters: constant values associated to the variables and the objective function,
- Linearity: although obvious at this point, both the objective function and the constraints must be linear.

At this point, the problem showcased in table 2.1 is not solved. The next subsection will describe some of the methods to solve this optimisation problem.

2.1.2 Graphical solution of a two-dimension LP problem

Continuing with the example of the factory's production, for didactic purposes and definition of further used concepts, we will solve this problem. Let x_1 and x_2 locate in the horizontal and vertical axis of fig. 2.1, respectively.

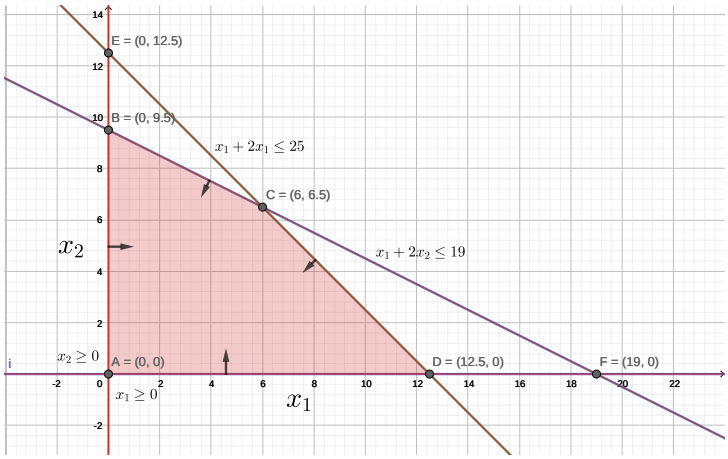

Figure 2.1: Graphical solution of the LP factory's production problem

If we graph the group of constraints of the problem, we can identify its intersection and joints known as vertices. This yields a shaded area where a **feasible solution** exists. This solution area is known as the **polyhedron**. The vectors that are coming *from* the constraints indicate the direction of the feasible shaded area. The vertices at points E and F are intersection points of the problem, but do not satisfy all constraints. Now that we have identified the area of the solution, we have

to remember that we are looking for a maximum. We create a group of new variables in the constraints of products A and B, that we will name the **slack variables** h_1 and h_2, and the inequalities will be transformed into equality constraints, as follows:

$$2x_1 + 2x_2 + h_1 = 25$$
$$x_1 + 2x_2 + h_2 = 19$$

These slack variables will be the unused production of items A and B, respectively. When the solution for this problem are the points of vertex A at $x_1 = 0$ and $x_2 = 0$, then we will have $h_1 = 25$ and $h_2 = 19$, it is valid to say that there is a *feasible solution*. The constraints of the problem are satisfied under these conditions, although the revenue under these conditions will be zero. These slack variables will be further discussed when we review the simplex method.

Now, we can start testing vertices B, C and D in these equations and the objective function z.

- vertex B = $\{0, 9.5\}$; $h_1 = 6,\ h_2 = 0,\ z = 760$
- vertex C = $\{6, 6.5\}$; $h_1 = 0,\ h_2 = 0,\ z = 790$
- vertex D = $\{12.5, 0\}$; $h_1 = 0,\ h_2 = 6.5,\ z = 562.5$

It can be seen that vertex in point C yields the largest objective function value and there are no unused products A and B. Thus this is the **optimal solution** of the LP problem. To summarise

- A *feasible solution* is the set of values of the variables of the problem that satisfy all the constraints of the LP problem,
- The *optimal solution* is the solution of the LP problem that cannot be improved,

Consequently, in the example above we have implicitly evoked the fundamental theorem of LP:

Theorem 1 *If there is an optimal solution of a LP problem, then the LP has at least one optimal solution that is a corner point solution.*

The proof of the theorem is further discussed in [33]. With this graphical solution of the factory's production problem, it is actually easy to enumerate the vertices where the solution exists. In the case that there are more variables in the problem and more constraints (which is the case of the UC problem), this would prevent us from following this approach, since the iterative process would be excessively time-consuming. A brief description of a technique to tackle this problem is shown in the next subsection.

2.1.3 The Simplex Method

As we could see, using the graphical solution to solve the LP problem is heavily time-consuming when there is a large number of variables. It was George Dantzig [63] who "translated" the geometric solution of the optimisation problem, into an algebraic form, known as the **simplex method**. This is known as the **standard form**. In the simplex method, the inequality constraints of the problem will be transformed into equalities, with the addition of the slack variables.

$$\begin{aligned} &\text{maximise} && z = 45x_1 + 80x_2 \\ &\text{subject to} \end{aligned}$$

$$2x_1 + 2x_2 + h_1 = 25 \tag{2.1.3}$$

$$x_1 + 2x_2 + h_2 = 19 \tag{2.1.4}$$

$$x_1, x_2, h_1, h_2 \geq 0 \tag{2.1.5}$$

Now there is a system of linear equations, where we have more variables $n = 4$ than equations $m = 2$. This means that the system has multiple solutions. Following a linear algebraic approach for this problem, we can equalise two of the variables to zero, so we can have the same number of variables and equations. This solution will

be known as a **basic solution**. The whole system can be solved as a simultaneous system of linear equations. Let $x_1 = 0$, $x_2 = 0$, then the slack variables h_1, h_2 that represent the capacity will be the fully unused product A and B, respectively, i.e. 25 and 19, and the revenue is zero. This solution is known as the **initial basic feasible solution**. These non zero variables will also be known as **basic variables**, whereas the variables with zero value will be known as **non basic variables**.

This **basic feasible solution** is a basic solution which satisfies the non-negativity constraints, and includes the basic and non basic variables in a standard form of the problem. The set of basic feasibile solutions correspond to the corner points of the linear program. It is possible for the simplex method to determine how many basic solutions exist, based on the number of equations and variables. The possible basic solutions are $n!/[m!(n-m)!]$, hence for this problem we have 6 alternatives, but it is possible that they cannot lead to basic solutions if one pair of equations are linearly dependent from each other.

The next logical step is to identify the path to find a new basic feasible solution. We are interested in another basic feasible solution only if it improves the value of the objective function. Then, at least one of the current non basic variables will be changing into a basic variable, because the number of basic variables must remain equal to the number of constraints. In the simplex method, this change happens once at a time per iteration. Intuitively, this change should only happen if it improves the objective function value. After observing the objective function, and bearing in mind that we want to maximise the revenue, we can see that the increment per unit of x_2 increases in £80 the objective function value, whereas x_1 increases it only £45. Thus, we can consider x_2 as the variable that will *enter the basis*, i.e. it will become non zero. The next step is to select which variable *leaves the basis*, i.e., will be assigned with a zero value. For this, there are two options: h_1 and h_2.

By looking at the fig. 2.1, we know that x_2 can not go beyond 9.5, and the slack variable associated with x_2 is h_2, hence h_2 will leave the basis, and become zero. Although this conclusion was obtained via visual inspection, this process can become automated by using the *minimum ratio test*, and consists in calculating the interceptions of the constraints with the variable x_2, as the ratio of the right hand

side to the the coefficient of the variable that will enter the basis, i.e., x_2. Thus, we would have the next expressions:

$$\text{intersection of restriction 1 and } x_2 = 25/2 = 12.5$$
$$\text{intersection of restriction 2 and } x_2 = 19/2 = 9.5$$

Next, we would have the next system of linear equations:

$$\begin{aligned} 2(0) + 2x_2 + h_1 &= 25 \\ (0) + 2x_2 + 0 &= 19 \\ x_1 = 0\,, x_2 = 9.5\,, h_1 = 6\,, h_2 &= 0 \end{aligned}$$

With this result, the slack variable h_1 represents an unused product A of 6 units. The next iteration searches for a new basic variable under the current system of linear equations. Applying the minimum test ratio, it is x_1 the variable that enters the basis, and h_1 its associated slack variable that will leave the basis. Thus, solving the next system of linear equations yields

$$\begin{aligned} 2x_1 + 2x_2 + (0) &= 25 \\ x_1 + 2x_2 + (0) &= 19 \\ x_1 = 6\,, x_2 = 6.5\,, h_1 = 0\,, h_2 &= 0 \end{aligned}$$

Finally, this is a feasible solution, since it statisfies all the constraints of the problem; and it is an optimal solution as well, since this solution can not be improved further. The results coincides with the graphical solution of the previous subsection. To summarise, the simplex method can be compacted in the next steps:

1. Transform the system of inequalities into standard form (equalities), and determine a feasible initial solution.

2. Select a non basic variable to enter the basis, using the optimality condition, seeking for the most negative reduced cost. A tie between coefficients can be broken arbitrarily.

3. Select the current basic variable to leave the basis, based on the feasibility condition that comes from the minimum test ratio. A tie can be broken arbitrarily.

4. Solve the system of linear equations considering the new basic and non basic variables. If the solution can be improved, return to step 2, otherwise, stops the process.

In essence, the simplex method keeps iterating until the solution cannot be improved and all the inequalities are met. A variation of this approach is known as the **dual simplex method**, which the reader can investigate further in [65]. Now we will show how the problem becomes more complex when integrality conditions are added to it.

2.2 The Non-Linearity of the UC problem and the frequency stability problem

In this section we address the UC problem from its natural non-linear form, and the motivations behind the frequency stability coupled with the power system dispatch, specifically addressing the inertia in the power system.

2.2.1 The UC problem in its non-linear form

So far we have discussed over how to tackle linear problems using LP. In this thesis, we work with the MILP modelling of the UC. The UC in its natural form is a NP-hard [24],non-linear problem, which will be shown in eq. (2.2.6):

$$\min_{\Phi} \sum_{t\in\mathcal{T}} \sum_{g\in\mathcal{G}} S_g(u_g^t - u_g^{t-1}) + F_g(P_g^t) \tag{2.2.6}$$

where $\Phi \coloneqq (P_g^t, u_g^t)_{g\in\mathcal{G}, t\in\mathcal{T},}$.

- $t \in \mathcal{T} \coloneqq \{1, \ldots, T\}$, where $\mathcal{T}$ is the set containing all timesteps in the planning horizon, and T is the final time point,

- $g \in \mathcal{G} \coloneqq \{1, \ldots, G\}$, where $\mathcal{G}$ is the set containing all synchronous generators, and G is the number of generators,
- u_g^t is the unit status (up or down) of unit g at time t, where $u_g^t \in \{0, 1\}$,
- P_g^t is the active power generation of unit g at time t, in MW,
- $S_g(u_g^t - u_g^{t-1}) \coloneqq C_g^{SU+} \max(u_g^t - u_g^{t-1}, 0) + C_g^{SD-} \max(u_g^{t-1} - u_g^t, 0)$ is the start-up and shutdown cost function which has a unit-dependent costs C_g^{SU+}, C_g^{SD-} per event,
- $F_g(P_g^t)$ is the fuel cost function of active power generation P_g^t which could be either quadratic or piece-wise linear.

The terms of the objective function in eq. (2.2.6) are convex, but non-linear. They can be linearised by adding some auxiliary constraints, a topic that will be further discussed in chapter 3. The AC power flow modelling equations describe the power balance at each bus. Such modelling is shown in eq. (2.2.7), and it is repeated at each time step of the UC optimisation, but for the sake of this example we will omit the t subscript:

$$SG_n^{\text{gen}} - SL_n^{\text{load}} - SZ_n^{\text{line}} - SS_n^{\text{shunt}} = 0 \qquad \forall n \in \mathcal{N} \tag{2.2.7}$$

where $\mathcal{N}$ is the set of buses in the system and $\mathcal{E}, \mathcal{E}^R \subseteq \mathcal{N} \times \mathcal{N}$ are the sets of forward and reverse paths of the transmission lines in the grid. This power balance equation follows the law of conservation of energy, which in our case it is power. The injected complex power by all generators connected at bus n is represented by SG_n^{gen}, whereas all the load connected to the bus n is represented by SL_n^{load}, in a complex form as well. The complex power flow transmitted from and to the adjacent nodes n is represented by SZ_n^{line}. The elements in shunt connection in node n are represented by SS_n^{shunt}. The set of generators is defined as $\mathcal{G} = \bigcup_{n \in \mathcal{N}} \mathcal{G}_n$, whereas the set of loads are $\mathcal{L} = \bigcup_{n \in \mathcal{N}} \mathcal{L}_n$, the set of transmission lines are $\mathcal{K} = \bigcup_{n \in \mathcal{N}} \mathcal{K}_n$, and the set of shunt elements is $\mathcal{M} = \bigcup_{n \in \mathcal{N}} \mathcal{M}_n$. Equation (2.2.7) is expanded in eq. (2.2.8)

$$\sum_{g\in\mathcal{G}_n} SG_g - \sum_{l\in\mathcal{L}_n} SL_l - \sum_{k\in\mathcal{K}_n} SZ_k - \sum_{m\in\mathcal{M}_n} (Y_m^{\text{shunt}})^* |V_n|^2) = 0 \qquad \forall n \in \mathcal{N} \qquad (2.2.8)$$

$$I_{ij} = Y_{ij}\big(V_i - V_j\big) \qquad \forall (i,j) \in \mathcal{E}, \qquad (2.2.9)$$

$$SZ_k = SZ_{ij} + SZ_{ji} \qquad \forall (i,j) \in \mathcal{E}, \qquad (2.2.10)$$

$$SZ_{ij} = V_i\big(I_{ij} + Y_{ij}^C V_i\big)^* \qquad \forall (i,j) \in \mathcal{E}, \qquad (2.2.11)$$

$$SZ_{ji} = V_j\big(-I_{ij} + Y_{ji}^C V_j\big)^* \qquad \forall (j,i) \in \mathcal{E}, \qquad (2.2.12)$$

The value of Y_m^{shunt} is the admittance of the shunt element m. Furthermore, at each node n the equation eq. (2.2.8) must be met by equalising to zero. The complex voltage V_n is the state variable of the optimisation problem. I_{ij} denotes the current flowing in the transmission line, from node i to node j. Y_{ij} and Y_{ij}^C represent the series admittance and the shunt admittance of the transmission line, from bus i to bus j, under a π-model transmission line [66]. SZ_{ij} is the complex power flow that moves from node i to node j, whereas the complex power SZ_{ji} flows to node i from node j. Thus, we can compact the previous formulation of the cost function eq. (2.2.6) and constraints in the following form:

$$\min_{\Phi} \; f(\Phi) \qquad (2.2.13)$$

where Φ is the vector of variables:

$$\Phi = \begin{bmatrix} u_g \\ V_n \\ P_g \end{bmatrix} \qquad (2.2.14)$$

$$\Phi_{min} \leq \Phi \leq \Phi_{max} \qquad (2.2.15)$$

subject to the power balance equality constraint in eq. (2.2.8), and eq. (2.2.15). Such cost function, equality and inequality constraints show the non-linearity of the UC problem in its natural form. In order to tackle this problem, there are techniques such as Mixed Integer Non Linear Programming (MINLP) approaches. For practical purposes, TSOs nowadays run a linear approximation of the UC problem. We elaborate further and fully on the linear version of the UC in chapter 3. Now we will

discuss the foundations behind the dynamics of the frequency in the power system, which is necessary to understand in order to couple them into the UC problem.

2.2.2 Frequency stability from the swing equation perspective

In this subsection we explain the dynamics of a power imbalance in the power system. This imbalance is directly translated into a change of speed in the rotor of the generator, which changes the the electrical frequency of the system. We can observe how this frequency in the grid is related to the mechanical rotational speed of the generators. As shown in fig. 2.2, conventionally the system frequency relies on the rotational speed of the generators whilst they are synchronised to the system and they are the main providers of conventional inertia to the system. Because of

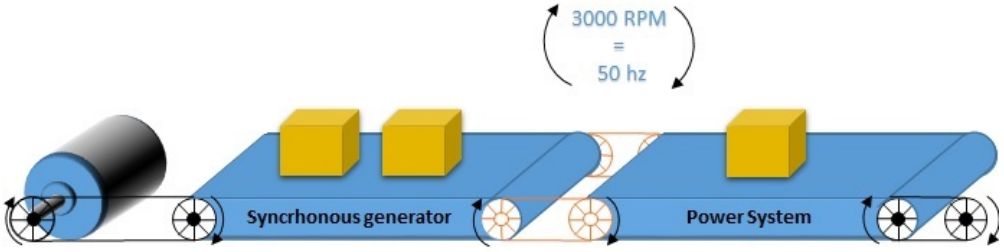

Figure 2.2: Synchronous link in power systems

this synchronous link between turbines and generators, the mechanical rotational speed ω_m is coupled with the electrical angular frequency ω_e. The imbalance between generation and demand is depicted as a mismatch between torques acting on the rotor[9], which is shown in:

$$T_a = T_m - T_e \tag{2.2.16}$$

where

- T_m is the mechanical torque in $N \cdot m$,
- T_e is the electrical torque in $N \cdot m$,
- T_a is the accelerating torque in $N \cdot m$

Since the combined inertia of the generator and the turbine is accelerated by this imbalance in torques, we have:

$$J\frac{d\omega_m}{dt} = T_a = T_m - T_e \tag{2.2.17}$$

where

- J is the moment of inertia of generator and turbine,
- ω_m is the angular velocity of the rotor, in rad/s,
- t time, s

the left side of the eq. (2.2.17) represents the kinetic energy stored in the turbine and generator. It can be expressed in seconds, if it is referred to a base in the system, or in MVA $\cdot\, s$. This is the time that a machine can deliver its nominal power output using only the kinetic energy stored in the rotating mass which is the inertia H for each generator in the system, as it is shown in:

$$H = \frac{1}{2}\frac{J\omega_{0_m}^2}{S_b} \tag{2.2.18}$$

where

- S_b is the base apparent power of the system.
- ω_{0_m} is the rated angular velocity in mechanical rad/s.

The moment of inertia from eq. (2.2.18) is:

$$J = \frac{2H}{\omega_{0_m}^2}S_b \tag{2.2.19}$$

Substituting eq. (2.2.19) in eq. (2.2.17), we have:

$$\frac{2H}{\omega_{0_m}^2}S_b\frac{d\omega_m}{dt} = T_m - T_e \tag{2.2.20}$$

Rearranging the eq. (2.2.20) we have:

$$2H\frac{d}{dt}\left(\frac{\omega_m}{\omega_{0_m}}\right) = \frac{T_m - T_e}{T_b} \tag{2.2.21}$$

where the base torque is $T_b = S_b/\omega_{0_m}$, so eq. (2.2.20) yields:

$$2H\frac{d\widehat{\omega_r}}{dt} = \frac{T_m - T_e}{T_b} \tag{2.2.22}$$

where in eq. (2.2.22), $\widehat{\omega_r}$ is:

$$\widehat{\omega_r} = \frac{\omega_m}{\omega_{0_m}} = \frac{\omega_r/p_f}{\omega_0/p_f} = \frac{\omega_r}{\omega_0} \tag{2.2.23}$$

where:

- ω_r is the angular velocity of the rotor in electrical rad/s,
- ω_0 rated value of this angular velocity,
- p_f is the number of poles.

As we can see, it is clear the effect that inertia has on the excursions of frequency when a generation imbalance happens, such an effect is to help the system to damp these frequency excursions due to the imbalance between load and generation. This can be seen as:

$$\frac{d\widehat{\omega_r}}{dt} = \frac{T_m - T_e}{2HT_b} \tag{2.2.24}$$

Considering RESs such as wind generation, the amount of conventional inertia in the system changes. Wind generation is treated as non synchronous generators, rotating in a variable speed. This is due to the intermittence of natural sources such as wind. This is depicted in fig. 2.3.

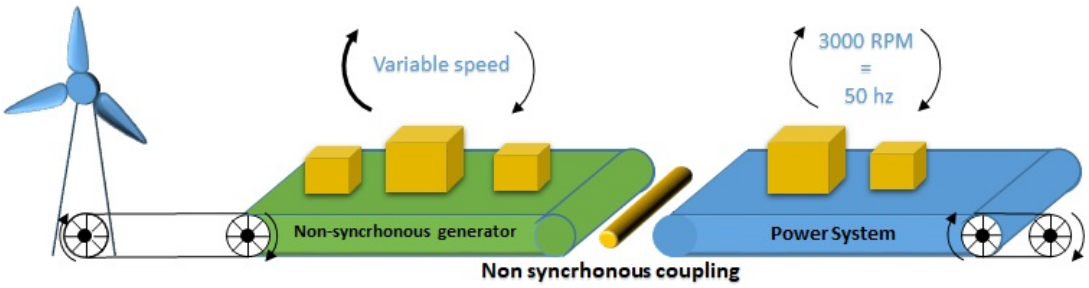

Figure 2.3: Non-synchronous link in power systems

Due to this non-synchronous link between RESs and the power system, these types of sources do not add conventional inertia, as a synchronous generator would do. In this thesis, we aim to incorporate into the UC optimisation, new modellings that include non-synchronous generation, such as wind or photovoltaic injections of power. At the same time, we will keep the post-fault frequency values into tolerance

limits within the power system dispatch. So far, we have covered the basis behind the UC problem in its non-linear form, and the motivations of the frequency stabilit problem of this thesis. It is necessary to define the foundations of the mathematical tool that solves the power system dispatch, and the tools necessary to tackle the non-linearities that may appear in the problem. This is discussed in the next section.

2.3 Basic MILP formulation

In order to elaborate on the UC problem, it is necessary to describe the foundations where this approach relies on. It is in the area of power system operations planning, and the purpose of the problem is to find an optimum operating state for the system. This normally involves maximising/minimising a specific utility (usually the cost to the operation of the system which is minimised). It is necessary to define where this analysis starts, and this section aims to scope this.

Before addressing the UC problem description, it is important to mention the types of operations planning problems (and their associated planning timescales) that exist in power system operations planning. This planning activity can range from decades-years timescale (for generation expansion/procurement and network adequacy studies), to minutes timescale (for operations planning type problems), which is commonly known as real time, and is part of the intra-day market. The timeline of these analyses is depicted in fig. 2.4.

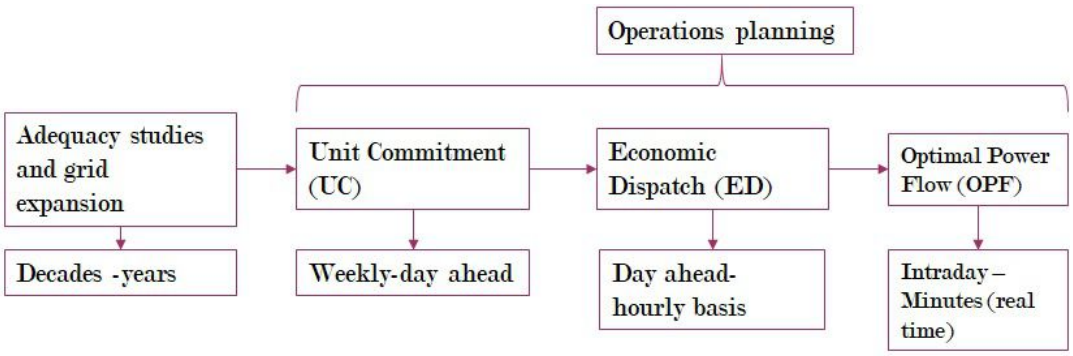

Figure 2.4: Planning horizon in the power system

In network adequacy studies, it is decided if the generation available in a future scenario is able to meet that future demand. The goal of this study is to determine

whether the system's generation capacity can cope with the demand growth in order to maintain a minimum level of reliability, known as Loss of Load Expectation (LOLE). In this problem, the uncertainty included is not only from the load, but from the renewable generation and the transmission system elements as well. It can be said that a study of generation adequacy is one of the areas of reliability analyses [67] when applied to power systems. The types of reliability analysis carried out in this thesis on the other hand are more focused on identifying operating states where system is no longer able to continue a secure operation, based on historic observed data. These are defined in the context of the planning timescales for operations planning purposes. The focus of this thesis is therefore on the UC optimisation problem. As a general way of describing the UC, it is the stage of operations planning where the decisions on which generator units to commit or de-commit are made, whilst adhering to the generation-demand balance condition. In its general form, the complete UC formulation is non-linear, due to the inclusion of the complex power balance equations, which are non-linear.

As it was reviewed in the previous section 2.2, the UC problem in its natural form comes from a non-linear modelling. However, using a MINLP approach to solve the UC problem is not practical for a daily-basis purpose. The connection and disconnection, besides being binary decisions, are nonlinear as well. Therefore, the full linear approach of the UC is discussed in chapter 3, but before doing so, we require that we review the MILP foundations in this section of the chapter, which is the mathematical tool to solve the scheduling problem in the power system. We will be using the example of table 2.1 problem. The considerations of the amount of products A and B are the same, although now we are not allowed to use fractionary ingredients x_1 and x_2 in the problem, but only integers. Therefore, the problem is

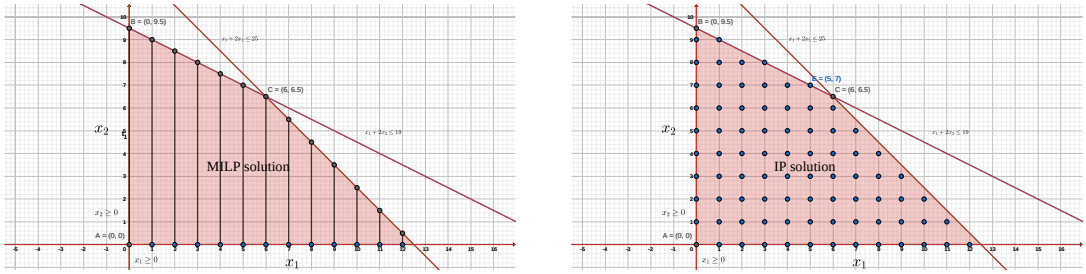

(a) MILP graphical solution

(b) IP graphical solution

Figure 2.5: MILP and IP solutions of the factory's production problem

an integer programming problem, according to:

$$\begin{aligned} \text{maximise} \quad & z = 45x_1 + 80x_2 \\ \text{subject to} \quad & \\ & 2x_1 + 2x_2 \leq 25 \\ & x_1 + 2x_2 \leq 19 \\ & x_1, x_2 \geq 0, \ x_1, x_2 \in \mathbb{Z} \end{aligned}$$

We can try to solve the problem by inspection under the graphical approach. Let's assume that, in fig. 2.5a, a MILP approach is followed, x_1 must be integer, and x_2 is a continuous variable. In fig. 2.5a, the problem is purely integer, thus it is an Integer Programming (IP) problem. The objective function value of the MILP problem is the highest, and slightly less for the IP one due to the integrality constraints. In the next subsections, it will be addressed how the integrality of the variables affects the solution and the different methods to work with this problem.

2.3.1 The branch and bound method

In this section a very brief description of the branch and bound method will be described to solve a MILP or IP problem. In essence, the branch and bound method starts with the so called LP relaxation, i.e. solving the problem in its continuous form. The solution of the LP relaxation is the next one:

- $x_1 = 6$, $x_2 = 6.5$, $z = 790$

This value will be known as the **upper bound** of the problem. The solution already indicates that x_1 is integer, then the variable x_2 will be the one that we will use for **branching**. In the branch and bound approach, sub-problems are created and then solved separately. Since $x_2 = 6.5$, the adjacent integers will be explored, i.e. 6 and 7. The corresponding LP problems will be:

$$\begin{aligned} \text{maximise} \quad & z = 45x_1 + 80x_2 \\ & \text{subject to} \\ & 2x_1 + 2x_2 \leq 25 \\ & x_1 + 2x_2 \leq 19 \\ & x_1 \geq 0\,, 0 \leq x_2 \leq 6,\ x_1, x_2 \in \mathbb{Z} \end{aligned}$$

and

$$\begin{aligned} \text{maximise} \quad & z = 45x_1 + 80x_2 \\ & \text{subject to} \\ & 2x_1 + 2x_2 \leq 25 \\ & x_1 + 2x_2 \leq 19 \\ & x_1 \geq 0\,, x_2 \geq 7,\ x_1, x_2 \in \mathbb{Z} \end{aligned}$$

Their corresponding solutions are:

- If $x_1 \geq 0$ and $x_2 \geq 7$, $z = 785£$, $x_1 = 5\,, x_2 = 7$,
- If $x_1 \geq 0$ and $0 \leq x_2 \leq 6$, $z = 772.5£$, $x_1 = 6.5$, $x_2 = 6$,

A graphical representation of the solution for each node of the branching process is shown infig. 2.6a and fig. 2.6b, respectively. Each of the darker shaded areas indicate where the solution of the problem lies, and their respective solution points of the LP problem.

The next branching will be over the adjacent integers of $x_1 = 6.5$, which are 6 and 7. Hence we have:

- If $0 \leq x_1 \leq 6$ and $0 \leq x_2 \leq 6$, $z = 750£$, $x_1 = 6\,, x_2 = 6$,

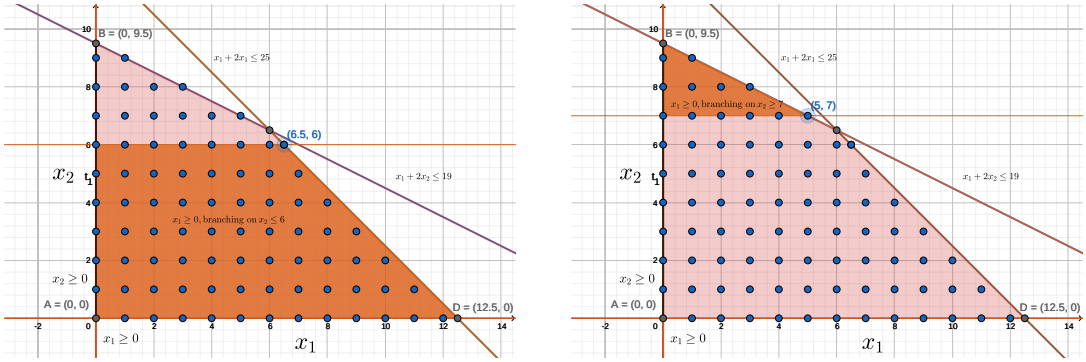

(a) Branching with $x_2 \leq 6$ (b) Branching with $x_2 \geq 7$

Figure 2.6: Solution areas when branching over $x_2 = 6.5$

- If $x_1 \geq 7$ and $0 \leq x_2 \leq 6$, $z = 755£$, $x_1 = 7$, $x_2 = 5.5$,

Graphically, the solutions will have the purple shaded area of fig. 2.7a and fig. 2.7b. We can see at this point that both values of the objective function are *below* the solution founded when branching with $x_2 \geq 7$. This is known as a lower bound, hence there is no need to keep branching over the non integer variables.

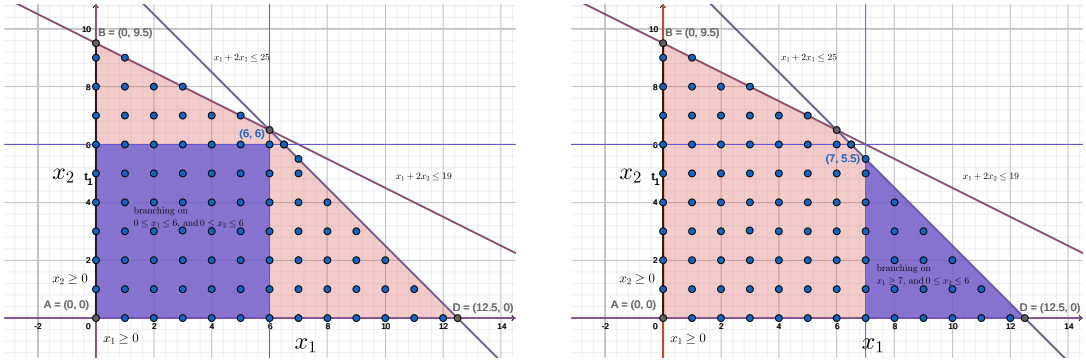

(a) Branching with $x_1 \leq 6$ (b) Branching with $x_1 \geq 7$

Figure 2.7: Solution areas when branching over $x_1 = 6.5$

The whole tree of solution search will have the structure of fig. 2.8. The problem terminates with the best values of 5 units of ingredient x_1 and 7 units of ingredient x_2 and an objective function value of $z = 790£$. In the next section, another approach to tackle the integrality of the MILP problem will be explained.

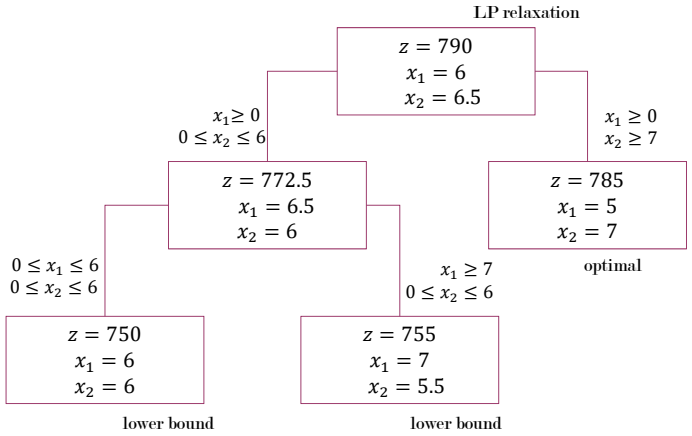

Figure 2.8: Branching tree of the MILP problem

2.3.2 The branch and cut method

The branch and cut method is an extension of the branch and bound method. "Cuts" are applied from the LP relaxation phase of the problem, then the branching starts in the different nodes of the search tree. We can start by defining only the general idea behind these cuts. We can consider the next MILP problem:

$$\text{maximise} \quad \sum_{k \in K} \sum_{i \in N} c_i x_i + e_k y_k \tag{2.3.25}$$

subject to

$$\sum_{k \in K} \sum_{i \in N} a_{ij} x_i + d_{kj} y_k \leq b_j, \qquad \forall j \in \{1, 2, \ldots, J\} \tag{2.3.26}$$

$$x_i \geq 0 \ , \in \mathbb{Z}_+^N$$

$$y_k \geq 0 \ , \in \mathbb{R}_+^K$$

Then, there is a set of feasible solutions of the MILP problem such that:

$$S := (x_{ij}, y_{kj}) \in \mathbb{Z}_+^N \times \mathbb{R}_+^K : Ax + Dy \leq b_j \tag{2.3.27}$$

where $A = (a_{ij})$ and $D = (d_{kj})$. The next LP relaxation solves the problem of eq. (2.3.27) since $S \subseteq P_0$:

$$\text{maximise } z_0 = \sum_{k \in K} \sum_{i \in N} c_i x_i + e_k y_k : (x, y) \in P_0 \tag{2.3.28}$$

We can assume that z_0 is the optimal value and (x^0, y^0) is an optimal solution. In this part enters the concept of "cuts". There can be cases when the solution (x^0, y^0) is not in S. The idea is to find an inequality $\alpha x + \gamma y \leq \beta$ that is satisfied by every point in S and that $\alpha x^0 + \gamma y^0 > \beta$.

$$P_1 := P_0 \cap \{(x, y) : \alpha x + \gamma y \leq \beta\} \tag{2.3.29}$$

Then we know that $S \subseteq P_1 \subset P_0$, the LP relaxation of the MILP problem P_1 is stronger than the initial natural LP relaxation of eq. (2.3.28), the optimal value of the objective function in eq. (2.3.30):

$$\text{maximise } \sum_{k \in K} \sum_{i \in N} c_i x_i + e_k y_k : (x, y) \in P_1 \tag{2.3.30}$$

is at least as good as an upper bound on the value z^* as z^0, while the optimal solution (x^0, y^0) of P_0 does not belong to P_1. Using this approach of defining **cutting planes**, we can generate more cuts in an iterative form. This iterative process is described as follows:

Starting with the initial LP relaxation, initialise with $i = 0$, repeat:

- **Step 1**: solve the LP problem $\max\{cx + ey :\in P_i\}$
  - If the optimal basic solution (x_i, y_i) exists in S, terminate the process.

- Otherwise solve the separation problem by finding the cutting plane $\alpha x + \gamma y$ separating (x_i, y_i) from S. Set $P_{i+1} := P_i \cap \{(x, y) : \alpha x + \gamma y \leq \beta\}$ and repeat step 1.

This separation problem is of high relevance in MILP problems. If (x_i, y_i) is outside the set of solution points of S, there are an infinite number of cuts that separates (x_i, y_i) from S. Instead of generating one single cut as it is shown in the previous algorithm, solvers usually add several cuts to P_i to generate the problem P_{i+1}.

In the branch and bound method, the upper bound is defined by the branching stage at each LP problem. For a tighter upper bound, the branch and cut method adds the necessary cutting planes *before* the branching process starts. A brief description of the branch and cut algorithm using the Gurobi solver[68] is described in the next steps:

Gurobi MILP bulding blocks

- **Step 1: Presolve**
  - This step reduces the size of the problem by modifying possible constraints susceptible of making them stronger than the original ones, e.g. reducing the coefficients' size. These new constraints must not discard any valid solutions.
- **Step 2: LP relaxation**
  - In this stage a LP relaxation is done, neglecting the integrality constraints of the problem and creating an objective function bound.
- **Step 3: Cutting planes strategy**
  - In this step is where the cutting planes are introduced to the problem. The solver decides in an empirical form to add the necessary cuts to the problem, based on the success of their addition. They are mostly added at the root node of the solution tree, and very few cuts are added in the later nodes of search.

- **Step 4: Branching phase**
  - Finally, in this branching phase the solver decides the branching variables. In a problem with thousands of variables, Gurobi classifies a "superb" variable as the one that finds infeasibility in both directions of the integer rounding.

Further reading of the solver settings and characteristics can be consulted in [68]. A review that expands on MILP and MINLP can be found in [69]. Now that we have covered the basic modelling of the MILP, which are the modelling foundations on the UC modelling, we have to tackle the cases when non linear expressions appear in the formulation. The inclusion of frequency stability constraints in the UC formulation requires to follow an approximation into a linear form. To address this problem, we will be introducing the separable programming approach that is incorporated into the MILP formulation in the next subsection.

2.3.3 Separable programming modelling

Previously, we have covered the LP and MILP problems where all the variables involved are linear. In the UC formulation addressed in this thesis, we follow a linear approach. For this reason, all non linear terms that appear in the cost function or the constraints of the problem, must be either linearised or approximated into a linear form.

This thesis includes a technique that approximates the non linearity of a term of the cost function or the constraints of the UC problem into a linear form, instead of trying to solve the problem directly, which under a MILP approach is not possible. We have shown that in LP problems the solutions are expected to be found in the vertices of the feasible region. With the inclusion of non linear terms, the solution might not be bounded by straight lines that inequality constraints add, or it could be the case that the solution could be found in the interior of the feasible region[70]. These types of problems arise in cases where the optimisation is expected to be modelled over a period of time, and it is expected that at each time point these non linearity constraints are approximated into linear forms. This is indeed the

case of the UC problem analysed in this thesis, and such non linearity problems will be discussed in depth in section 2.2.2 and chapter 3. In order to handle this Nonlinear Programming (NLP) problem, we use an approach known as **separable programming**[71]. If the objective function or constraint that includes the non linear term can be represented in the next form:

$$\phi(x_1, \ldots, x_n) = \sum_{j=1}^{n} \phi_j(x_j) \tag{2.3.31}$$

then it is called a **separable function** since all of its terms can be expressed as the sum of each function $\phi_1(x_1) + \phi_2(x_2) + \cdots + \phi_j(x_j)$. Another condition is that the function must be convex, guaranteeing a global optimum, since inside of the polyhedron can be traced by a straight line between each solution point, without interfering with another solution point or region of the polyhedron. In practical terms, all the points can be *seen* at any position inside the solution region. The j term of eq. (2.3.31) represents all the possible variables to be linearised in the objective function. As an example, the linear function:

$$\phi(x_1, x_2, x_3, x_4) = 2x_1 + 5x_2 + x_3 + 6x_4$$

is separable, since each of its terms is not multiplying with another, or included inside a different function, plus no quadratic term is embedded either and the function is convex. An example of a non-linear but convex function is shown in:

$$\phi(x_1, x_2) = 2x_1 + 5x_2^2$$

whereas the function:

$$\phi(x_1, x_2, x_3, x_4) = x_1 + 5(x_1 x_2) + x_1 \sin(x_3 + x_4) + x_4^2$$

is not directly separable since there are variables that multiply each other inside the function, and also have a sinusoidal and quadratic form; hence the nonlinearity of the function.

In the UC problem addressed in the aforementioned section 2.2 and expanded further in chapter 3 in its linear form, we will be working with a parameter known as the largest infeed (ΔP_L^{max}), which is the largest credible outage of a generator

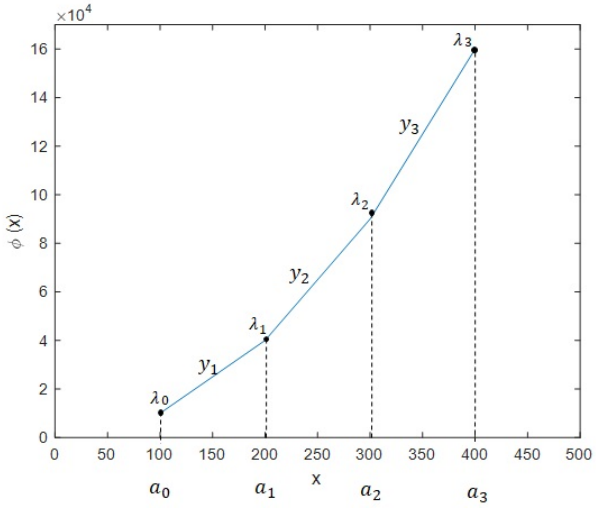

Figure 2.9: Discretisation of x value

that can happen in the power system. Due to the problem modelling this parameter becomes quadratic, as in $(\Delta P_L^{max})^2$. The quadratic modeling of this value will be further discussed in chapter 3. For the sake of the example, let's assume that we want to add it as a decision variable in the optimisation problem, since it could be the case we want to add that flexibility of letting the solver choose optimally the size of the largest infeed. We would need to approximate it into a linear form in order to include it in the MILP, hence substituing ΔP_L^{max} as the x variable to approximate into linear, we will have:

$$x = \Delta P_L^{max} \tag{2.3.32}$$

$$\phi(x) = (\Delta P_L^{max})^2 \tag{2.3.33}$$

As a modelling strategy of approximating $\phi(x)$ as linear, we show the value of x as a piecewise linear function with some r affine segments, considering a range of outages of $[100, 400]$ MW in the power system. This can be shown in fig. 2.9

First we perform a discretisation with lower l and upper u bounds of a_r values of the form $l \equiv a_0 < a_1 < \cdots < a_R \equiv u$. The less distance between each point, and the more points of the discretisation, the better the approximation. There is an obvious tradeoff between the number of breaking points, and the results of the optimisation. One strategy can be to observe result of the x value in question, and add more granularity between the adjacent breaking points. Next we have to model

the coordinates $(a_r, \phi(a_r))$ as a convex combination associated with the weights λ_r for each $r = 0, \ldots, R$ and associate each transition between the a_r points with the binary variable $y_r$where $y_r \in \{0, 1\}$ to reflect the selection of each affine segment in the interval $r = 1, \ldots, R$. This formulation is shown as follows:

$$x = \sum_{r=0}^{R} a_r \lambda_r \quad \text{and} \quad \phi(x) \approx \sum_{r=0}^{R} \phi(a_r)\lambda_r \tag{2.3.34}$$

where:

$$\sum_{r=0}^{R} \lambda_r = 1, \quad \sum_{r=1}^{R} y_r = 1 \tag{2.3.35}$$

$$\lambda_0 \leq y_1, \quad \lambda_r \leq y_r + y_{r+1} \text{ for all } r \in \{1, \ldots, R-1\}, \quad \lambda_R \leq y_R \tag{2.3.36}$$

$$\lambda_r \geq 0, \quad y_r \in \{0, 1\}, \quad \text{for all } r \in \{0, 1, \ldots, R\}; \tag{2.3.37}$$

The value of λ_r must meet the next condition:

Adjacency condition: At most two λ_r weights are positive. If two weights are positive, then they are adjacent, i.e., of the form $\lambda_r + \lambda_{r+1}$. This is also known as a SOS2 *Special Ordered Set 2* condition [70, 72, 73, 74]. The λ_r operators will look to select fractional values of the adjacent coefficients a_r and a_{r+1}, where the sum of two of them will yield the approximated linearised value. The use of the binary operators y_r ensures that one slope is selected between two adjacent points. This strategy will guarantee and enforce and a global optimum in the optimisation since the problem keeps its convexity[75]. This whole approach will result in the approximation of the squared value of ΔP_L^{max}.

The non-linearities in the optimisation can appear in different forms, not only as a squared variable. Fortunately, there are different techniques that are capable to induce a linear form. Let x_1 and x_2 be the variables that are members of a nonlinear term, either in the objective function or a constraint of the problem, and let y_1 and y_2 be auxiliary variables. Some of the transformations necessary to induce linearity are shown in table 2.2.

More transformations can be implemented to avoid the direct inclusion of non-linear terms in the optimisation problem [76], but so far these are useful examples of how by adding extra variables and constraints helps to include them in the MILP formulation. For a graphical representation, let's assume that the variables

Table 2.2: Variable transformations to approximate nonlinear terms into linear terms

Inducing separability

Term	Substitution	Additional constraints	restriction
x_1^2	$x = \sum_{r=0}^{R} a_r \lambda_r$, $\phi(x) \approx \sum_{r=0}^{R} \phi(a_r)\lambda_r$	$\sum_{r=0}^{R} \lambda_r = 1$ $\lambda_r \geq 0$, for all $r \in \{0, 1, \ldots, R\}$	SOS2 condition, and convex solution area
$x_1 x_2$	$x_1 x_2 = y_1^2 - y_2^2$†	$y_1 = 0.5(x_1 + x_2)$ $y_2 = 0.5(x_1 - x_2)$	none
$x_1 x_2$	$x_1 x_2 = y_1$	$\log y_1 = \log x_1 + \log x_2$	$x_1 > 0$, $x_2 > 0$

†This substitution is non-convex

$x_1, x_2, y_1, y_2 \in [-1, 1]$, and we are interested in approximating into linear the product of $x_1 x_2$. We can see the non-convex feasible region of the product of the two variables x_1 and x_2 in fig. 2.10a. When we develop this last expression into the transformation of $y_1^2 - y2^2$, and subject to the respective constraints shown in the third column of table 2.2, the feasible region is shown in fig. 2.10b, and it is non convex as well. With these cases, the SOS2 condition can not be met without the inclusion of additional constraints; contrarily it is possible to do so with the case of the convex function x_1^2 shown in fig. 2.9. The necessary additional constraints are shown in eqs. (2.3.35) to (2.3.37). The integrality of the constraints guarantees a global optimum, even for the non-convex cases [77].

These are the foundations of the MILP formulations, that will be used later throughout this research work, applied to power systems operations planning, but specifically the UC problem. The next step in this work is to include the uncertainty in the UC problem. The basic formulation of the techniques used to address this problem will be covered in the next section of this chapter.

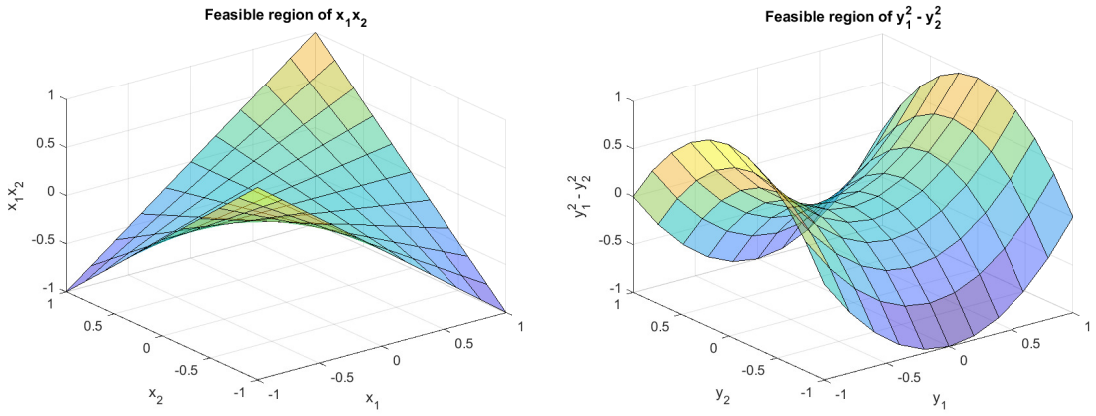

(a) x_1x_2 feasible region

(b) $y_1^2 - y_2^2$ feasible region

Figure 2.10: Feasible region of variable transformations

2.4 Inclusion of uncertainty in the MILP formulation: Stochastic Programming

Thus far, we have covered how to tackle the problem of MILP, which is the mathematical programming tool to model the UC optimisation problem. It is in the UC problem where the decisions of connecting and disconnecting generation units happen. Nonetheless, the UC in its deterministic form may not necessarily contain any uncertain variables. There are different perspectives to include this uncertainty, such as:

- Load perspective: based on past behaviour and history, and depending on the time frame from the scenario to analyse, load forecasting is a tool where the demand's behaviour is predicted.

- Generation perspective:The uncertainty that comes from some of the RES, specifically those that do not have a constant source of power, such as the wind and solar resource.

- Contingency analysis: Due to unforeseen circumstances, there is uncertainty on the continuous functioning of the elements that belong the power system. Via contingency analysis under a probabilistic modelling, and using the respective historic data, we can obtain the probability for an element to fail

(i.e., a contingency). This input can be included as a source of uncertainty in the context of power systems planning problems.

All these sources of uncertainty can be acknowledged in the modelling as *random variables*. Other classifications on the source of uncertainty depending on the nature of problem may also exist but the categories above comprise the cases that apply to most problems. In this thesis work, we model the uncertainty using Stochastic Programming (SP). Via SP techniques we can include these sources of uncertainty in the optimisation problem. The difference with an optimisation based on deterministic and constant inputs is that such approach only covers one "path" of results, based on the single-path input data. A deterministic modelling of the UC is a useful approach when the certainty of the input data is rather high. On the other hand, Using SP we can capture the uncertainty of the aforementioned perspectives, and it is in the interest of this work to understand how the linearisation techniques can be implemented at the presence of uncertain variables. Next we will be covering in general form some of the techniques to work under a SP environment.

2.4.1 Scenario generation and selection

The UC is an optimisation processed that is performed for a specific planning horizon. This will be discussed in detail in chapter 3. As it was mentioned earlier, the uncertainty from the load and RESs can be included in the problem. There are different approaches to do this, and they are discussed here:

Probability model

This is possibly the mostly known form of characterising the random variables. Using the historical data from RESs or load, we can model the probability density function (PDF) or cumulative distribution function (CDF) which describe the behaviour of these random variables[78]. This historical data can be sourced from real readings from available meters or simulated output. We will describe one statistical approaches to estimate the PDF: parametric estimation. With parametric estimation it is assumed that the historical values follow a probability distribution

dependent on the parameters of interest. The case of wind energy is an example for this statement. It is usually assumed in empirical studies that the speed of the wind (x) follows a Weibull distribution, such as:

$$PDF(x;\lambda,k) = \begin{cases} \frac{k}{\lambda}(\frac{x}{\lambda})^{k-1}e^{-(x/\lambda)^k} & x \geq 0, \\ 0 & x < 0, \end{cases} \tag{2.4.38}$$

where k is Weibull form parameter. It indicates the shape of the Weibull distribution, which a small value of k indicates very variable wind speed, and more constant wind speed is characterised by large values. The value of λ is the scale parameter; a measure of the characteristic wind speed of the distribution. This value is proportional to the mean wind speed. Both of these values can be estimated through methods such as the maximum likelihood estimator, Bayes estimator, etc. [79]. So far, it should have become evident that it is not possible to include the probabilistic behaviour to the MILP optimisation directly. The function in eq. (2.4.38) is not linear and not convex either. Different methods able to handle this input are the chance constraint and Value at Risk[80], but both of them are not used in this thesis work.

Multiple scenarios

Continuing with the different perspectives of analysing the uncertainty to be included in the UC, we reach the scenario generation and classification [81]. The aim of this approach is to capture the behaviour of historical data in different *strata* of the random variables (load or RES). These strata should represent the extreme points of the historical data, and this data will be grouped depending previously defined thresholds. Once the data is allocated to their respective strata, the next step is to randomly select the data points from the stratum. This is known as **stratified sampling** [82]. A graphical representation is shown in fig. 2.11. The red dots at each stratum will be the randomly selected elements. The selection of the scenarios should comply with the next characteristics:

- Compactness: The number of strata that group the data should be a number that fairly represent the distribution of the data. This number will also depend

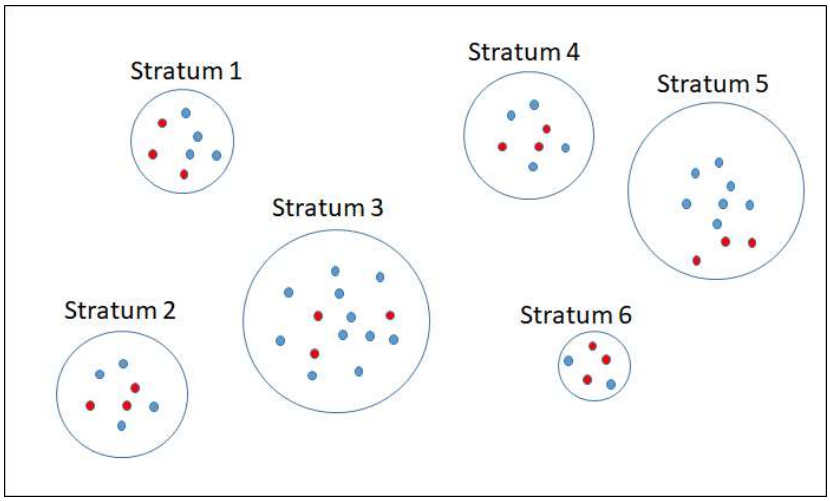

Figure 2.11: Schematic representation of scenario selection via stratified sampling

on the number of realisations needed for the analysis.

- Diversity: The scenarios selected should represent not only the mean values of the historic data, but the extreme cases as well. Hence the importance of the stratum construction.

- Representativeness: The scenarios selected should represent the whole data, but not be redundant or repetitive.

Now let's assume that we are looking to create the strata for a historic data of wind resource. For the sake of the example, we can omit to specify the output of this resource, either energy or wind speed. In fig. 2.11 the stratum classification can represent sources that are geographically allocated in different areas. Hence, if we look at one year of hourly observations, due to the seasonality of the wind resource, it could very well be the case that certain amount of wind is available for a region in the system at certain week of the year, whereas this is not the case for another region of the system, and vice versa. This approach improves the representativeness of the historical data in each stratum. Now we will analyse some of the approaches to model the uncertainty into the MILP and hence the UC.

2.4.2 Two-stage stochastic programming

Previously we have covered how we can define the MILP problem. So far, the input data has been assumed to be constant and deterministic. This is useful when the problem is modelled under a short term horizon. In order to add the aforementioned scenarios into the formulation, we will use in this thesis work the **two-stage stochastic programming (TSSP)** approach [80, 83, 84]. This approach is known to **commit** to decisions on the first stage of the problem, also known as the **here-and-now** decision; and the second stage of the optimisation, the **recourse**, takes into account the different scenarios according to their respective probability. Under this approach, the optimal decision ensures the minimum or maximum total cost of the objective function in an expected value sense. In order to remember the original deterministic MILP problem, we will show again the eq. (2.1.1):

$$\text{maximise (minimise)} \quad \sum_{i \in N} c_i x_i \tag{2.1.1 revisited}$$

subject to

$$\sum_{i \in N} a_{ij} x_i \leq b_j, \qquad \forall j \in \{1, 2, \ldots, J\} \tag{2.1.2 revisited}$$

$$x_i \geq 0, x_i \in \mathbb{R}$$

The modified eq. (2.1.1) under a two-stage stochastic programming becomes and matrix form is:

$$\text{maximise (minimise)} \quad c^{\intercal} x + \sum_{\xi \in \Xi} \pi_{\xi} q_{\xi}^{\intercal} y_{\xi} \tag{2.4.39}$$

$$\text{s.t. } Ax \leq b, \tag{2.4.40}$$

$$R_{\xi} x + G_{\xi} y_{\xi} \leq h_{\xi}, \qquad \forall \xi \in \{1, 2, \ldots, \Xi\} \tag{2.4.41}$$

$$x \geq 0,\ y_{\xi} \geq 0,\ \forall k \in \{1, 2, \ldots, \Xi\}$$

where:

- $c_i\, q_\xi$ are the cost coefficients associated with the first and second stages of the problem, respectively;
- x is the variable vector of the first stage of the problem,
- y_ξ is the variable vector of the second stage of the problem, at each scenario ξ
- π_ξ is the probability of the scenario $\xi = \{1, 2, \ldots, \Xi\}$,
- A is the coefficients matrix of the first stage of the problem,
- R_ξ, G_ξ are the coefficients matrix of the second stage, at each scenario ξ, and h_ξ is the right hand side of the inequality.

To summarise the whole optimisation problem: the solution of eq. (2.4.39) is given by one optimal solution of $\overline{x}$ and the $\xi - th$ optimal solutions of $\overline{y_\xi}$, and the vector of variables y_ξ repeats at each $\xi - th$ scenario. Under these conditions, the term $G_\xi y_\xi$ picks up the slack if there is a deviation of the term $R_\xi x \leq h_\xi$, once the uncertain data is revealed. The cost of this handling this deviation is amounted by $q_\xi^\intercal y_\xi$. Under this approach, we assume that the process under analysis is solved repeatedly under random conditions that do not significantly change over a period of time. This stochastic formulation will be expanded for the UC in chapter 5.

This last section of the chapter has been the last one regarding the MILP formulation and how to include the stochasticity in the optimisation. One of the motivations of this thesis work is to understand the dynamics of the frequency stability, and include their behaviour for the UC problem. The next chapter covers the frequency stability foundations of this thesis work. In the subsequent section we will elaborate on the test system used in throughout this thesis.

2.5 The Reliability Test System (RTS) - updated NREL version

The three area test system shown in fig. 4.8 is a test system that is based originally from the IEEE Reliability Test System 96 [85]. Recently, changes have been applied

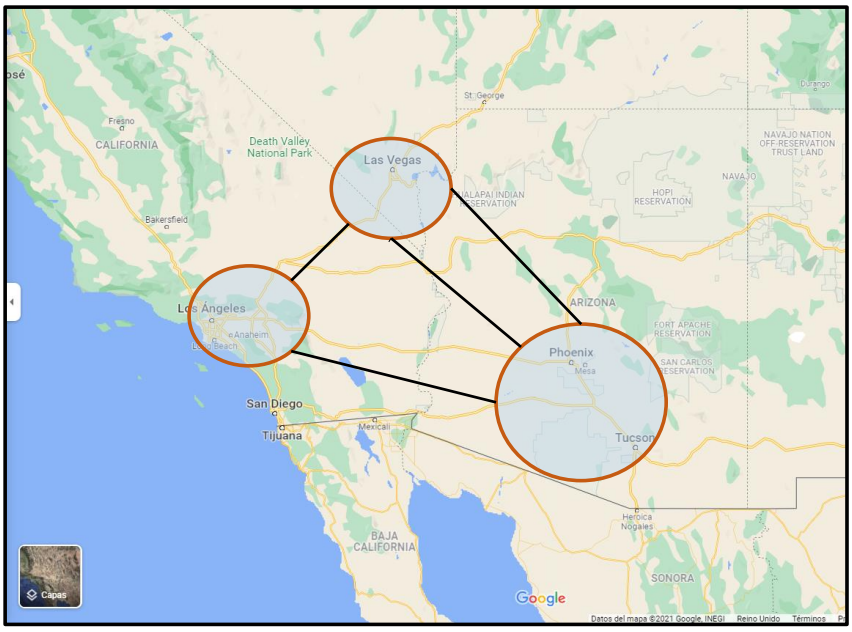

Figure 2.12: Three area RTS geographical representation[60]

to it to be suitable for modern power system analytical needs. This is a task that is under the National Renewable Energy Laboratory (NREL) supervision. The changes can be consulted in the reference [60]. A geographical representation of such test system is included in the fig. 2.12

2.6 Chapter remarks

In this chapter we covered the foundations of the UC optimisation problem, starting from reviewing the mathematical programming tools that are needed to solve it. A simple LP optimisation problem involves variables that are continous and with a lower bound greater than zero. We use simple examples as a two-variable problem to show that the basic feasible solutions are in the corner points of the feasible region. These basic feasible solutions must satisfy all the constraints of the LP problem, and there will be one single solution, known as *optimal solution* which it cannot be improved. This definition is part of the basic theorem of LP.

We have reviewed the natural UC problem in its non-linear form as well. This is of high importance because it shows the necessity of using another mathematical programming tool that allows us to solve the UC problem, since it is non-linear and

involves binary decision variables that are not handled in a natural LP problem. Thus in this chapter we reviewed the MILP basic formulation needed to further understand the UC problem in chapter 3.

The inclusion of non-linear constraints involves modelling them in such a form that it is capable for the solver to understand a model that is linear. In this thesis work, we will be adding constraints that capture the frequency stability of the power system. In order to do so, we will be using a technique called separable programming, which the basic formulations have been explained in this chapter as well.

Finally, we need to expand the modelling of the UC to include the uncertainty that RESs such as solar and wind bring into the system. To tackle this problem, we have covered the foundations of the approach followed in this thesis, such as the TSSP. This technique *commits* to include the necessary information in the first stage of the problem, then the variation and the uncertainty of the second stage is covered by introducing different scenarios in the modelling.

In the next chapter we will be reviewing on the linear formulation of the UC and the inclusion of the frequency stability constraints into the problem, with their respective simulations and results.

Chapter 3

Frequency Stability in the day-ahead to week-ahead generation scheduling

Parts of this chapter follow from the paper "Inclusion of Frequency Stability Constraints in Unit Commitment Using Separable Programming" with the assigned Manuscript Number EPSR-D-21-00126R2, now under minor review status. The problem of frequency stability was explained in chapter 1, and in chapter 2 the foundations of MILP formulations were given. It is within the scope of this thesis to cover the models necessary for operational planning for systems with low inertia. To this end, our aim in this chapter is to incorporate the frequency stability constraints within the unit commitment (UC) problem for operational planning purposes.

3.1 Introduction

Continuing with the day-ahead to week-ahead generation scheduling, specifically the UC problem, we look to understand it from a security standpoint, thus creating a security-constrained unit commitment SCUC optimisation problem. In this class of UC, we add security criteria, either for generator outages or branch outages, in the form of equality or inequality constraints. In this work, we adopt an N-1 security criterion. Generally speaking, this criterion means that at minimum the system

must withstand any disturbance (i.e. contingency) caused by the outage of any one single component (e.g. transmission line or generator, and in specified cases, large loads). In our work, we are specifically looking at power imbalances produced by the outage of the largest generator or interconnector. From the TSO perspective, this yields a minimum number of units to be committed in order to withstand a possible frequency excursion due to the loss of the largest infeed. The transient responses from the controls of Synchronous Generatorss (SGs) and CIGs units are not in the scope of this research.

As mentioned earlier in Chapter 2, the UC problem is a mathematical tool with which network operators, namely TSO, determine, over a set planning timescale, an optimum set of generating units that are to be committed to maintain network operational security. If in the course of the UC problem, a security criterion (e.g., $N-1$ criterion) is considered, then the ensuing problem becomes a SCUC problem. Notwithstanding this, the UC problem, at its core, contains the set of constraints pertaining to the network operational requirements (i.e. nodal power balance constraints, transmission thermal limit constraints, etc.) as well as generating units limits (i.e. maximum capacity, ramp limits, inter-temporal constraints, minimum up and down times, etc.) as specified in previous chapter, section 2.2. However, additional constraints such as frequency stability constraints, may be added to the core UC problem if need be [66, 86]. For instance, authors in [87] propose to include the primary and tertiary reserves in the UC problem, which is defined as a multi-period optimisation problem over a 24-hours planning period.

The UC problem formulation may include a stochastic formulation to tackle the inherent uncertainty in renewable resource (e.g. wind) and demand forecasts. For example, in the work of [88], a UC stochastic formulation is used to take into account multiple scenarios of demand and wind realisations. The wind input is modelled as an auto regressive (AR) process. The time window of analysis is performed for a whole year of UC optimisation. Transmission network constraints are not considered. The authors in [89] include frequency stability constraints in the UC optimisation by extracting a priori the bounds of the variables that have an influence in the constraints. Although this method runs faster than a piece-wise linearisation of the

nonlinear constraints of frequency stability, it is affected by the size of the system. This approach is tested on a 20 synchronous generators system.

More recently, scholars working to overcome the challenges of low-rotational inertia have proposed different approaches to tackle the frequency stability constraints into the UC [90, 91]. In [90] authors use two methods to achieve this: overestimating planes, and binary expansion with the big-M method, whereas in [91] the authors introduce the frequency constraints as mixed integer second order cone program Mixed Integer Second Order Cone Programming (MISOCP), based on the fact that binary variables and the big-M method is used as well in this approach, when certain conditional statements are met in the proposed formulation. MISOCP problems are out of the scope of this thesis, suffice is to say that they can represent sometimes relaxations or reformulations of MINLP or MILP. For further reading on this technique, the reader can consult [92]. The works Badesa et al. [90, 91] are implemented within a stochastic framework and include frequency services with different time responses.

In [93] the virtual inertial response from wind farms are specifically modelled from their mechanical power generated, and the whole problem is solved as a stochastic chance-constrained frequency constrained UC problem. Furthermore, in the work of [94], authors introduce the concept of frequency security margin. This expression is non linear, thus it is linearised via a piecewise linearisation method and using a deterministic UC approach.

Authors in [95] incorporate scenarios with de-loaded modes of wind turbines variable speed, providing PFR and frequency response as well. The way they tackle the non linearity of the Frequency Nadir is by adding binary and continuous variables to the problem. This is all formulated as a stochastic MILP problem, and solved via Generalised Bender Decomposition (GBD). The work is based on a six-bus system. What differentiates this latest literature from the work presented in this paper is the approach to the frequency nadir non linearity. Whereas the above authors linearise it through the methods mentioned earlier, in this thesis work we approach the frequency nadir linearisation via separable programming.

Indeed, we solve the UC problem as a MILP problem. We incorporate three

sets of frequency stability constraints namely, the RoCoF, the Frequency Nadir and the Quasi Steady-State Minimum Frequency Recovery. For the three constraints we follow the frequency deviation limits set in the UK grid code by the UK TSO, National Grid ESO [96] to select an acceptable value of RoCoF. Inclusion of the three frequency stability constraints, ensures that within a specified planning timescale, the optimum unit commitment schedule not only adheres to the network's operational boundaries but also meets the inertia and PFR requirements to withstand the frequency disturbances due to the loss of the largest in-feed. As mentioned above, we use separable programming techniques as a way to linearly approximate the Frequency Nadir constraint, which is nonlinear. Via separable programming technique we can approximate a nonlinear term into a linear term, by translating it into a larger linear program that involves additional binary variables. The use of this extra binary variables guarantees a global optimum. To apply this technique, the function in question must be in separated terms. This is the case of the Frequency Nadir, which we will elaborate later. It goes without saying that the addition of frequency stability constraints converts the UC problem into a SCUC one.

To respond to the frequency excursions, in our work we added the possibility of including so-called Synthetic Inertia (SI), or virtual inertia emulation (assuming it as an additional control). This response takes advantage of the stored kinetic energy in the rotating blades of the wind turbines. Since wind turbines rotate at a non-synchronous speed, their coupling with the grid frequency is normally provided through a power electronic converter interface, and with the proper control settings, they can provide almost instantaneous power response, as long as the wind turbines have the room to deliver this power to the grid [97]. We assume in this work that the wind turbines are able to deliver this response. We note that time-domain frequency and transient stability analysis is beyond the scope of this research as our focus is on operations planning ahead of real-time operation in form of the solution of a multi-period SCUC problem.

For the test system we use the updated IEEE Reliability Test System [60] using the three areas of the original system, and we run the simulations in a Matlab™ environment, using a modified version of the Matpower Optimal Scheduling Tool

(MOST) [98, 99]. The optimisation process is solved via the Gurobi solver.

The chapter is organised as follows. In section 3.2 we describe the UC modelling including frequency stability constraints. In section section 3.3 we cover the simulation and results obtained. Finally, in section section 3.5 we draw the conclusions and discuss future work.

3.2 The UC optimisation process

In the first stage of power systems short-term operational planning we focus on the problem of allocating units in order to meet demand at a certain point in time. The optimum schedule of *committed* generators is the result of solving a UC problem [100], which was introduced earlier as a MINLP in previous chapter. Based on the available resources of each unit and their running costs, the aim of the UC problem is to minimise the cost of synchronising and desynchronising generators to the grid and meet the demand. This is usually a problem that is run at least a day ahead. The time step, which could range from minutes to hourly-basis, has to be coherent with the rate of change of power output of each unit. This is usually performed on hourly or half hourly basis. For practical purposes, the UC problem is typically formulated as a MILP [33, 65] rather than the original MINLP since for the specified planning timescale voltage variations can be effectively neglected especially for transmission systems. Notwithstanding this, the problem still contains mixed integer variables representing the binary decisions that occur to synchronise or disconnecting the units. Other types of problems, such as UC where voltage limits and reactive power injections are included in the constraints, are solved as MINLP [101] due to the non-linearity that these restrictions bring to the problem.

In the next subsection we define the mathematical modelling of the UC applied in this chapter.

3.2.1 UC objective function

The aim is to optimise the objective function in eq. (3.2.1) where:

$$\min_{\Phi} \sum_{t\in\mathcal{T}} \sum_{g\in\mathcal{G}} \left(S_g(u_g^t - u_g^{t-1}) + F_g(P_g^t) + C_g^0 u_g^t + C_g^+ R_g^t + \delta_g(P_g^t - P_g^{t-1})\right) \quad (3.2.1)$$

where $\Phi \coloneqq (P_g^t, R_g^t, u_g^t, \theta_v^t)_{g\in\mathcal{G},\, t\in\mathcal{T},\, v\in\mathcal{M}}$ and where P_g^0 and u_g^0 are known.

- $t \in \mathcal{T} \coloneqq \{1, \ldots, T\}$, where $\mathcal{T}$ is the set containing all timesteps in the planning horizon, and T is the final time step,
- $g \in \mathcal{G} \coloneqq \{1, \ldots, G\}$, where $\mathcal{G}$ is the set containing all synchronous generators, and G is the number of generators,
- u_g^t is the unit status (up or down) of unit g at time t, where $u_g^t \in \{0, 1\}$,
- $S_g(u_g^t - u_g^{t-1}) \coloneqq C_g^{SU+} \max(u_g^t - u_g^{t-1}, 0) + C_g^{SD-} \max(u_g^{t-1} - u_g^t, 0)$ is the start-up and shutdown cost function which has a unit-dependent costs C_g^{SU+}, C_g^{SD-} per event,
- $F_g(P_g^t)$ is the fuel cost function. In our modelling we use a piecewise linear form where $F_g(P) := \max_{i=1}^{n_g} a_{gi}P + b_{gi}$, with parameters a_{gi} and b_{gi} such that $F_g(0) = 0$.
- P_g^t is the active power generation of unit g at time t, in MW,
- θ_v^t is the voltage angle of node v in radians and at time t,
- C_g^0 is the no-load cost of unit g at time t, that is the cost of a unit that is active ($u_g^t = 1$) but that is not generating ($P_g^t = 0$). A classic example is a synchronous condenser, which can be synchronised at $P_g^{min} = 0$,
- R_g^t is the available Primary Frequency Response of unit g at time t, in MW. C_g^+ is the cost associated with the day ahead PFR offered.
- $\delta_g(P_g^t - P_g^{t-1}) \coloneqq C_g^{\delta+} \max(P_g^t - P_g^{t-1}, 0) + C_{gt}^{\delta-} \max(P_g^{t-1} - P_g^t, 0)$ represents the ramp up and down reserve cost functions for each unit g in time t. Both are dispatch-dependent of P_g^t.

Physical constraints

$$u_g^t P_g^{\min} \leq P_g^t \tag{3.2.2}$$

$$P_g^t + R_g^t \leq P_g^{\max} u_g^t \tag{3.2.3}$$

$$0 \leq R_g^t \leq \min(R_g^{\max}, \Delta_g^{\max}), \tag{3.2.4}$$

$$\sum_{g \in \mathcal{G}_v} P_g^t - P_{Dv}^t - \sum_{\substack{w \in \mathcal{M} \\ v \neq w}} B_{vw}(\theta_v^t - \theta_w^t) = 0, \qquad \forall v \in \mathcal{M} \tag{3.2.5}$$

$$B_{vw}(\theta_v^t - \theta_w^t) \leq L_{vw}^{\max}, \qquad \forall\ v, w \in \mathcal{M} \tag{3.2.6}$$

$$\delta_g^{\min} \leq P_g^t - P_g^{t-1} \leq \delta_g^{\max}, \tag{3.2.7}$$

$$u_g^t - u_g^{t-1} \leq u_g^{\tau_g^1} \qquad \forall\ g \in \mathcal{G};\ \ t \in \{2, \ldots, T-1\};\ \ \tau_g^1 \in \{t+1, \ldots, \min\{t + \Lambda_g - 1, T\}\} \tag{3.2.8}$$

$$u_g^{t-1} - u_g^t \leq 1 - u_g^{\tau_g^0} \quad \forall\ g \in \mathcal{G};\ \ t \in \{2, \ldots, T-1\};\ \ \tau_g^0 \in \{t+1, \ldots, \min\{t + \phi_g - 1, T\}\} \tag{3.2.9}$$

where we used the following constants:

- $P_g^{\min}$ is the lower limit of active power generation of unit g at time t, in MW (can be zero),
- $P_g^{\max}$ is the upper limit of active power generation of unit g at time t, in MW,
- $\mathcal{G}_v$ is the set of generators connected to node v,
- P_{Dv}^t is the power demand of node v at time t, in MW,
- B_{vw} is the susceptance of transmission line (v, w) in S,
- $L_{vw}^{\max}$ is the thermal limit of transmission line from bus v to w, in MW,
- $\mathcal{M}$ is the set of nodes, and $\mathcal{G}_v \subseteq \mathcal{G}$ is the set of generators connected to node $v \in \mathcal{M}$,
- $R_g^{\max}$ is the available offer of primary frequency response of unit g, in MW,
- $\Delta_g^{\max}$ is the physical capacity of primary frequency response of unit g, in MW,

- $\delta_g^{\max}$ upward physical limit of ramping capacity of unit g, in MW/h,
- $\delta_g^{\min}$ downward physical limit of ramping capacity of unit g, in MW/h,
- Λ_g is the minimum time the unit must be online after being connected to the system,
- ϕ_g is the minimum time the unit must be offline after being disconnected from the system,

The nonlinear functions S_g, F_g, and δ_g can be transformed into linear form with additional constraints and variables as below. As such, in its MILP linearised form, eq. (3.2.1) becomes:

$$\min_{\Phi'} \sum_{t\in\mathcal{T}}\sum_{g\in\mathcal{G}} \left(C_g^{S+}S_{gt}^{+} + C_g^{S-}S_{gt}^{-} + f_g^t + C_g^0 u_g^t + C_g^{+}R_g^t + C_g^{\delta+}\delta_{gt}^{+} + C_g^{\delta-}\delta_{gt}^{-}\right) \quad (3.2.10)$$

where $\Phi' \coloneqq (S_{gt}^{+}, S_{gt}^{-}, P_g^t, f_g^t, R_g^t, u_g^t, \delta_{gt}^{+}, \delta_{gt}^{-}, \theta_v^t)_{g\in\mathcal{G}, t\in\mathcal{T}, v\in\mathcal{M}}$. We use the standard transformation to turn a maximum of linear functions into an auxiliary variable and a set of linear inequalities [75, pp. 150-151].

Auxiliary constraints

$$S_{gt}^{+} \geq u_g^t - u_g^{t-1}, \quad (3.2.11)$$

$$S_{gt}^{+} \geq 0, \quad (3.2.12)$$

$$S_{gt}^{-} \geq u_g^{t-1} - u_g^t, \quad (3.2.13)$$

$$S_{gt}^{-} \geq 0, \quad (3.2.14)$$

$$f_g^t \geq a_{gi}P_g^t + b_{gi}, \qquad \forall i \in \{1, \ldots, n_g\} \quad (3.2.15)$$

$$\delta_{gt}^{+} \geq P_g^t - P_g^{t-1}, \quad (3.2.16)$$

$$\delta_{gt}^{+} \geq 0, \quad (3.2.17)$$

$$\delta_{gt}^{-} \geq P_g^{t-1} - P_g^t, \quad (3.2.18)$$

$$\delta_{gt}^{-} \geq 0, \quad (3.2.19)$$

where:

- S_{gt}^{+}, S_{gt}^{-} are the startup and shutdown auxiliary variables for unit g at time t, respectively,

- a_{gi}, b_{gi} denote the power-cost coefficients of generator g,
- f_g^t is the auxiliary cost variable of generator g.
- δ_{gt}^+ is the ramp up auxiliary variable of unit g in time t, in MW,
- δ_{gt}^- is the ramp down auxiliary variable of unit g in time t, in MW.

3.2.2 Inclusion of frequency stability constraints

In this section, we analyse the frequency stability constraints to be included in the UC formulation given in the previous section. In order to ensure a minimum level of inertia in the system that is capable of responding to a frequency excursion, it is necessary to include this constraint in the UC problem. This new constraint must be linear as well as our aim is to solve UC as a linear programme. First, it is necessary to define the role the value plays in an actual power system. If we model the turbine-generator set as a rotating two-mass model, as in eq. (2.2.16), then the ensuing dynamics on the turbine-generator shaft can be defined as shown in eq. (3.2.20):

$$P_a = P_m - P_e \tag{3.2.20}$$

where

- P_m is the mechanical power in MW,
- P_e is the electrical power in MW,
- P_a is the accelerating power in MW.

P_a is the amount of *accelerating* (or *decelerating*) power on the shaft of the turbine-generator set caused by any imbalance between mechanical power of the turbine and electrical power output of the generator defined as a function of the total inertial of the turbine-generator, and the change in frequency (rotor electrical speed). This is defined as a first-order Ordinary Differential Equation (ODE) in eq. (3.2.21):

$$\frac{2H}{f_0}\frac{d\Delta f(t)}{dt} + D\,P_D\,\Delta f(t) = P_m - P_e \tag{3.2.21}$$

where:

- H is the inertia in the system, in MW $\cdot$ s,
- f_0 is the system nominal frequency in Hz, which is 50 Hz in this study,
- P_m is the mechanical response from generators, in MW,
- P_e is the electrical imbalance, in our case unit tripped, in MW
- D is the damping element, in 1%/Hz,
- P_D is the total power demand in the system, in MW.

The damping D indicates the sensitivity of the load to the frequency problem, i.e., load that is susceptible to be disconnected from the grid due to large frequency excursions. This includes loads such as motors, which represent heavily inductive elements. Selecting a damping value of 1% from the total load is an approximation of the actual value of the nonlinear load that can be disconnected in the light of a generator or interconnector outage.

3.2.3 Rate of Change of Frequency constraint

For steady state purposes, we can define that the change in power is a result of a loss of generation in the system. Therefore, eq. (3.2.21) can be represented as:

$$\Delta P_L^{max} = P_a = P_m - P_e \tag{3.2.22}$$

Following National Grid ESO grid code regulations, the maximum Rate of Change of Frequency $RoCoF_{max}$ acceptable in the system is set at 0.5 Hz/s. Notice that from now on, we have dropped the t superscript, considering that these calculations are performed for every time step in the planning horizon.

The available inertia in the system is calculated as in:

$$H = \sum_{g \in \mathcal{G}} H_g P_g^{max} u_g - \Delta P_L^{max} H_L^{max} + P_g^{wind} H_g^{wind} \tag{3.2.23}$$

where:

- H is the total inertia in the system after an outage in MW $\cdot$ s,

- H_g is the inertia per generator g, in MW $\cdot$ s,
- P_g^{max} is the rated power of unit g, in MW,
- ΔP_L^{max} is the maximum lost unit generation, in MW, known in advance in our work, and this is further elaborated in section 3.3,
- H_L^{max} is the maximum lost inertia of ΔP_L^{max}, in MW $\cdot$ s, known in advance in our work, and this is furter elaborated in section 3.3,
- P_g^{wind} is the power output of wind farm generator g,
- H_g^{wind} is the available synthetic inertia of wind farm generator g.

Following any unit outage in the power system, a mismatch between generation and demand arises. This leads to excursions of frequency in the system caused by the imbalance between generation and demand. In the very short term, the response of the governors in the generators is negligible. The first element to alleviate this mismatch is the inertia. Therefore, the maximum RoCoF is proportional to the power lost and inversely proportional to the system inertia. The next step is to substitute eq. (3.2.22) and eq. (3.2.23) in eq. (3.2.21) This minimum level of inertia based on a maximum RoCoF requirement is obtained in:

$$H \geq \left| \frac{\Delta P_L^{max} f_0}{2RoCoF_{max}} \right| \tag{3.2.24}$$

This is now a linear constraint which can be added to the UC problem and the MILP formulation directly.

3.2.4 Frequency Nadir constraint inclusion

From eq. (3.2.21) now P_m can include two elements, such as the total enhanced frequency response in the system R_s^{tot} which is the response from storage units, and the total primary frequency response in the system R_g^{tot} which is the governor's response in the conventional generators. Both values are obtained for each time step of the UC optimisation. The storage units in this work are considered as the Battery Energy Storage systems (BESS), which quoting the IEEE standard, is defined as

"A system which is used to store electric energy by means of electrochemical materials, typically includes batteries, power conversion system, and battery management system". Consequently, taking into account the two responses, eq. (3.2.21) turns into:

$$\frac{2H}{f_0}\frac{d\Delta f(t)}{dt} + DP_D\Delta f(t) = R_S^{tot} + R_G^{tot} - \Delta P_L^{max} \tag{3.2.25}$$

where $\mathcal{S}$ is the set of available storage units to respond after a power imbalance, and $\mathcal{G}$ are the available conventional units. These two values happen in certain time step t each one according to:

$$R_S^{tot} := \begin{cases} \sum_{s\in\mathcal{S}} R_s t/T_s & \text{if } t \le T_s \\ \sum_{s\in\mathcal{S}} R_s & \text{if } t > T_s \end{cases} \tag{3.2.26}$$

$$R_G^{tot} := \begin{cases} \sum_{g\in\mathcal{G}} R_g t/T_g & \text{if } t \le T_g \\ \sum_{g\in\mathcal{G}} R_g & \text{if } t > T_g \end{cases} \tag{3.2.27}$$

where

- R_S^{tot} is the total response from storage units in MW, for each time step
- T_s is the delivery time from storage units in seconds s,
- R_G^{tot} is the total response from conventional units in MW, for each time step
- T_g is the delivery time from units in seconds s.

Assuming that t^* is the time when nadir is reached, this time should range in the interval of $t \in [T_s, T_g)$ without actually reaching the governor time T_g. If the nadir occurs at time T_g this would have already activated the low frequency demand disconnection schemes, since the recovery of the frequency did not start after inertia had arrested the effect of the power imbalance. Hence for Frequency Nadir we have eq. (3.2.28):

$$|\Delta f_{nadir}| = |\Delta f(t = t^*)| \le \Delta f_{max} \tag{3.2.28}$$

Now we identify the different regions of action from $R_s(t)$ and $R_g(t)$. Four sections have been depicted in fig. 3.1 in green and blue colours, the red colour indicates the imbalance of power in the grid, and the action commences at t_0. $R_s(t)$

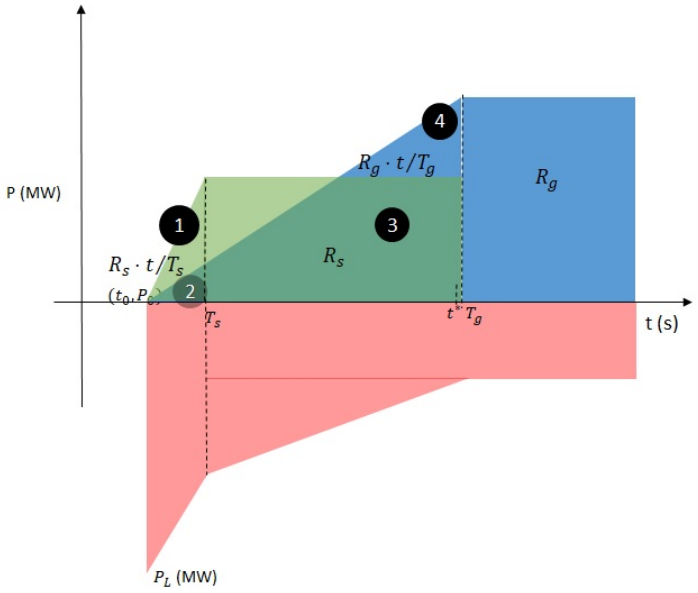

Figure 3.1: Power response vs. Power imbalance

starts to respond until it reaches its full response at T_s. This is done faster than the conventional generators, hence the steepest ramp of section (1). This power changes with time, according to the ratio t/T_s, until it reaches its full output R_s at time T_s.

At the same time t_0, the response from conventional generators starts to be deployed by the governors $R_g(t)$, which is the region (2). The full deployment of the storage and governor responses can be identified by sections (3) and (4), with the governor response taking more time to provide its maximum response. The rest of the frequency will be recovered by the secondary and tertiary frequency responses.

Next in our modelling,at the nadir the system frequency reaches the lowest point after the largest generation or interconnector loss. At time t^*, the RoCoF must be zero, and it is assumed that no further deviation of the frequency happens from this step in time. Also, in a conservative approach and for the sake of simplicity of eq. (3.2.25), we can assume no damping D effect is present. Thus, with these considerations in mind we can integrate eq. (3.2.25) and we have:

$$\Delta f(t^*) = \frac{f_0}{2H}\left[R_G^{tot}\frac{(t^*)^2}{2\,T_g} + R_S^{tot}(t^* - \frac{T_s}{2}) - \Delta P_L^{max} t^*\right] \tag{3.2.29}$$

It is worth noting that certain considerations should be taken into account for eq. (3.2.25). Assuming the system frequency is at the nadir, $\Delta f(t^*)$ should be zero and full power output from the storage units has been reached, therefore the

time when the nadir occurs is:

$$t^* = \frac{T_g}{R_G^{tot}}(\Delta P_L^{max} - R_S^{tot}) \tag{3.2.30}$$

Substituting eq. (3.2.30) in eq. (3.2.29) we have:

$$\Delta f(t^*) = \frac{f_0}{2H}\left[-\frac{T_g}{2R_G^{tot}}(\Delta P_L^{max} - R_S^{tot})^2 - \frac{R_S^{tot}T_s}{2}\right] \tag{3.2.31}$$

Next, substituting eq. (3.2.31) in eq. (3.2.28) we have:

$$\left(\frac{H}{f_0} - \frac{R_S^{tot}T_s}{4\Delta f_{max}}\right) R_G^{tot} \geq \frac{T_g(\Delta P_L^{max} - R_S^{tot})^2}{4\Delta f_{max}} \tag{3.2.32}$$

And this is the case when we consider energy storage. In this chapter however, we only analyse the case with the governor response from conventional generators, even thought the formulation is able to include effects from storage units as well if need be. We can integrate eq. (3.2.25), and if we include the damping effect in eq. (3.2.32) then we have:

$$H R_G^{tot} - \frac{f_0\, T_g (\Delta P_L^{max})^2}{4\,\Delta f_{max}} + \frac{D\, P_D\, T_g\, \Delta P_L^{max}\, f_0}{4} \geq 0 \tag{3.2.33}$$

Equation (3.2.33) is a separable function where every term is constant but the product $H R_G^{tot}$. In section 2.3.3 we show the example of linearisation for a single variable, such as $(\Delta P_L^{max})^2$ assuming that the largest infeed is a variable in the optimisation problem. The specific case of the product of two continuous variables is shown in appendix A.1, which is the case of our test system. The product $H R_G^{tot}$ is suitable to be represented as in the next change of variables:

$$H\alpha R_G^{tot}\beta = x_1^2 - x_2^2 \tag{3.2.34}$$

$$\frac{x_1 + x_2}{\alpha} = H \tag{3.2.35}$$

$$\frac{x_1 - x_2}{\beta} = R_G^{tot} \tag{3.2.36}$$

This is now a separable function that we linearise in the same fashion as the $(\Delta P_L^{max})^2$ value from the example of section 2.3.3. The variables x_1 and x_2 are obtained in their linearised form as in eq. (B.1) and eq. (B.2), from the appendix A.1, respectively. They follow the modelling strategies discussed in section 2.3.3. The factors α and β help by scaling the difference between inertia H and the reserve

R_G^{tot} bounds, assuming that they are in per unit values. This helps to improve the numerical stability of the solution.

The boundaries of the new variables $H(x_1, x_2, \alpha)$ and $R_G^{tot}(x_1, x_2, \beta)$ for the UC optimisation are:

$$H_{min} \leq \frac{x_1 + x_2}{\alpha} \leq H_{max} \tag{3.2.37}$$

$$R_{Gmin} \leq \frac{x_1 - x_2}{\beta} \leq R_{Gmax} \tag{3.2.38}$$

Finally, substituting eq. (3.2.34) in eq. (3.2.33) we have:

$$x_1^2 - x_2^2 \geq f^* \tag{3.2.39}$$

where f^* in eq. (3.2.39) is:

$$f^* = f(f_0, T_g, \Delta P_L^{max}, \Delta f_{max}, \alpha, \beta)$$

Bearing in mind that f^* is in function of the values in eq. (3.2.33) and this is calculated for each time step t. Equation (3.2.24) changes to the following form, using eq. (3.2.35):

$$\frac{x_1 + x_2}{\alpha} \geq \left| \frac{\Delta P_L^{max} f_0}{2RoCoF_{max}} \right| \tag{3.2.40}$$

We analyse the constraint of the steady-state minimum frequency recovery in the subsequent section.

3.2.5 Steady-state minimum frequency recovery

According to eq. (3.2.21), the third constraint depicts the behaviour of the frequency when the strategy aims to recover the frequency to a minimum acceptable value. This minimum acceptable recovery value of frequency is the difference between the nominal frequency and the aimed frequency in post-disturbance state, Δf_{ss}. For this constraint, it is correct to assume that the frequency excursion has been arrested, therefore the RoCoF it is zero. This third and last constraint solely depends on the amount of PFR available from the units, and it is also a linear constraint.

$$\frac{x_1 - x_2}{\beta} \geq \Delta P_L^{max} - D\, P_D\, \Delta f_{ss} \tag{3.2.41}$$

In the next section we show the study case with its respective results.

3.2.6 Literature comparison of Frequency Nadir handling

As mentioned in the introduction of this chapter, recently published papers have approached Frequency Nadir linearisation in novel ways. To compare these works with our current paper, we show in table 3.1 the similarities and differences between these approaches. Our work follows the formulation of the frequency stability constraints of the works shown in the table, but we handle the Frequency Nadir non linearity in a different manner.

Table 3.1: Comparison of works on nadir linearisation

	Works on nadir linearisation		
concept	Badesa et al 2019[90]	Badesa et al 2020[91]	Ferrandon et al 2021
nadir linearisation technique	overestimating planes, binary expansion with big-M method	mixed integer second order cone program (MISOCP)	separable programming and SOS2 conditions
modelled problem	MILP	MISOCP	MILP
test system used	GB 2030 system	GB 2030 system	RTS updated version[60]
synthetic inertia provision	✓	✓	✓
storage response	✓	✓	✓*
scheduling time	Four months	one year	5 working days
load damping	✓	✓	✓
stochastic approach	✓	✓	✗

*Modelled, but not included in this work

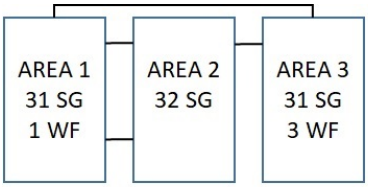

Figure 3.2: Three area RTS[60] schematic diagram

3.3 Case Study

We work with the modified and updated version of the IEEE-RTS-96 power system [60, 85]. Physical capabilities and cost-related information of the power plants are included in updated version of the test system, which consider also the wind farms. In our work, we only consider the fuel costs of the power plants, so in the case of renewable energy generation it is set as zero. We do not consider fixed costs of the power plants for this UC problem, with the only exception of the start up and shut down costs. If the reader is interested in studies that include the fixed costs of renewable energy sources, some of this information can be found in [102]. UK grid code is applicable to this system, as is the case in [89]. We use the three-area version, including 95 synchronous generators and 4 wind farms located at different nodes in the system. The rotational inertia is provided by the synchronous generators and we have considered synthetic inertia by the wind farms. This system depicts how a power system is starting its transition to non-synchronous renewable energy sources, since the majority of the generators are conventional ones. The system is shown in an schematic diagram in fig. 3.2.

Using the IEEE-RTS-96 test system, we simulated a scheduling period of 5 days (120 hours) during the working week, whereas the costs, mean values of aggregated system inertia (H_{agg}), PFR provision, convergence times and total wind energy in the simulation are reported in table 3.3 and table 3.4. We worked with the base case, which has no frequency stability constraints, and four cases with frequency stability constraints but different levels of synthetic inertia provision. We selected the framework of the working-days week because in such scenario demands follows a more consistent pattern than during weekends. A long-term UC problem can deliver a scheduling of one year, as it is the case of [44], but in this study we wanted

to observe the behaviour of a UC with frequency stability constraints for a week, more towards what the control room operators have to work with for purposes of short-scale scheduling in power systems operational planning scenarios [103].

At the moment, we only consider the outage of the largest in-feed in this system, which is the nuclear power plant comprising for 400 MW, following an $N-1$ security criterion. The list of power plants of this test system is shown in Table 3.2. "CT" stands for "combustion turbine", whereas "ST" means "steam turbine". "CC" is combined cycle power plant. In the second column of the table, the acronym "SG" stands for synchronous generators. Although the hydro power plants are synchronous generators as well, the distinction is made to observe the flexibility of inter-temporal ramping and reserve that hydro sources add to the system. Although some of the wind power exceeds the nuclear power of the system, due to the transmission lines thermal limits these power outputs do not exceed the 400 MW. This is part of the UC optimisation results.

Table 3.2: Power plants available in the RTS-96 (updated version[60])

Unit Group	figures acronym	Pmax per gen (MW)	Unit Type	Category	Fuel	number of power plants	inertia per gen (s)
U12	SG	12	Steam	Oil ST	Oil	7	2.8
U20	SG	20	CT	Oil CT	Oil	12	2.8
U50	Hydro	50	Hydro	Hydro	Hydro	19	3.5
U55	SG	55	CT	Gas CT	NG	27	2.8
U76	SG	76	Steam	Coal	Coal	7	3
U155	SG	155	Steam	Coal	Coal	7	3
U350	SG	350	Steam	Coal	Coal	2	5
U355	SG	355	CC	Gas CC	NG	10	7
U400	SG	400	Nuclear	Nuclear	Nuclear	1	5
Sync cond	n/a	0	Sync cond	Sync cond	Sync cond	3	0
Wind farm 1	Wind	713	Wind	Wind	Wind	1	6
Wind farm 2	Wind	847	Wind	Wind	Wind	1	6
Wind farm 3	Wind	122	Wind	Wind	Wind	1	6
Wind farm 4	Wind	799	Wind	Wind	Wind	1	6

We use the next constants for the frequency stability constraints in the UC (they are following National Grid standards):

- nominal frequency (f_0) is 50 Hz,
- Delivery time (T_g) is 10 seconds,
- RoCoF is 0.5 Hz/s,
- Δf_{max} is 0.8 Hz,
- Δf_{ss} is 0.5 Hz.

Two scenarios with their respective sub-scenarios are considered in this work and the costs obtained are the total costs for the five days simulation. No low wind and low demand scenario was considered, since this scenario poses the less risk againts frequency excursions, due to the sufficient provision of inertia in the system.

- High wind - low demand (HWLD),
  - Base case: no frequency stability constraints enforced, and no synthetic inertia provision from wind. The allocation of the PFR for this case is done under the criterion of minimum PFR of the [104], of at least 6% of the total load in the system. In the figures, this case is recognised as " HWLD" and "W/O FC",
  - Frequency stability constrained case, with synthetic inertia provision of $H_{wind} = 6\,s$ per wind farm. In the figures, this case is recognised as "HWLD" and "W/FC",
- High wind - high demand (HWHD),
  - Base case: no frequency stability constraints enforced, and no synthetic inertia provision from wind. At least 6
  - Frequency stability constrained case, with synthetic inertia provision of $H_{wind} = 6\,s$ per wind farm. In the figures, this case is recognised as "HWHD" and "W/FC",

It is the interest of this work to understand how inertia and reserve will be allocated in the UC under frequency stability constraints with the extreme levels of demand, yielding a more robust approach toward security-constrained operations planning in systems with high wind injection. As a consequence, regarding the wind farms' high power injection levels for both levels of demand, we aimed to observe the impact of incorporating such frequency stability constraints in the light of high wind input. In the data from [60] we selected the week working days with the highest wind level. The data is available for a whole year. For both cases of demand, we optimise for two sub-scenarios: one including synthetic inertia provision from wind and one without it. Synthetic inertia has been explained in the earlier part of this work. The simulation is run on a 64-bit Operating System, with an Intel(R) Core(TM) i5-8350U CPU at 1.70 GHz, with 8 GB of RAM.

3.3.1 High wind - low demand

The results for this simulation are shown in table 3.3. We performed a sensitivity analysis for different values of synthetic inertia provision from wind. Even for this case of low demand, where less units are connected to the system, the cost of increasing the units connected and the allocation of PFR increases compared to the unconstrained case.

Table 3.3: Results - HWLD

Case : High wind and low demand					
concept	base case	$H_{wind} = 0\,s$	$H_{wind} = 4\,s$	$H_{wind} = 5\,s$	$H_{wind} = 6\,s$
system cost	£4,955,261.77	£6,553,263.13	£6,551,028.37	£6,550,958.37	£6,545,450.76
reserves cost	£61,255.00	£224,980.00	£229,458.30	£228,648.43	£223,100.00
convergence time (s)	163	176.27	480.00	466.67	192.28
avg H_{agg} [min H_{agg},max H_{agg}] (s)	3.88 [3.51 4.64]	3.4 [3.12 4.31]	4.28 [4.26 4.36]	4.5 [4.37 4.547]	4.71 [4.38 4.83]
avg R_G^{tot} [min R_G^{tot}, maxR_G^{tot}] (MW)	355.98 [233.3 481.09]	1037.43 [1020.1 1055.84]	1035.24 [1016.75 1057.91]	1046.08 [1015.91 1217.71]	1034.55 [1015.07 1058.67]
wind energy (MWh)	177259.83	168090.46	167889.84	167889.77	167888.36

Power profile

This is the power profile in the case without frequency constraints and including frequency constraints. They are shown in fig. 3.3a and fig. 3.3b, respectively. The hydro input adds a higher share of PFR in order to comply with the Frequency Nadir, which is the constraint that has a bigger weight in the simulation. It is important to highlight the RES penetration percentage, which can reach up to 50% in some time steps.

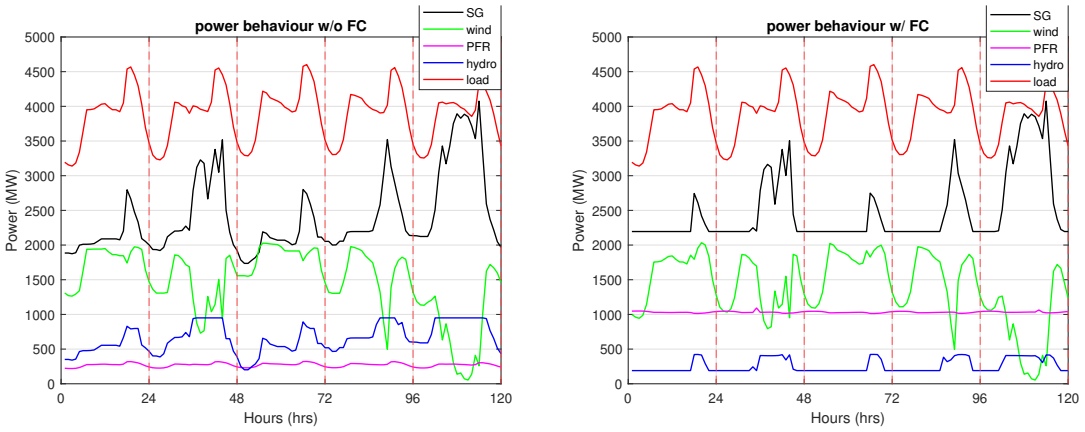

(a) Power profile without freq. constraints - HWLD

(b) Power profile with freq. constraints - HWLD

Figure 3.3: Power profiles - HWLD

RoCoF and inertia

RoCoF behaviour is purely limited by the inertia available in the system. We show the RoCoF and inertia level for both cases: with and without frequency constraint in the optimisation, in fig. 3.4a and fig. 3.4b, respectively.

In this work, the frequency stability constraints are enforced from the beginning of the optimisation. This fully sets a minimum level of inertia from the outset. Even though the limit is to be no greater than 0.5 Hz/s, the actual value of the RoCoF is significantly lower than this value for the constrained case. It should be noted that this grid is characterized by a recent proliferation of renewable generation. This explains the presence of a fair amount of inertia in the system even in the case

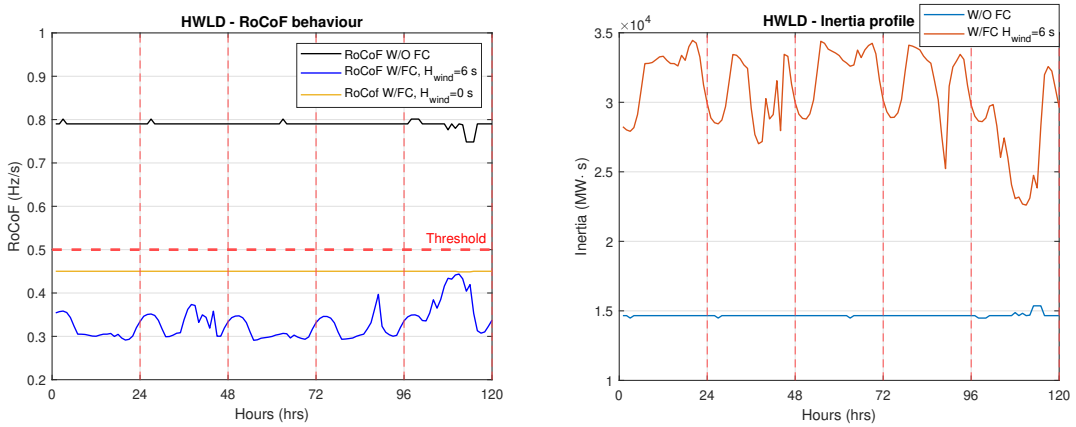

(a) RoCoF - HWLD

(b) Inertia - HWLD

Figure 3.4: RoCoF and inertia behaviour - HWLD

without frequency stability constrains. This will be further elaborated with the Frequency Nadir constraint.

Frequency Nadir constraint and Δf_{max}

Now we observe the Frequency Nadir constraint. The nadir is lowest value that the frequency in the power system can reach when a generation or interconnector outage occurs, shown in the schematic graphical representation in fig. 3.5 as Δf_{min}. For each time step of the simulation, we obtain the theoretical value of Δf_{max}, from the resulting scheduling of the UC via eq. (3.2.33). Such value is shown in fig. 3.6. For example, a value of Δf_{max} of 0.25 Hz would imply, for a 50 Hz system, a Frequency Nadir of 49.75 Hz after a generation or interconnector outage.

The product HR_G^{tot} controls the Frequency Nadir constraint. This product essentially ensures that at the solution the frequency remains within bounds in the light of the largest in-feed from the day ahead perspective. This means that Δf_{max} is no greater than 0.8 Hz if such a contingency occurs.

Next we show the minimum value of frequency recovery. Although this is not a transient stability analysis per se, and these are only the values of the constraints after the optimisation is performed, it is an approximation on how the system frequency should behave. Compared to the case without frequency stability constraints, where a higher frequency drop is present, the case with frequency stability

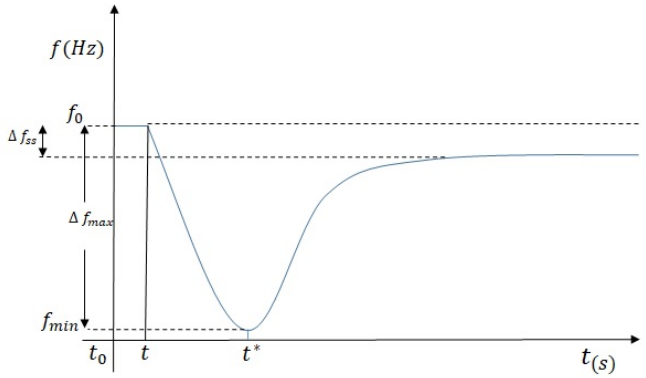

Figure 3.5: Frequency behaviour after a disturbance

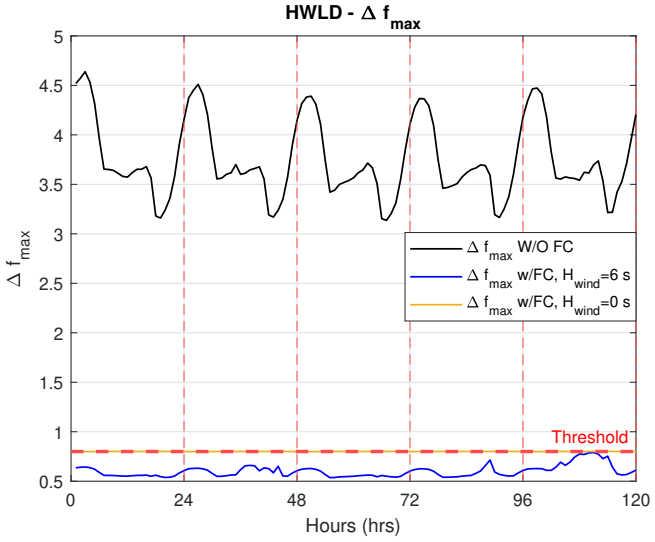

Figure 3.6: Nadir behaviour - HWLD

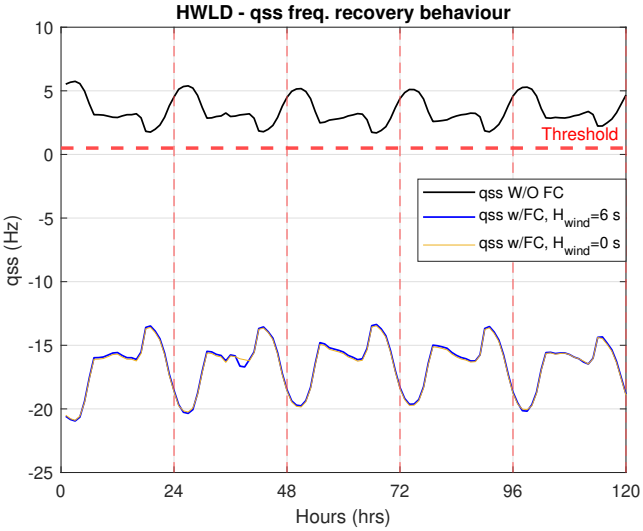

Figure 3.7: QSS behaviour - HWLD

constraints remains under the threshold of the red dotted line of fig. 3.6. The value of the Δf_{max} for the case without frequency stability constraints is shown in fig. 3.6 in the black curve of the graph. Obviously, before reaching these values of Frequency Nadir, the load shedding schemes will be activated, which is an undesirable operational stance and should be avoided.

QSS frequency recovery

The quasi-steady state (QSS) frequency recovery value solely depends on the amount of PFR available in the system. The fig. 3.7 is interpreted as follows: the frequency must recover at least to an acceptable deviation of 0.5 Hz from the nominal frequency of the system in a determined time. We should remember that the values shown in fig. 3.7 do not come from a transient stability study, and they are only the value of Δf_{ss} obtained from the eq. (3.2.41). The negative values of frequency in the graph indicate that there is enough PFR to recover the frequency to acceptable levels in the cases with frequency stability contraints, whereas this would not be the case for the case without frequency stability constraints. In the next subsection we show the case for HWHD.

3.3.2 High wind - high demand

This scenario shows the behaviour of the system with a high demand condition. This condition poses less severity on the $N-1$ contingency against an excursion of frequency, since in order to meet the demand it has to start from a different operational stance (more units connected from the beginning). The costs results are shown in table 3.4.

Table 3.4: Results - HWHD

Case 2 : High wind and high demand					
concept	base case	$H_{wind} = 0\,s$	$H_{wind} = 4\,s$	$H_{wind} = 5\,s$	$H_{wind} = 6\,s$
system cost	£9,129,900.00	£9,752,400.00	£9,753,158.00	£9,715,261.00	£9,717,900.00
reserves cost	£88,661.00	£169,940.00	£170,348.00	£172,862.62	£172,070.00
convergence time (s)	45.07	273.11	254.47	334	351.6
mean H_{agg} [min ,max] (s)	3.88 [3.51 4.64]	5.03 [4.85 5.12]	5.03 [4.86 5.12]	5.05 [4.88 5.14]	5.02 [4.85 5.11]
mean R_G^{tot} [min, max] (MW)	355 [233.3 481.09]	701.12 [676.3 736.37]	701.69 [678.87 734.17]	706.02 [684.87 758.17]	707.243 [672.04 761.07]
wind energy (MWh)	160913.15	158479.40	158850.57	159146.45	167888.36

Power profile - HWHD

The high demand power profiles for the unconstrained and constrained cases are shown in fig. 3.8a and fig. 3.8b, respectively. When contrasting the previous case (low demand) with this current case (high demand), there is a lower value of PFR allocated for the high demand case. Although it might seem counter intuitive at first sight, we must acknowledge that the higher demand forces the solution to connect more units from the beginning of the optimisation, sharing the physical effort (inertia and PFR product) of arresting the Frequency Nadir in a different manner, compared to the low demand case. Furthermore, the hydro input plays a paramount role in the high demand case, responding to the inter-temporal ramping up and down constraints due to its faster responses.

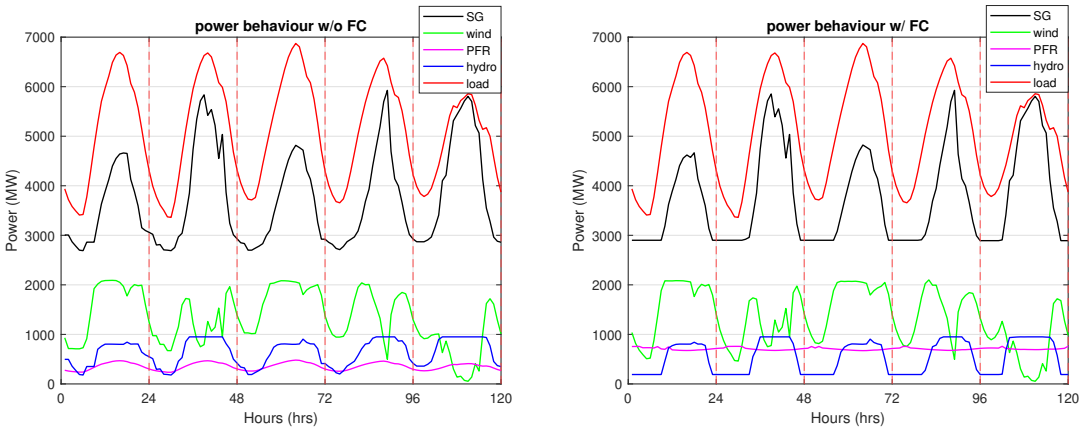

(a) Power profile without freq. constraints - HWHD

(b) Power profile with freq. constraints - HWHD

Figure 3.8: Power profiles - HWHD

RoCoF and Inertia - HWHD

The operational point the system starts under the high demand condition sets a different starting level of inertia in the system, compared to the low demand case. It is important to highlight that for both cases, synthetic inertia becomes a rather important player in the system that fluctuates following the wind behaviour pattern. With its inclusion on inertia provision, RoCoF value is kept in a lower value compared to the unconstrained and no synthetic inertia case. This is shown in fig. 3.9a

and fig. 3.9b.

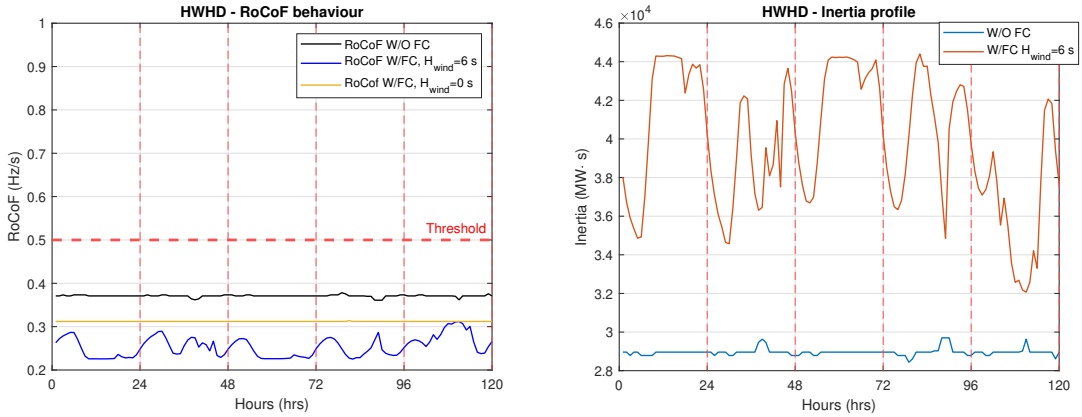

(a) RoCoF - HWHD

(b) Inertia - HWHD

Figure 3.9: RoCoF and inertia behaviour - HWHD

Frequency Nadir - HWHD

The HDHW Frequency Nadir is shown in fig. 3.10. Again, without the share of synthetic inertia the system would be almost right over the constraint value (0.8 Hz). We see this behaviour at the times of low wind in the system, where the gap of the nadir and the constraint is reduced.

QSS frequency recovery - HWHD

In the HWHD case is shown that with lower share of PFR compared to the HWLD case, frequency can be recovered in minimum time previously set. This is shown in fig. 3.11.

3.4 Discussion

3.4.1 Relevance of Frequency Nadir constraint

For both cases (HWLD and HWHD) the determinant constraint is the nadir. This is extremely important, because inertia only attenuates the speed of the frequency excursion, but it is the combination of inertia and PFR the one that arrests the

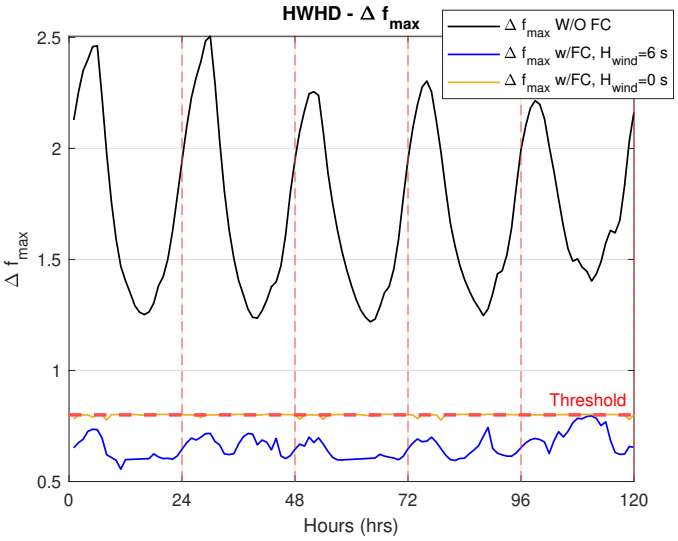

Figure 3.10: nadir behaviour - HWHD

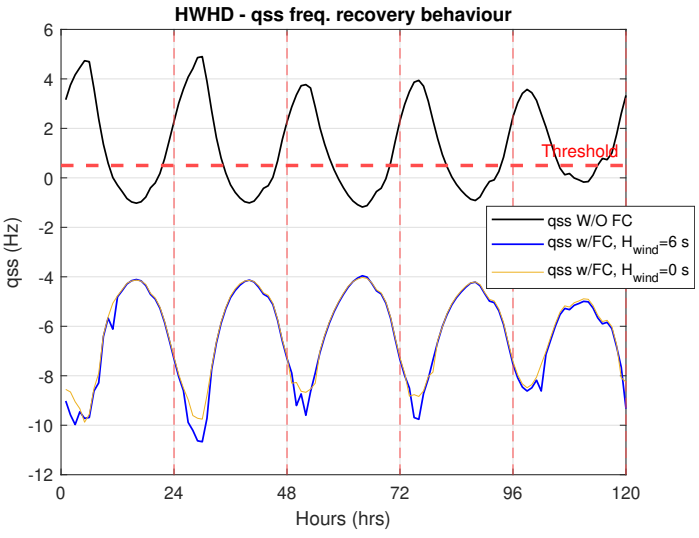

Figure 3.11: QSS behaviour - HWHD

frequency drop (nadir). The combination of both is bounded by the optimisation solution, so a lower value of PFR does not necessarily mean a higher frequency drop, since this low value of PFR should be covered by the available inertia in the system. This interaction between inertia and PFR is shown for HWLD and HWHD in fig. 3.12 and fig. 3.13, respectively.

3.4.2 Role of synthetic inertia in the UC with frequency stability constraints

While looking at the results obtained in table 3.3 and table 3.4 we notice the intrinsic value that the synthetic inertia has over the costs of running this test system. Four cases with frequency stability constraints and different values of synthetic inertia are run, ranging from 0 seconds, then from 3 to 6 seconds of inertia emulation from the wind farms. The highest value of inertia is taken from [89]. We do not intend to define a valuation method of the synthetic inertia for this test system. We do want to discuss how having an inertia emulation response affects the overall costs of the system. For this study, we did not assign any cost to the synthetic inertia. For the HWHD case, the solution indicates that the more synthetic inertia available, the higher input of wind is sought after in the optimisation, since both the variable costs and synthetic inertia from the wind have zero cost. This reduces the overall costs of the system, because it either reduces the use of units that do have non-zero variable costs, PFR costs, or both. For avoiding market distortions, it is necessary to do further studies on the synthetic inertia provision to define when this response becomes a necessity in the system, rather than just an "emulation" of natural inertia from conventional generators. Possibly, this scenario would be when the vast majority of the generation fleet is formed from converter-based resources, which is not the case of this transition-to-low-carbon system.

3.4.3 Linearisation breaking points

In this section we observe the advantages and drawbacks of using less or more linearisation points in the separable programming problem. For the case of HWLD,

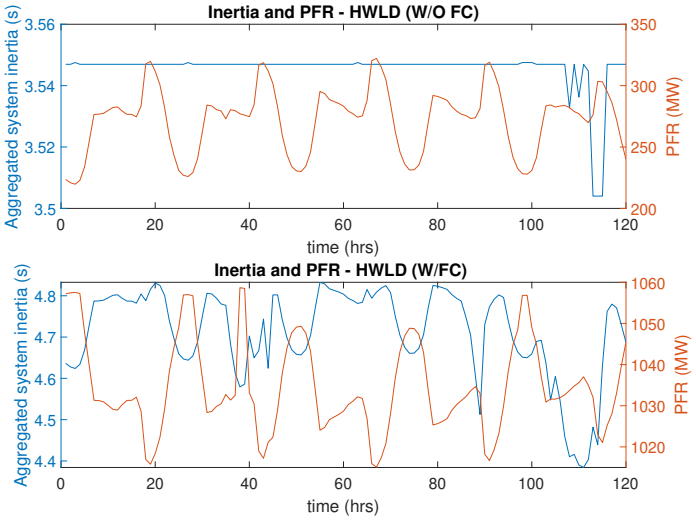

Figure 3.12: H and PFR interaction - HWLD

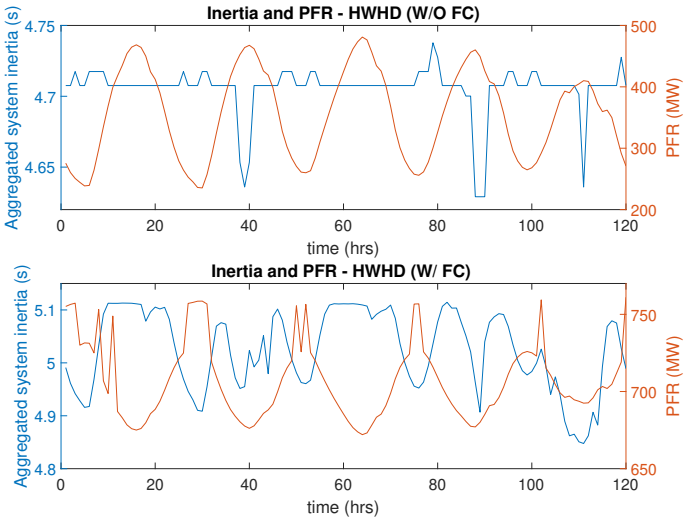

Figure 3.13: H and PFR interaction - HWHD

we show the results from 5, 8, 10, 15, and 20 breaking points in table 3.5. Recalling that the problem is set with a duality gap [65] of at least 2%, the case with 15 breaking points yields the smallest duality gap. Although choosing this approach would increase the convergence time by approximately 26 times the 10 breaking points case. In this scenario of HWLD, choosing a 5 breaking points approach would yield a better final duality gap, although the convergence time becomes an obstacle to use as a solution. We acknowledge that H_{agg} and R_G^{tot} remain very similar, regardless the selection of the number of breaking points. A cost-benefit analysis between the drawbacks and benefits of each thus lead us to choose to work with 10 breaking points for this scenario. In the case of the HWHD scenario, the solution with the lowest final duality gap uses the 10 breaking points scenario as well. For this scenario, the convergence time is quite similar between different breaking points, as well as the H_{agg} and R_G^{tot}. In this scenario, it is plausible to choose the 5 breaking points solution approach. although that would imply to have a higher duality gap. All in all, the number of breaking points for this work was calibrated upfront, depending mostly in two factors: final duality gap reached, and convergence time, and these factors are highly influenced by the scenario under analysis.

Table 3.5: Different number of linearisation breaking points - HWLD

Case : High wind and low demand, $H_{wind} = 6s$					
concept	5 bp	8 bp	10 bp	15 bp	20 bp
system cost	£6,509,749.81	£6,549,671.32	£6,545,450.76	£6,535,630.99	£6,625,835.55
reserves cost	£212,099.27	£223,556.53	£223,100.00	£221,721.38	£222,315.84
convergence time (s)	7501.74	62.47	192.28	5170.19	11481.98
duality gap	0.59%	1.71%	0.86%	0.18%	1.41%
mean H_{agg} [min ,max] (s)	4.711 [4.3768 4.8327]	4.711[4.3761 4.8326]	4.71 [4.38 4.83]	4.712 [4.380 4.832]	4.706 [4.376 4.828]
mean R_G^{tot} [min , max] (MW)	1003.94 [976.03 1221.25]	1033.80 [1014.659 1053.943]	1034.55 [1015.07 1058.67]	1030.55 [1011.96 1221.75]	1032.08 [1014.309 1052.078]
wind energy (MWh)	167905.84	168090.38	167888.36	167888.44	167484.71

Table 3.6: Different number of linearisation breaking points - HWHD

Case : High wind and high demand, $H_{wind} = 6s$					
concept	5 bp	8 bp	10 bp	15 bp	20 bp
system cost	£9,668,606.09	£9,757,420.05	£9,717,900.00	£9,784,849.62	£9,758,753.41
reserves cost	£172,161.55	£174,028.95	£172,070.00	£171,815.34	£171,448.83
convergence time (s)	164.88	428.09	351.60	356.81	340.40
duality gap	1.31%	1.77%	0.59%	2.00%	1.72%
mean H_{agg} [min,max] (s)	5.03 [4.85 5.12]	5.03 [4.86 5.12]	5.02 [4.85 5.11]	5.03 [4.85 5.12]	5.03 [4.85 5.12]
mean R_G^{tot} [min, max] (MW)	706.62 [681.08 766.08]	699.7 [678.2 888.58]	707.24 [672.04 761.07]	706.36 [679.61 735.87]	704.53 [679.61 736.38]
wind energy (MWh)	158867.42	159638.77	159709.75	159013.05	158847.54

3.5 Chapter remarks

In this chapter we looked for a new way to include frequency constraints in the unit commitment optimisation process, with the objective of minimising the system cost. The optimisation solution respects the physical boundaries of the system variables. No time-domain simulation was performed, but the results can provide an starting point for a time-domain simulation. Via separable programming, this new approach approximates the non-linearity of the Frequency Nadir constraint to a linear form. The Frequency Nadir indicates the lowest value the frequency reaches after the largest in-feed.

In contrast, the Rate of Change of Frequency and Quasi-steady state frequency recovery constraints are both linear. The Frequency Nadir constraint involves the product of inertia and primary frequency response variables, and therefore becomes a non-linear constraint that can not be added to the unit commitment formulation in its original form. We tackled the non-linearity of the Frequency Nadir via separable programming. Based on the power system to optimise, there is flexibility in the number of breaking points to use for the approximation of the linearisation. Tuning the number of breaking points and the scaling factors allows us to improve the convergence time of the problem.

At every step, we made sure the system is covered against the loss of the largest in-feed under an $N-1$ security criterion. We included the transmission system constraints through a DC load flow perspective, guaranteeing that the power flows remain below transmission line ratings. Our work has a practical application with power systems where the energy transition to a carbon neutral is at its early stage, and where we need to meet a minimum on-line commitment of units in the system for frequency stability and reliability reasons. This approach, along with the right electricity market framework, could incentivise new ancillary services such as inertia provision and different time windows of primary frequency response. This would help to avoid market distortions, by taking into account the inertia provision from renewable energy sources and the possible primary frequency response that they can deploy. We can expect in low carbon grids that the frequency stability is addressed not only by conventional generators, but from renewable energy sources too.

Chapter 4

Contingency Ranking Via Reliability Rates

This chapter of the thesis closely follows from the conference paper "Contingency Ranking in Power Systems Via Reliability Rates" and it can be consulted in[62]. After getting the results from the UC, as it was covered in chapter 3, each time step of these results can work as a starting point for specific analysis. They can work as initial stage of an OPF problem, a classical load flow studies problem, or even dynamic stability studies. It is also a starting point where the transmission lines loading can be verified, and this can be done through contingency ranking algorithms. This widely used tool in the control room, such as contingency ranking algorithms, is the topic to discuss in this chapter of the thesis.

4.1 Introduction

In any power system, maintaining the security is paramount for the correct functioning of the flexible grid of the future with high levels of RESs and Distributed Generation (DG) integrated, mostly CIG sources. Contingencies or disturbances are events that are always present in any power system in the world. This chapter aims to determine the severity of a contingency in the system, and for that we have implemented and added a contingency ranking algorithm in Matpower[98] in a Matlab™ environment. This computation allows us to rank which contingencies are the most

severe. Using an AC power flow algorithm [50, 51] we get the state variables for each contingency scenario. These output variables are used to get two indices, one that measures the severity and post-contingency thermal limit of transmission lines, and one that assesses the severity of bus voltages violations. All calculations are carried out whilst upholding an N-1 criterion as this is the current level of security upheld by most TSOs such as the National Grid ESO.

We use the updated IEEE Reliability Test System [60, 85] which is essentially a three-area system with renewable energy resources integrated, and updated thermal limits for lines as well as load injections. Using a state sampling approach, we get the state probabilities for each N-1 scenario. Combined with the Performance Index (PI) under each post-contingency state, this results in the actual risk of the system, which combines the severity and probability for such a post-contingency scenario. Using the contingency ranking algorithm weighted by probabilities of each outage scenario (i.e., contingency) will give an analytical tool for ranking contingencies in the order of their risk.

The chapter is organised as follows. Section 4.2 contains the description of the contingency ranking algorithm used in this thesis. Section 4.3 covers the probabilistic approach used in this work and its modelling via risk evaluation. In section 4.4 we show the simulation and results obtained. Finally; in section 4.5 we draw the conclusions.

4.2 Contingency ranking algorithm

In this work, we use an AC load flow algorithm[105, 106] to determine thermal limit violations in a post-contingency scenario. We calculate the PI for each scenario under the N-1 criterion. The most critical scenarios are identified through a scattered plot according to the PI value. Using the reliability data from the IEEE three-area Reliability Test System[60, 85], we obtain the probability of each N-1 branch outage case. Probabilities for each case are calculated with state enumeration [107, 108], and these probabilities are verified using a Monte Carlo simulation[109]. The main purpose of this comparison is that the Monte Carlo simulation allows us to observe

the full behaviour of the system under possible contingencies scenarios. In our case it is restricted to a N-1 case, but other types of reliability criteria could equally be applied depending on the nature of the study. The product of the PI and the probability for each case gives a reliability PI, which includes the probability of the contingency and its severity. At the final part of the simulation, we calculate the conditional expected value of the PI and this is compared to the value obtained from Monte Carlo simulation.

4.2.1 Performance Index: Thermal Violations

We calculate the PI [59, 110, 111] that indicates the severity of a contingency as follows eq. (4.2.1):

$$PI(P_1, P_2, \ldots, P_n) = \sum_{k \in lines} w_k \left(\frac{P_k}{P_k^0} \right)^{\alpha} \tag{4.2.1}$$

where

- k is the line or branch number,
- $w_k \in [0, 1]$ is the weight factor for each line,
- P_k is the active power flowing through the line,
- P_k^0 is the practical operational limit of the branch,
- $\alpha > 1$.

Equation (4.2.1) is calculated for each N-1 condition scenario. The weight factor can be selected by the operational necessities of the TSO, since the topology of the grid is changing throughout the day, whether it is because of scheduled maintenance or fortuitous events in the system. In our case, we run a power flow study under peak load conditions. According the loading conditions obtained in each transmission line, we select the weight factor by calculating how much power the transmission line is carrying compared to the total load in the system.

The use of α helps to avoid the so called masking effect in contingency ranking. This effect leads to wrongly ranking contingencies above ones that should be in

the top of the rank [109]. $\alpha = 2$ was selected in this work, since it discriminated correctly the contingencies, separating the worst from the contingencies that did not pose a real threat in thermal limitations or bus magnitude voltages.

4.2.2 Performance Index: Bus Voltage magnitude violations

Since an AC power flow algorithm is used in this work, nodal voltage magnitudes are part of the state variables. We consider a contingency as any fault that leads to a branch outage, but now the observe the voltage magnitudes in the grid, instead of the thermal limits of the transmission lines. The PI for voltage magnitude analysis [112] yields a measure on the severity when an voltage magnitude violation of security thresholds occurs, either this is because of a branch outage and then this produces a redistribution of load flows as a result, or an outage of generation unit(s) in the system. The PI for voltage magnitude analysis (PI_v) is shown in eq. (4.2.2):

$$PI_v = \sum_{b \in PQ} w_{v_b} \left(\frac{|V_b| - |V_b^0|}{\Delta V_b^0} \right)^{\alpha} \tag{4.2.2}$$

where

- b is the PQ bus number,
- $w_{v_b} \in [0, 1]$ weight factor for each bus,
- V_b voltage magnitude of bus b in post contingency state,
- V_b^0 voltage magnitude of bus b specified in pre contingency state (usually 1 PU),
- ΔV_b^0 voltage deviation tolerance and

And this is calculated for each N-1 scenario. The voltage deviation tolerance can be interpreted as the allowable change in bus voltages magnitudes whilst maintaining the system under security thresholds. This will depend on the operational scenario the system is found, which can be normal, alert, emergency or restorative [113]. Under the convention of using the PU system, a normal state a ±5%PU of bus voltage magnitude is accepted; whilst for an emergency state, the system should

withstand ±10%PU some minutes at such condition. This will also depend on the voltage magnitude level addressed [114].

4.3 Evaluating System Risk

In this thesis, power systems risk evaluation [109] is considered as a steady state problem, where steady state probabilities are calculated. We have used two methods for calculating the probabilities of outages of system components namely, a state enumeration approach and a Monte Carlo simulation approach.

4.3.1 Branch outage transitions

A state-space diagram is built [107], considering the transition between states of the element under study, as is shown in fig. 4.1 where λ is the failure rate and μ is the repair rate.

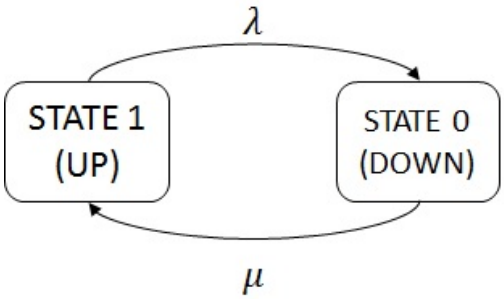

Figure 4.1: State Space Diagram

We can calculate the expected time that the element takes to make the transition from state 1 to state 0, as in eq. (4.3.3). This is known as the mean time to failure (MTTF)

$$E(T) = \frac{1}{\lambda} \tag{4.3.3}$$

Similarly to eq. (4.3.3), we can model the transition of a variable from state 0 (not working), to 1 (fully working), according to eq. (4.3.4):

$$E(T) = \frac{1}{\mu} \tag{4.3.4}$$

And this is the mean time to repair (MTTR). Now we will model the transitioning of states through time in section 4.3.2.

4.3.2 Markov chain and state enumeration

We assume the outage event in each branch can be modelled as a Markov process in which the transition time between a healthy state to a failed state (and vice versa) follows an exponential distribution. We therefore model each branch as a two-state Markov process. Considering that a Markov process [115] can be at a finite or infinite number of states $0, 1, 2, \ldots$ at time t, it is correct to interpret that the status of the process at time t is described by $X(t)$ and equals the state j that the process has at that moment. Assuming that the process is in state i at time t_0, the probability that the process transitions into the state j at time $t_0 + t$ is given by:

$$P_{ij}(t_0, t) = P\{\mathrm{X}(t_0 + t) = j | \mathrm{X}(t_0) = i\} \tag{4.3.5}$$

From (4.3.5) it is seen that the transition probability is independent of the history of the process $\mathrm{X}(t)$ prior to the instant t_0. The transition probability from state i to state j does not depend on the initial moment t_0 but only on the elapsed time between the transitions. Therefore, the eq. (4.3.5) reduces to:

$$P_{ij}(t) = P\{\mathrm{X}(t_0 + t) = j | \mathrm{X}(t_0) = i\} \tag{4.3.6}$$

In the case of the single repairable component shown in fig. 4.1, the steady state probabilities are:

$$\lim_{t\to\infty} P(\mathrm{X}(t) = 1 \mid X(0) = i) = p = \frac{\mu}{\mu + \lambda} \tag{4.3.7}$$

and

$$\lim_{t\to\infty} P(\mathrm{X}(t) = 0 \mid X(0) = i) = q = \frac{\lambda}{\lambda + \mu} \tag{4.3.8}$$

These *steady state* probability expressions are applicable irrespective of whether the system starts in the operating state 1 or in the failed state 0. Consequently we define the vector S to contain all system states when the system is in an N-1 state. That is, $S = 0$ means that all branches are working, and $S = i$, with $i \in \{1, \ldots, N\}$, means that the ith branch is failed, but all other branches are connected.

The probability of $S = i$, for $i \neq 0$, is:

$$P(S = i) = q_i \prod_{\substack{m=1 \\ m\neq i}}^{N} p_m \tag{4.3.9}$$

and when $i = 0$ (no outage):

$$P(S = 0) = \prod_{m=1}^{N} p_m \tag{4.3.10}$$

The value p_m is the steady state probability of each branch that remained connected after a contingency happens, i.e. when they are working. This value p_m comes from the eq. (4.3.7) for each single repairable component, which is a transmission line in this analysis.

The value q_i represents the steady state probability of a branch when it is disconnected from the grid due to a contingency. This value q_i comes from the eq. (4.3.8), and it represents the probability of the branch i to be under a contingency scenario.

Finally, the overall steady state probability of the system to be under a contingency scenario $S = i$ is represented in eq. (4.3.9), whereas the overal steady state probability of the system to be without contingencies ($S = 0$) is obtained via eq. (4.3.10).

4.3.3 Reliability performance indices

After obtaining the state probabilities and the performance indices for N-1 states, the reliability performance indices are calculated. First, the Reliability Performance Index (RPI) of thermal violations for each ith N-1 scenario is calculated as in:

$$RPI_i = P(S_i) \times PI_i \tag{4.3.11}$$

where:

- $P(S_i)$ state probability of ith scenario,
- PI_i performance index for thermal violations of ith scenario.

Secondly, the reliability voltage PI is calculated in similar fashion according to:

$$RPIv_i = P(S_i) \times PIv_i \tag{4.3.12}$$

where:

- $P(S_i)$ state probability of ith scenario,

- PIv_i performance index for thermal violations of ith scenario.

Both indices are encircling the severity of a contingency, but observing different variables in the system. The one in eq. (4.3.11) observes thermal limit violations, whereas eq. (4.3.12) observes bus voltage magnitude limits violations. Both include the probability of the system of being at certain state S_i and this yields a different ranking compared to the ones obtained by eq. (4.2.1) and eq. (4.2.2). Moreover, we obtain the conditional expected value of the PI via the analytical computation, for both indices, as shown in the next subsection.

4.3.4 Performance Index Conditional Expectation: Analytical Computation

The conditional expected value[108] of the PI is calculated according to eq. (4.3.13). This value represents the average value of the PI over the probability of N-1 branches outages scenarios, including the case of no outage, i.e. $i = 0$.

$$E(PI \mid S_0 \cup S_1 \cdots \cup S_N) = \frac{\sum_{i \in S} PI_i \, P(S_i)}{\sum_{i \in S} P(S_i)} \tag{4.3.13}$$

This value is obtained for thermal and bus voltage magnitude violations, respectively. Finally, via Monte Carlo simulation, we obtain the state probabilities in order to compare to the results obtained via the analytical computation.

4.3.5 Monte Carlo simulation

In this section the probabilities for each state are calculated via Monte Carlo simulation [109]. M = 10,000 samples were drawn. $PI_{i(j)}$ is the PI value where $i(j)$ is the N-1 state in the jth sample. The sample mean of the PI is calculated with eq. (4.3.14):

$$\widehat{PI} = \sum_{j=1}^{M} \frac{PI_{i(j)}}{M} \tag{4.3.14}$$

This value, as well as eq. (4.3.13), is obtained for thermal an bus voltage violations, respectively. Lower and upper limits with a 95% level of confidence for the $\widehat{PI}$ are

calculated with:

$$\widehat{PI} \pm 1.96\frac{s}{\sqrt{M}} \tag{4.3.15}$$

The sample standard deviation is calculated according to:

$$s = \sqrt{\frac{\sum_{j=1}^{M}(PI_{i(j)} - \widehat{PI})^2}{M-1}} \tag{4.3.16}$$

In the next section, we present the results for the test system we worked with.

4.4 Simulation and results

We use the test system that was introduced in section 2.5. In this system we only used the normal rates (i.e. thermal limits under normal operation) for each branch included in the data. For determining the value of PI we use the two approaches: analytical and via simulation. The results are shown in the next two subsections.

4.4.1 Performance index for three area system via calculation

In fig. 4.2 the distribution of the PI (PI_i) value is shown. In the fig. 4.3 we show the RPI (RPI_i) distribution.

The conditional expected value obtained using eq. (4.3.13) is:

$$E(PI \mid S_0 \cup S_1 \cdots \cup S_N) = 0.3172$$

And for the voltage PI we have:

$$E(PI \mid S_0 \cup S_1 \cdots \cup S_N) = 0.5860$$

Next, we can understand the figs. 4.2 to 4.5 in this way: the main difference between the classical performance index and the reliability performance index (either if we analyse loading or voltage magnitude violations) relies in that the ranking obtained via the reliability performance index captures the probability of the contingency to happen. By observing specifically the case of thermal limit violations, we can look at the outage probability from branch 84 when it is combined with

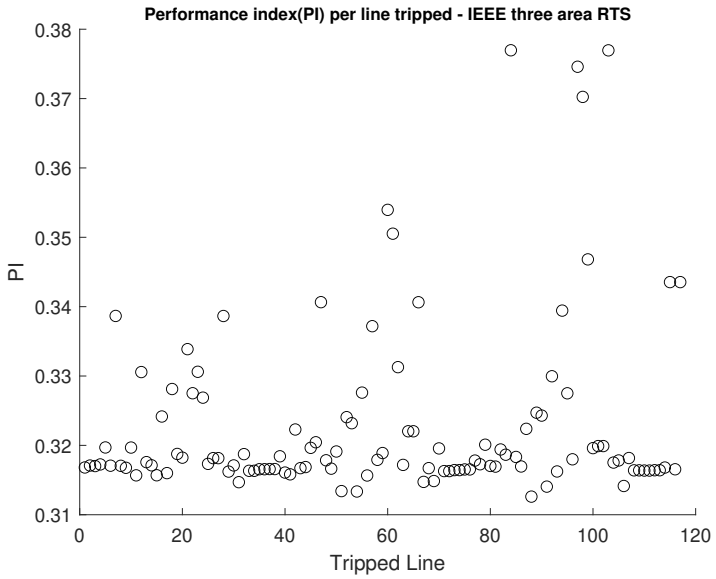

Figure 4.2: Performance index - Three area system

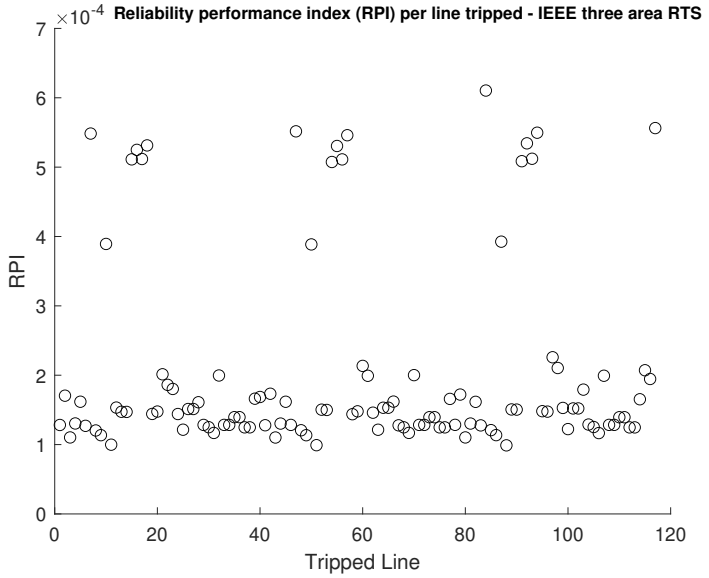

Figure 4.3: Reliability performance index - Three area system

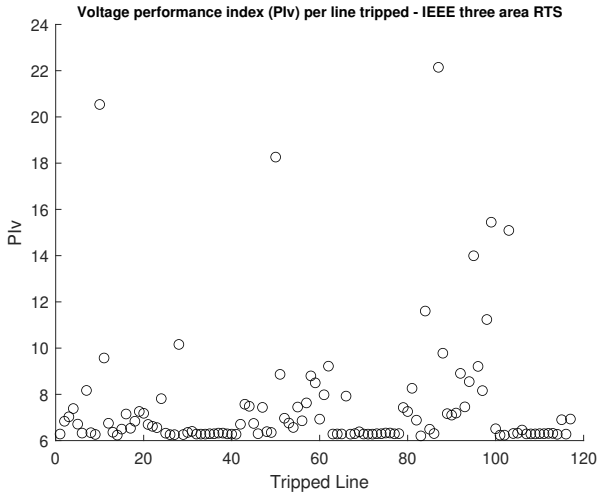

Figure 4.4: Voltage performance index - Three area system

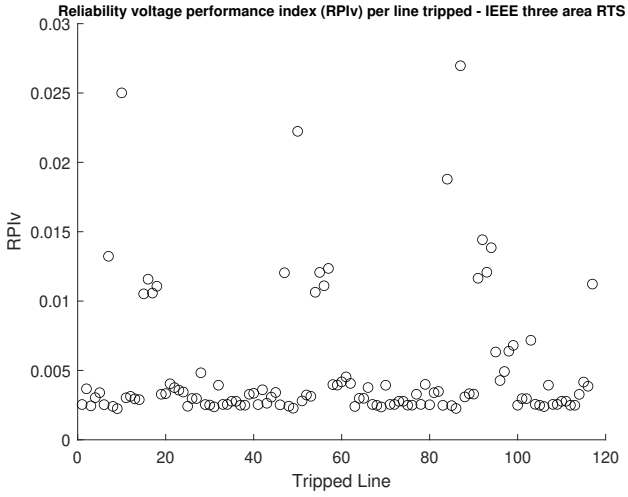

Figure 4.5: Reliability voltage performance index - Three area system

the severity, yielding the highest contingency ranked in the system. Whereas if we follow the classical approach of the performance index, the most critical contingency is when line 103 is out. Also, using the RPI_i ranking we can identify a threshold of contingencies that range in the interval $(0.0005, 0.0006)$, whereas using the PI_i contigency ranking approach, we may overlook contingencies that do not appear in the RPI_i classification. The observations for the bus voltage magnitude violations can be inferred in a similar fashion as the thermal limit violations of transmission lines.

4.4.2 Performance indices for three area system via simulation

In this section, we calculated the probabilities of contingencies using Monte Carlo simulation rather than direct analytical calculations. The advantage of using Monte Carlo simulation is in that we can also derive the distribution of the PI rather than just a point calculation as it is evident in fig. 4.6 (thermal limit index) and fig. 4.7 (voltage magnitude limit index).

- $\widehat{PI} = 0.3173$
- confidence bounds were $[0.3172, 0.3174]$

For the voltage PI we obtained:

- $\widehat{PI_v} = 0.5825$
- confidence bounds were $[0.5726, 0.5924]$

Regarding the type of contingencies, the sample results are shown in table 4.1:

Table 4.1: Types of contingencies

Total samples	**No outage**	**N-1 events**	**N-2 events**	**N-3 events**
10000	9254	713	31	2

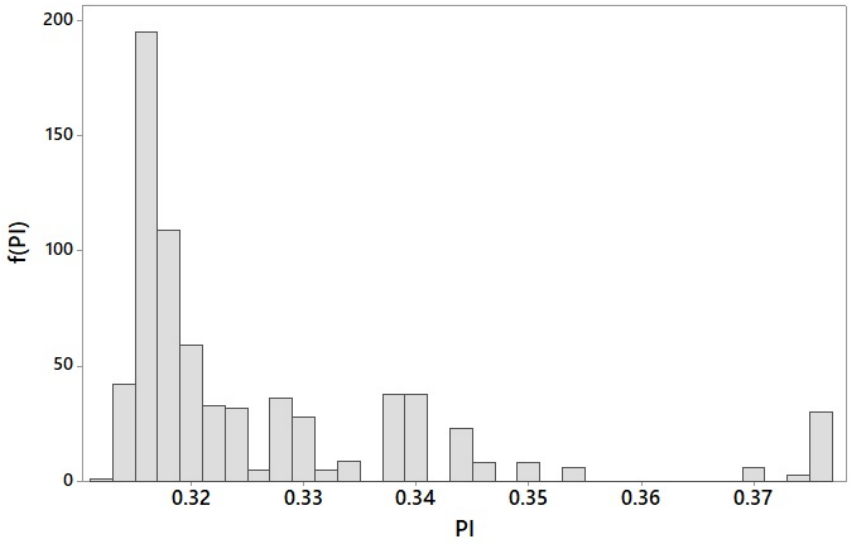

Figure 4.6: Performance index (PI) distribution - IEEE three area RTS [60]

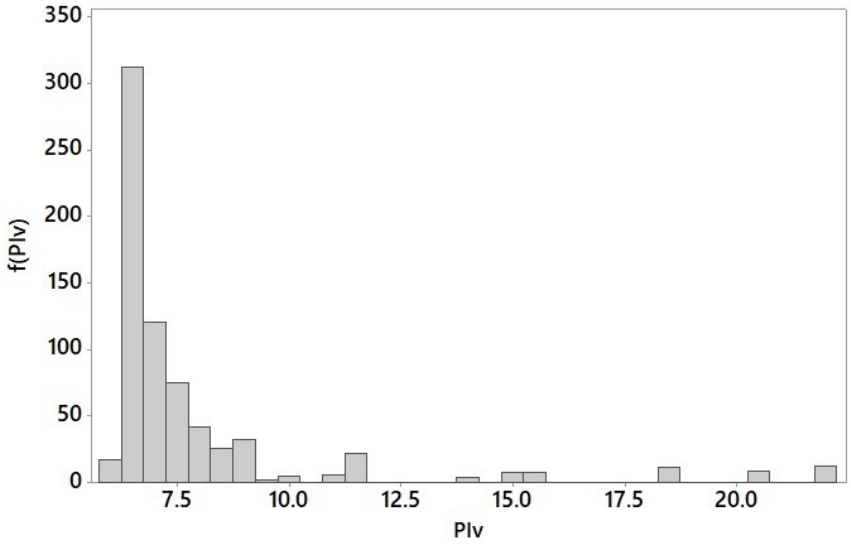

Figure 4.7: Voltage Performance index (PIv) -IEEE three area RTS [60]

The figs. 4.6 and 4.7 indicate that the vast majority of the contingencies simulated occur between the bounds $[0.3172, 0.3174]$ for the thermal limit violations, and between $[0.5726, 0.5924]$ for bus voltage magnitude violations. This is in line with the state probabilities obtained via the reliability rates of the RTS data.

comments on histograms

4.5 Chapter remarks

This potential difference in rankings is important when it comes to analysing the steady state security of the system and therefore a probabilistic approach leads to a more reliable estimation of the system's risk. Depending on the physical quantity to observe in the grid, either transmission lines load flows or voltage magnitudes in buses, we can choose to use the two performance indices discussed in this chapter. Risk evaluation can be added to the contingency ranking analysis as well, through the use of reliability rates. Overlooking a critical scenario in the bulk power system can happen, especially for large-scale systems. Implementing a more careful probabilistic contingency ranking analysis such as the one introduced in this chapter, in real time with a time step of minutes is beneficial to the operator and the whole crew in the control room. More realistic decisions can be made based on the severity of the contingency and also the probability to happen rather than a deterministic approach. We can use this method for other systems as well, since the IEEE RTS system we used in this chapter is essentially a connection of three identical smaller systems.

With the large-scale integration of renewable generation expected in the future, it is necessary to determine new control variables different from transmission line loading and bus voltage magnitude violations. Since the generation fleet is expected to be flexible (synchronising and desynchronising) through the day, inertia is changing with it too. This variable can be looked at if a disturbance happens in the system, following a similar approach as shown in this chapter. Moreover, it is interesting to perform this task via time based simulation, since the constant changing conditions (load and renewable energy injections) of the system will also

change the distribution of both rankings.

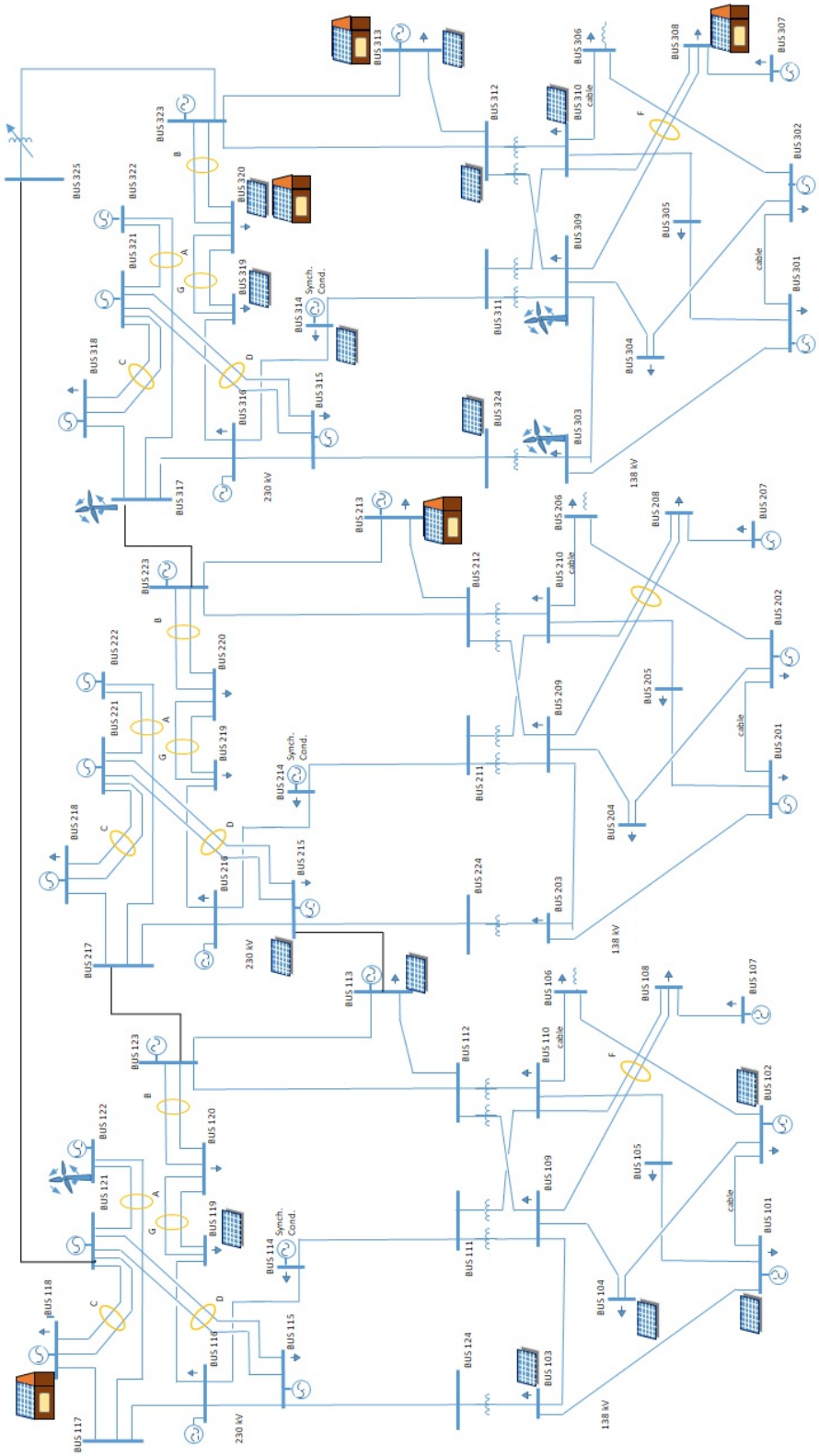

Figure 4.8: Three area 73 bus system

Chapter 5

Two-stage Stochastic Unit Commitment with Frequency Stability Constraints Using Separable Programming

In chapter 3 we covered the modelling of the UC problem in its linear version. The frequency stability constraints were introduced and modelled into the formulation, using a technique called separable programming. So far, we have used a deterministic approach, with only one single trajectory of RESs that is introduced in in the UC input data, and it is assumed to be known, for instance from a forecast based on historic data. In reality, when we are analysing future energy scenarios, ranging from weeks-ahead to months-ahead, we need to incorporate ways to take into account the uncertainty that these RESs add to the UC problem. Therefore, the aim of this chapter is to formulate a stochastic UC optimisation that incorporates the linearised frequency stability constraints via separable programming. It should be noted that parts of this chapter will form a future publication. We will keep using the test system used throughout this thesis namely, the one in [60], and we will expand on using provided historic data on solar and wind resources from this reference.

5.1 Introduction

Previously, we covered the inclusion of frequency stability constraints into a MILP model that solves the UC problem. In chapter 3 we used the wind resource of the RTS, using only the highest input of wind energy, and this scenario selection was done in a deterministic fashion. In order to cover a broad and significant spectrum of wind scenarios in one single UC simulation, we need to investigate and explore techniques that allow us to model the uncertainty in wind. Two-stage stochastic programming [116] is one of the tools that we will be using throughout this chapter of the thesis. The generalised formulation of two-stage stochastic programming was introduced in section 2.4.2. Furthermore, we are not limiting the UC optimisation to just a single type of RES: besides wind, we will be including solar as well. Both of these CIGs sources will be distributed into scenarios as input data for the two-stage stochastic programming.

Before reviewing the history of UC under a stochastic framework, we review the origins of stochastic programming. The first authors to investigate stochastic programming problems are Beale and Dantzig, in 1955 [83]. Later, Bale revisited his own work in [117], giving the following definition on stochastic programming: "Stochastic Programming, is the Art and Science of deciding on the best plan of action (in some expected-value sense) while hedging against the myriad of possible ways the best laid plans can go awry" Basically, stochastic programming belongs to the general field of planning under uncertainty. Since then, stochastic programming has been applied in different fields, ranging from finance, agriculture, generation scheduling (this thesis work), to name a few.

Regarding the UC problem, authors of [118] present a stochastic approach for a so called multi-stage stochastic unit commitment (MSSUC) where the different scenarios of load and availability of grid elements are uncertain, and this information is not given all at once, but it is becoming a known information as the problem is moving in time. This uncertainty is introduced in the form of *scenario trees*. The schematic representation of this scenario tree is shown in fig. 5.1:

Following up with the MSSUC modelling, Strbac and his team have further explored the use of this technique in recent years for the UC optimisation problem

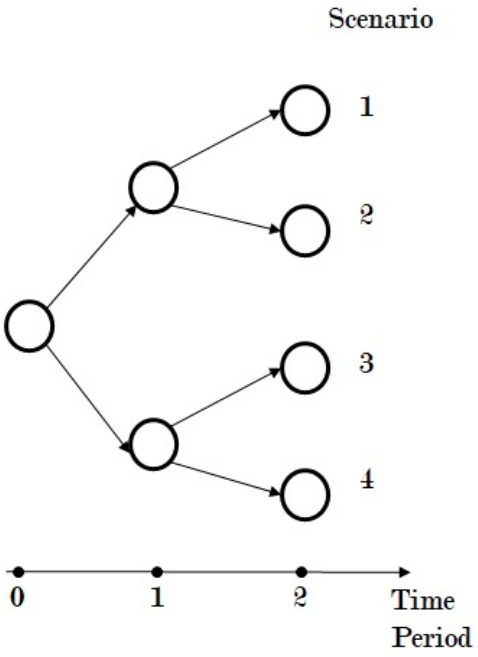

Figure 5.1: Scenario trees

[37, 45, 90, 91, 119, 120]. Meanwhile, other authors have used MSSUC technique in [121]. It is in the interest of this thesis to investigate how we can add the frequency stability constraints using separable programming into a two-stage stochastic framework; the basics of the formulation of which were described in section 2.4.2. In this thesis we will model the stochastic framework in the UC as a TSSUC, where the decisions on switching on and off the generators are taken in the first stage of the problem, and in the second stage we handle any deviations due to the uncertainty of RESs, such as wind and solar. Previous work where a two-stage stochastic approach is followed for including the uncertainty in the the UC can be found in [47, 95, 122, 123] and a review on both methods: multi-stage and two-stage, amongst others, can be found in [124]. However, none of these approaches include separable programming in their formulation for incorporating linearised constraints. Using separable programming into a MILP takes advantage of the already existing modelling with binary variables, and optimises the objective function as a single MILP problem. The expansion of the formulation of the deterministic UC, presented in chapter 3 is included here in this chapter.

Before reviewing the modified UC within a stochastic framework, we need to

further elaborate on the inclusion of the uncertainty in the problem. This is discussed in the next section.

5.2 Uncertainty handling and Scenario Generation

In this section of the chapter we will explain how to include the uncertainty of RESs into the UC formulation. We will continue working with the test system used in section 3.3, but we will be using the historical data that is provided in [85] and updated in [60] to model the uncertainty of these RESs, namely the wind and solar inputs. The available data is from one year of observations, on an hourly basis. These observations are given in the form of power output, distributed at specific nodes of the test system. The weather conditions are not included in the available data, although the authors of the updated test system have considered to include them in the future. Thus for our work, it was not possible to use weather data that could serve as estimators, in order to produce a forecast of the power output of the RES generators. This raises the question as to how to capture the extreme cases that happened throughout a year, with the available data.

As a result, we use the method of stratified sampling, as presented in section 2.4 to account for such extreme cases. More specifically, to generate the required scenarios from the input RES data we followed the steps below:

1. Extract the historical data in time-series format, using the hourly-basis format at each node with a solar/wind input based on the data in RTS96 [85].

2. Allocate the available data into weekly-basis groups, identifying the start and end of a week by Monday to Sunday, respectively. This will be done for both solar and wind resources.

3. Select the number of scenarios that will become the "strata" of the stratified sampling. These strata will range from the lowest amount of wind and coincidental solar power production, to the highest one, accumulated in one week's time. The proposed strata for the wind resources will therefore as follows:

- LL (low-low) scenario: $0 \leq \text{LL} \leq 0.2\, P_{Wweek}^{max}$,
- LM (low-medium) scenario: $0.2\, P_{Wweek}^{max} < \text{LM} \leq 0.4\, P_{Wweek}^{max}$,
- MM (medium-medium) scenario: $0.4\, P_{Wweek}^{max} < \text{MM} \leq 0.6\, P_{Wweek}^{max}$,
- MH (medium-high) scenario: $0.6\, P_{Wweek}^{max} < \text{MH} \leq 0.8\, P_{Wweek}^{max}$,
- HH (high-high) scenario: $0.8\, P_{Wweek}^{max} < \text{MH} \leq 1.0\, P_{Wweek}^{max}$,

where P_{Wweek}^{max} represents the maximum accumulated wind production in one week's time. This process will repeat with each wind injection that is present in the test system. In this case, there are 4 large wind inputs in 4 different buses.

4. Group the available weekly data into the previously specified stratums, using the "group_by()" function in Rstudio, and randomly sample one element of the stratums using "sample_n()" in Rstudio as well [125, 126].

In order to maintain the spatio-temporal correlation, the solar resource data will *follow* the randomly selected week of the year of wind input at a reference node n. For example, if the sample selects the week 21 for wind resource at certain node n of the system, in the stratum LM, all the solar input in the system will use the data from week 21 for the stratum LM at every node n that has a solar resource included. The number of strata should follow the practices on representativeness discussed in section 2.4. Each stratum represents a scenario, and it is assigned with a probability π with the following condition:

$$\sum_{\xi \in \Xi} \pi_{\xi} = 1 \tag{5.2.1}$$

and each π_{ξ} is the probability of the corresponding scenario ξ. A criterion to assight this probability can be to acknowledge the proportion of cases in each stratum. Finally, all this information will be sent to be used in MATLAB©, using the extensively modified MOST®, from MATPOWER®to solve the two-stage stochastic UC problem formulated in the next section.

5.3 Two-stage stochastic UC modelling

In this section we present the linear formulation of the UC problem similar to the one covered in chapter 3, albeit suitable for a stochastic MILP. The ensuing formulation therefore converts the deterministic UC into a two-stage stochastic UC (i.e., TSSUC) problem [116]. Meanwhile, we will again incorporate in the TSSUC formulation, the linearised frequency stability constraints presented in chapter 3 using the method of separable programming.

5.3.1 The Objective Function in the two-stage stochastic UC problem

The objective function for the TSSUC problem takes the following form:

$$\min_{\Phi} \sum_{t\in\mathcal{T}}\sum_{g\in\mathcal{G}}(S_g(u_g^t - u_g^{t-1}) + C_g^u u_g^t + \sum_{\xi\in\Xi}[\pi_\xi(F_g(P_{g\xi}^t) + C_g^R R_{g\xi}^t + \dots + \delta_g(P_{g\xi}^t - P_{g\xi}^{t-1}) + \sum_{v\in\mathcal{M}} \text{Voll}_v\, \ell_{v\xi t})]) \tag{5.3.2}$$

where $\Phi \coloneqq (P_{g\xi}^t, R_{g\xi}^t, u_g^t, \theta_{v\xi}^t, \ell_{v\xi t})_{g\in\mathcal{G}, t\in\mathcal{T}, v\in\mathcal{M}, \xi\in\Xi}$, where $P_{g\xi}^0$ and u_g^0 are known.

- $g \in \mathcal{G} \coloneqq \{1, \dots, G\}$, where $\mathcal{G}$ is the set containing all dispatchable generators, and G is the number of generators,
- $\mathcal{M}$ is the set of nodes in the system, where each node is identified by the index v,
- $t \in \mathcal{T} \coloneqq \{1, \dots, T\}$, where $\mathcal{T}$ is the set containing all time steps in the planning horizon, and T is the final time point,
- $\xi \in \Xi \coloneqq \{1, \dots, \mathcal{X}\}$, where Ξ is the set containing the scenarios of the test study and $\mathcal{X}$ is the number of scenarios to include,
- π_ξ is the probability of scenario ξ,
- u_g^t is the unit status (up or down) of unit g at time t, where $u_g^t \in \{0, 1\}$,

- $S_g(u_g^t - u_g^{t-1}) \coloneqq C_g^{S+} \max(u_g^t - u_g^{t-1}, 0) + C_g^{S-} \max(u_g^{t-1} - u_g^t, 0)$ is the start-up and shutdown cost function which has a unit-dependent costs C_g^{S+}, C_g^{S-} per event,

- $F_g(P_{g\xi}^t)$ is the fuel cost function. In our modelling we use a piecewise linear form where $F_g(P) := \max_{i=1}^{n_g} a_{gi}P + b_{gi}$,

- $P_{g\xi}^t$ is the active power generation of unit g at time t for scenario ξ, in MW,

- $\theta_{v\xi}^t$ is the voltage angle of node v at time t of scenario ξ, in radians,

- $C_g^u u_g^t$ is the no-load cost of unit g at time t, that is the cost of a unit that is active ($u_g^t = 1$) but that is not generating ($P_g^t = 0$). A classic example is a synchronous condenser.

- $R_{g\xi}^t$ is the available Primary Frequency Response of unit g at time t of scenario ξ, in MW. C_g^R is the cost associated with the day ahead PFR offered.

- $\delta_g(P_{g\xi}^t - P_{g\xi}^{t-1}) \coloneqq C_g^{\delta+} \max(P_{g\xi}^t - P_{g\xi}^{t-1}, 0) + C_{gt}^{\delta-} \max(P_{g\xi}^{t-1} - P_{g\xi}^t, 0)$ represents the ramp up and down reserve cost functions for each unit g in time t of scenario ξ. Both are dispatch-dependent of $P_{g\xi}^t$,

- Voll_v is the cost of the load shedding, also known as value of lost load, in £/MWh, corresponding to the interruptible load connected at node v,

- $\ell_{v\xi t}$ is the lost load in scenario ξ and node v, at the time point t, in MW.

Physical constraints

$$u_g^t P_g^{\min} \leq P_{g\xi}^t \tag{5.3.3}$$

$$P_{g\xi}^t + R_{g\xi}^t \leq P_{g\xi}^{\max} u_g^t \tag{5.3.4}$$

$$0 \leq R_{g\xi}^t \leq \min(R_g^{\max}, \Delta_g^{\max}), \tag{5.3.5}$$

$$\sum_{g \in \mathcal{G}_v} P_{g\xi}^t - (P_{D\xi v}^t - \ell_{\xi vt}) - \sum_{\substack{w \in \mathcal{M} \\ v \neq w}} B_{vw}(\theta_{v\xi}^t - \theta_{w\xi}^t) = 0, \qquad \forall v \in \mathcal{M} \tag{5.3.6}$$

$$0 \leq \ell_{v\xi t} \leq P_{D\xi v}^t \tag{5.3.7}$$

$$B_{vw}(\theta_{v\xi}^t - \theta_{w\xi}^t) \leq L_{vw}^{\max}, \qquad \forall\ v, w \in \mathcal{M} \tag{5.3.8}$$

$$\delta_g^{\min} \leq P_{g\xi}^t - P_{g\xi}^{t-1} \leq \delta_g^{\max}, \tag{5.3.9}$$

$$u_g^t - u_g^{t-1} \leq u_g^{\tau_g^1} \qquad \forall\ g \in \mathcal{G};\ \ t \in \{2, \ldots, T-1\};\ \ \tau_g^1 \in \{t+1, \ldots, \min\{t + \Lambda_g - 1, T\}\} \tag{5.3.10}$$

$$u_g^{t-1} - u_g^t \leq 1 - u_g^{\tau_g^0} \quad \forall\ g \in \mathcal{G};\ \ t \in \{2, \ldots, T-1\};\ \ \tau_g^0 \in \{t+1, \ldots, \min\{t + \phi_g - 1, T\}\} \tag{5.3.11}$$

where we used the following constants:

- $P_g^{\min}$ is the lower limit of active power generation of unit g at time t, in MW,
- $P_{g\xi}^{\max}$ is the upper limit of active power generation of unit g at time t, in MW. We define that this value can be different for each scenario for any unit, but specifically for wind generation, where this value could be different depending on the wind, and scoped by its maximum output,
- $\mathcal{G}_v$ is the set of synchronous generators connected to node v,
- $P_{D\xi v}^t$ is the power demand of node v at time t, in MW, of scenario ξ,
- B_{vw} is the susceptance of transmission line (v, w) in S,
- $L_{vw}^{\max}$ is the thermal limit of transmission line from bus v to w, in MW,

- $\mathcal{M}$ is the set of nodes, and $\mathcal{G}_v \subseteq \mathcal{G}$ is the set of generators connected to node $v \in \mathcal{M}$,
- $R_g^{\max}$ is the available offer of primary frequency response of unit g, in MW,
- $\Delta_g^{\max}$ is the physical capacity of primary frequency response of unit g, in MW,
- $\delta_g^{\max}$ upward physical limit of ramping capacity of unit g, in MW/h,
- $\delta_g^{\min}$ downward physical limit of ramping capacity of unit g, in MW/h,
- Λ_g is the minimum time the unit must be online after being connected to the system,
- ϕ_g is the minimum time the unit must be offline after being disconnected from the system,

The non-linear functions $S_g,\ F_g(P_{g\xi}^t)\,, R_{g\xi}^t,\ \delta_g$ can be transformed into linear form with additional constraints and variables as follows. In its MILP linearised form, eq. (5.3.2) becomes:

$$\min_{\Phi'} \sum_{\xi\in\Xi}\sum_{t\in\mathcal{T}}\sum_{g\in\mathcal{G}} \big(C_g^{S+}S_{gt}^{+}+C_g^{S-}S_{gt}^{-}+C_g^{(0)}u_g^t+\pi_\xi\big(f_{g\xi}^t+C_g^{+}R_{g\xi}^t+C_g^{\delta+}\delta_{gt\xi}^{+}+C_g^{\delta-}\delta_{gt\xi}^{-}+\text{Voll}\, l_{\xi vt}^{shed}\big)\big) \tag{5.3.12}$$

where $\Phi' \coloneqq (S_{gt}^{+}, S_{gt}^{-}, P_{g\xi}^t, f_{g\xi}^t, R_{g\xi}^t, u_g^t, \delta_{gt\xi}^{+}, \delta_{gt\xi}^{-}, \theta_{v\xi}^t, l_{\xi vt}^{shed})_{g\in\mathcal{G},\, t\in\mathcal{T},\, v\in\mathcal{M},\xi\in\Xi}$. We use the standard transformation to turn a maximum of linear functions into an auxiliary variable and a set of linear inequalities [75, pp. 150-151].

Auxiliary constraints

$$S^+_{gt} \geq u^t_g - u^{t-1}_g, \tag{5.3.13}$$

$$S^+_{gt} \geq 0, \tag{5.3.14}$$

$$S^-_{gt} \geq u^{t-1}_g - u^t_g, \tag{5.3.15}$$

$$S^-_{gt} \geq 0, \tag{5.3.16}$$

$$f^t_{g\xi} \geq a_{gi} P^t_{g\xi} + b_{gi}, \qquad \forall i \in \{1, \ldots, n_g\} \tag{5.3.17}$$

$$\delta^+_{gt\xi} \geq P^t_{g\xi} - P^{t-1}_{g\xi}, \tag{5.3.18}$$

$$\delta^+_{gt\xi} \geq 0, \tag{5.3.19}$$

$$\delta^-_{gt\xi} \geq P^{t-1}_{g\xi} - P^t_{g\xi}, \tag{5.3.20}$$

$$\delta^-_{gt\xi} \geq 0, \tag{5.3.21}$$

where:

- S^+_{gt}, S^-_{gt} are the startup and shutdown auxiliary variables for unit g at time t, respectively,
- a_{gi}, b_{gi} denote the power-cost coefficients of generator g,
- $f^t_{g\xi}$ is the auxiliary cost variable of generator g.
- $\delta^+_{gt\xi}$ is the ramp up auxiliary variable of unit g in time t, in MW,
- $\delta^-_{gt\xi}$ is the ramp down auxiliary variable of unit g in time t, in MW.

We can observe that the two-stage stochastic modelling shares a similar modelling as in the deterministic case. Under a two-stage stochastic formulation the first stage of the modelling is identified by the variables that do not share the subscript ξ, which indicate the corresponding scenario. The first stage variables belong to the *here-and-now* decisions, which are the binary operators u^t_g. These variables remain outside the second stage of the optimisation problem, committing *ex-ante* the possible variations from the power dispatch $P^t_{g\xi}$ at each wind and solar injections scenario.

Now we will show the comparison with similar works that take into account a stochastic framework in the UC. We show in table 5.1 the works of [47] and [91] that have been recently developed. It is the work of Paturet et al that has more

common points with the work that is develop in this thesis. The a priori extration bounds of the relevant variables is a process that it is performed upfront before the optimisation begins, based on the possible combinations of scheduling dispatches under an N-1 security criterion. Under this approach, they obtain the limits of the variables that maintain a Frequency Nadir value inside an security critierion of maximum frequency deviation after the largest generation outage in the system. This technique is used in the modified two-area system of 20 generators and 16 wind farms.

The strength of our technique lies in the fact that there is no need extract the bounds of inertia and PFR. The bounds are already included inside the modelling, leaving the linearisation work to the separable programming extra variables $(\lambda_{\xi 1r}, \lambda_{\xi 2r}, y_{\xi 1r}, y_{\xi 1r})$. We add the constraints since the beginning of the simulation and the full three area [60] system.

5.3.2 Separable programming for the TSSUC problem

In this section, we will include the the linearisation of frequency constraints for the TSSUC formulation. The variables $x_{\xi 1}$ and $x_{\xi 2}$ that model H (total inertia) and PFR are included for each scenario ξ. Consequently, $\lambda_{1\xi r}$ and $\lambda_{2\xi r}$ operators will follow a scenario-based modelling as in:

$$x_{\xi 1} = \sum_{r=0}^{R} a_{1r}\lambda_{\xi 1r} \quad \text{and} \quad \phi_{\xi 1}(x_{\xi 1}) = x_{\xi 1}^2 \approx \sum_{r=0}^{R} a_{1r}^2\lambda_{\xi 1r} \quad \text{for} \quad \xi \in \{, 1, 2 \ldots, \mathcal{X}\} \tag{5.3.22}$$

$$x_{\xi 2} = \sum_{r=0}^{R} a_{2r}\lambda_{\xi 2r} \quad \text{and} \quad \phi_{\xi 2}(x_{\xi 2}) = x_{\xi 2}^2 \approx \sum_{r=0}^{R} a_{2r}^2\lambda_{\xi 2r} \quad \text{for} \quad \xi \in \{, 1, 2 \ldots, \mathcal{X}\} \tag{5.3.23}$$

$$a_{1r} \coloneqq \frac{r}{2R}(\alpha H_{\max} + \beta R_{G\max}), \quad \text{for} \quad r \in \{0, 1, \ldots, R\} \tag{5.3.24}$$

$$a_{2r} \coloneqq \frac{r}{2R}(\alpha H_{\max} - \beta R_{G\max}), \quad \text{for} \quad r \in \{0, 1, \ldots, R\} \tag{5.3.25}$$

$$\lambda_{\xi 10} \leq y_{\xi 11}, \quad \lambda_{\xi 1r} \leq y_{\xi 1r} + y_{\xi 1,r+1}, \quad \text{for} \quad r = 1, \ldots, R-1, \quad \lambda_{\xi 1R} \leq y_{\xi 1R} \tag{5.3.26}$$

$$\lambda_{\xi 20} \leq y_{\xi 21}, \quad \lambda_{\xi 2r} \leq y_{\xi 2r} + y_{\xi 2,r+1}, \quad \text{for} \quad r = 1, \ldots, R-1, \quad \lambda_{\xi 2R} \leq y_{\xi 2R} \tag{5.3.27}$$

Table 5.1: Comparison of works on nadir linearisation in a stochastic framework

	Stochastic Unit Commitment approaches comparison		
concept	Paturet et al 2019[47]	Badesa et al 2020[91]	Ferrandon et al 2021
nadir linearisation technique	A priori extraction bounds of relevant variables	mixed integer second order cone program (MISOCP)	separable programming and SOS2 conditions
modelled problem	MILP	MISOCP	MILP
test system used	RTS two-area system	GB 2030 system	RTS three-area updated version [60]
synthetic inertia provision	✓	✓	✓
storage response	✗	✓	✓*
scheduling time	Five working days	one year	5 working days
moment of frequency constraints implementation	At hour 67 of the simulation	From the start of the simulation	From the start of the simulation
load damping	✓	✓	✓
stochastic approach	TSSUC	MSSUC	TSSUC

*Modelled, but not included in this work

$$\sum_{r=0}^{R} \lambda_{\xi 1 r} = 1, \quad \sum_{r=0}^{R} \lambda_{\xi 2 r} = 1, \quad \sum_{r=1}^{R} y_{\xi 1 r} = 1, \quad \sum_{r=1}^{R} y_{\xi 2 r} = 1 \tag{5.3.28}$$

and

$$\lambda_{\xi 1 r} \geq 0, \quad \lambda_{\xi 2 r} \geq 0, \quad y_{\xi 1 r} \in \{0, 1\}, \quad y_{\xi 2 r} \in \{0, 1\},$$
$$\text{for all } r \in \{0, 1, \ldots, R\}, \quad \text{and} \quad \text{for all } \xi \in \{1, 2, \ldots, \mathcal{X}\};$$

where:

- a_{1r} and a_{2r} are the breaking points in point r of the variables $x_{\xi 1}$ and $x_{\xi 2}$, respectively. Each breaking point is a constant which will have a diferent value based on the scenario ξ, according to the lambda operators,
- $\lambda_{\xi 1 r}$ and $\lambda_{\xi 2 r}$ are the weights associated with each transition between breaking points a_{1r} and a_{2r} for breaking point r. Lambda operators could be different for each scenario ξ
- $y_{\xi 1 r}$ and $y_{\xi 2 r}$ are the binary operators that select the affine segment of the linearisation, based on scenario ξ,

and finally, the updated set of variables to optimise in the problem will be:

$$\Phi' := (S^+_{gt}, S^-_{gt}, P^t_{g\xi}, f^t_{g\xi}, R^t_{g\xi}, u^t_g, \delta^+_{gt\xi}, \delta^-_{gt\xi}, \theta^t_{v\xi}, \lambda_{\xi 1 r}, \lambda_{\xi 2 r}, y_{\xi 1 r}, y_{\xi 2 r})_{g \in \mathcal{G}, t \in \mathcal{T}, v \in \mathcal{M}, \xi \in \Xi} \tag{5.3.29}$$

Over a time horizon, the variables $x^t_{\xi 1}$ and $x^t_{\xi 2}$ now are calculated for each time point t and for each scenario ξ. Both represent the calculation of inertia (H^t) and PFR ($R^t_{g\xi}$), which have been modelled in chapter 3. Now we will move on the test system and the results obtained under this two-stage approach.

5.4 Test system and results

As it was mentioned in the beginning of this chapter, we will be working with the RTS model, under the updated version of[60]. In chapter 3 we only used wind as the source of RES. In this chapter we will use wind and solar resources available from

the data. The updated data of the available generators are shown in table 5.2. One year of observations will be used to create the scenarios for theTSSUC, and they will follow the strata structure discussed in section 5.2. The frequency constraints are enforced for the deterministic UC and the TSSUC case. For the deterministic UC problem, we will obtain the average of determined results that are obtained separately, namely total active power generated in the system, aggregated system inertia, et cetera. These number of separate UC schedulings do not necessarily need to be equal to the number of scenarios of the TSSUC, hence the differentiation in terminology that will be used from now on.

Table 5.2: Power plants available in the RTS-96 (updated version [60]) with solar resource

Unit Group	figures acronym	Pmax per gen (MW)	Unit Type	Category	Fuel	number of power plants	inertia per gen (s)
U12	SG	12	Steam	Oil ST	Oil	7	2.8
U20	SG	20	CT	Oil CT	Oil	12	2.8
U50	Hydro	50	Hydro	Hydro	Hydro	19	3.5
U55	SG	55	CT	Gas CT	NG	27	2.8
U76	SG	76	Steam	Coal	Coal	7	3
U155	SG	155	Steam	Coal	Coal	7	3
U350	SG	350	Steam	Coal	Coal	2	5
U355	SG	355	CC	Gas CC	NG	10	7
U400	SG	400	Nuclear	Nuclear	Nuclear	1	5
Sync cond	n/a	0	Sync cond	Sync cond	Sync cond	3	0
Wind farm 1	Wind	713	Wind	Wind	Wind	1	6
Wind farm 2	Wind	847	Wind	Wind	Wind	1	6
Wind farm 3	Wind	122	Wind	Wind	Wind	1	6
Wind farm 4	Wind	799	Wind	Wind	Wind	1	6
Solar	Solar	25.3-188.2	Solar	Solar	Solar	25	0

Furthermore, for both of the deterministic UC and the TSSUC, we will only analyse the case where we have $H_{wind} = 6\ s$ of synthetic inertia provision from wind farms, since the cases with lower levels of synthetic inertia provision have been already covered in the deterministic case of chapter 3. These 6 seconds of virtual inertia emulation coming from the large wind farms are assumed to be provided even in low wind output conditions by the converter, but there will be no virtual inertia provision if the wind output is zero, which could be the case for the lowest value of wind of the deterministicUC, or the LL stratum of the TSSUC.

In this section we compare the results of 5 deterministic cases, each one representing a different scenario, against a one single run of TSSUC that accounts for the whole 5 scenarios. These 5 deterministic cases represent the scenarios of the strata that where described in section 5.2.

5.4.1 Active power results, deterministic vs. TSSUC

We will start by comparing the active power between the average of the 5 deterministic cases, and the expected value of the power from the generators in the TSSUC case, which is calculated as eq. (5.4.30).

$$avg\ (P_G^t) = \frac{1}{\mathcal{J}} \sum_{j \in \mathcal{J}} (P_g^t)_j \ \text{ for all } t \in \{1, 2, \ldots, T\} \tag{5.4.30}$$

where:

- $\mathcal{J}$ is the set of deterministic UC that are run separately, and $j \in \mathcal{J} := \{1, \ldots, J\}$, where J is the number of deterministic cases run in the problem,

The expected value of the total generation P_G is calculated as in eq. (5.4.31).

$$\mathbf{E}(P_g^t) = \sum_{\xi \in \Xi} \pi_\xi P_{g\xi}^t \ \text{ for all } t \in \{1, 2, \ldots, T\} \tag{5.4.31}$$

As shown in fig. 5.2a, the active power injection of wind power remains in a higher level compared to the stochastic case of fig. 5.2b.Although it may initially seem that more wind power is scheduled in the average of the deterministic cases, this approach overestimates the availability of wind when we compare it to the

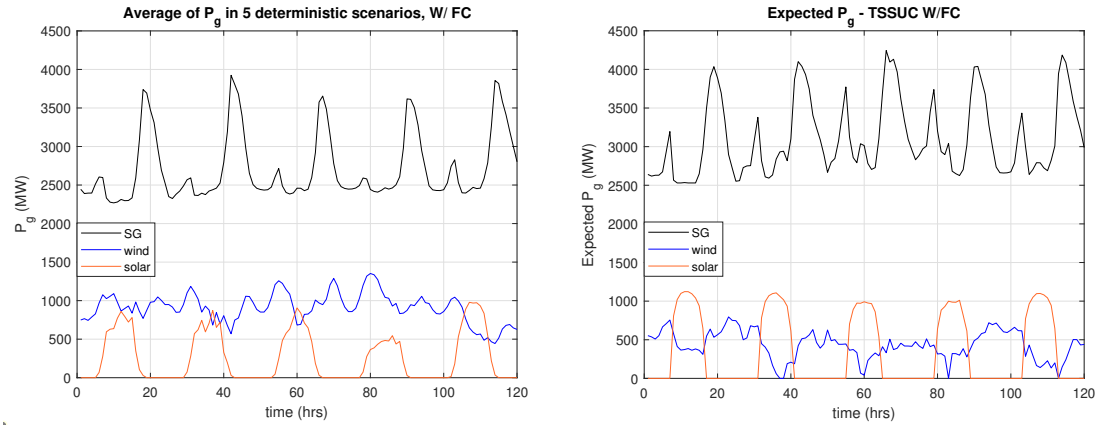

(a) Avg P_g, deterministic cases

(b) Expected P_g, TSSUC

Figure 5.2: Expected P_g, deterministic vs. TSSUC

TSSUC case. Also, more active power from solar resources can be accommodated in the system in the stochastic case.

5.4.2 Inertia, deterministic vs. TSSUC

Following on from the previous section, in here we will observe the allocation of inertia for both of deterministic and stochastic cases. The expected inertia of the stochastic case in fig. 5.3b has more pronounced fluctuations throughout the simulation, if compared with fig. 5.3a. Let us remember we have not assigned an economic value to the inertia provision of this work, as it was seen in chapter 3, hence the solver tends to use the zero-cost of synthetic inertia with a higher priority in the stochastic case. Let us also remember that the Frequency Nadir depends on the amount of inertia and PFR allocated in the system, therefore the product of both limits the frequency drop, hence the observed fluctuations of inertia in the grid in the stochastic case.

We obtain the inertia values as

$$avg\ (H)^t = \frac{1}{J}\sum_{j\in\mathcal{J}}(H)^t_j \ \text{ for all } t \in \{1,2,\ldots,T\} \tag{5.4.32}$$

$$\mathbf{E}(H^t) = \sum_{\xi\in\Xi}\pi_\xi H^t_\xi \ \text{ for all } t \in \{1,2,\ldots,T\} \tag{5.4.33}$$

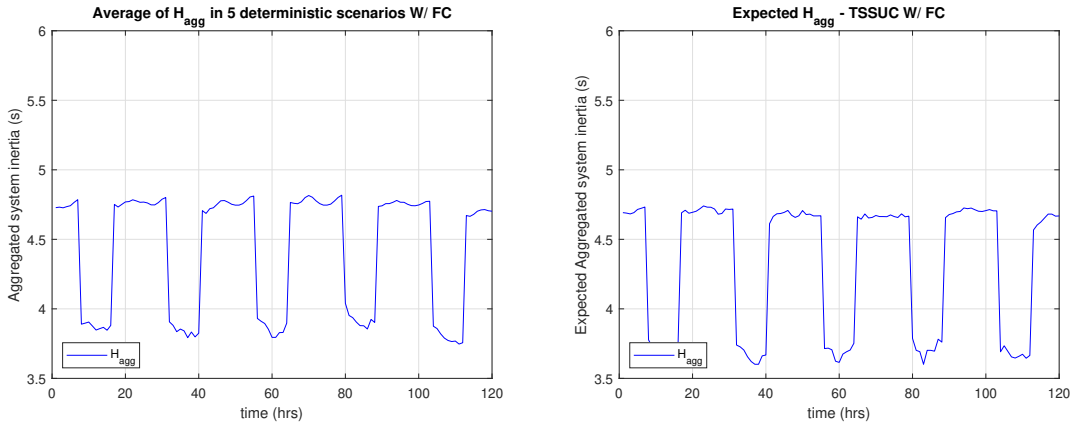

(a) Avg H_{agg}, deterministic cases (b) Expected H_{agg}, TSSUC

Figure 5.3: H_{avg}, deterministic vs. TSSUC

And the inertia considering an N-1 condition in the grid, and considering different wind power inputs, is calculated as in eq. (5.4.34). We assume this calculation is performed at each time step t, and we will omit the superscript.

$$H_{\xi} = \sum_{g \in \mathcal{G}} H_{g\xi} P_{g\xi}^{max} u_g - \Delta P_L^{max} H_L^{max} \tag{5.4.34}$$

We will now review the PFR to assess its impact on the average of the deterministic case and the fully stochastic case.

5.4.3 PFR, deterministic vs. TSSUC

Next, regarding on the amount of total PFR that is allocated at each time point for each of the two cases, we have the results on fig. 5.4. The level of PFR remains relatively flat for the stochastic case, as seen in fig. 5.4b. Due to the large amount of the average of wind power injection, the system would need a higher share of PFR to cover against the largest in-feed, whereas with the stochastic case, in an expected sense, less PFR is needed to handle a generation N-1 disturbance in the power system. This will be further clarified when we analyse the Frequency Nadir constraint.

We calculate the average PFR as eq. (5.4.35), and the expected value of the the PFR obtained as in eq. (5.4.36).

$$avg\ (R_G^{tot})^t = \frac{1}{J}\sum_{j\in\mathcal{J}}(R_G^{tot})_j^t \ \text{ for all } t \in \{1,2,\ldots,T\} \tag{5.4.35}$$

$$\mathbf{E}(R_G^{tot})^t = \sum_{\xi\in\Xi}\pi_\xi(R_{G\xi}^{tot})^t \ \text{ for all } t \in \{1,2,\ldots,T\} \tag{5.4.36}$$

For each time step, the updated equation that calculates the allocated PFR in the scheduling is modelled as in eq. (5.4.37), therefore we can ommit the superscript t in this case.

$$R_{G\xi}^{tot} = \sum_{g\in\mathcal{G}} R_{g\xi} \ \text{ for all } \xi \in \{1,2,\ldots,\mathcal{X}\} \tag{5.4.37}$$

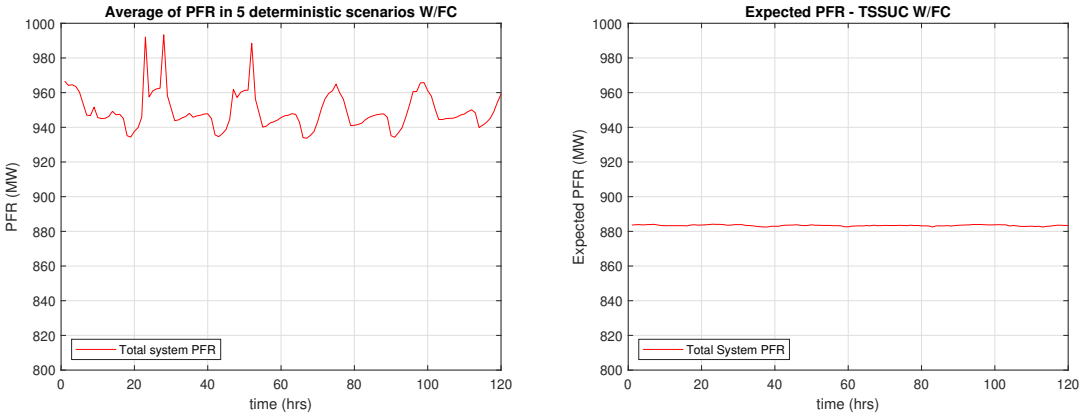

(a) Avg PFR, deterministic cases

(b) Expected PFR, TSSUC

Figure 5.4: Expected PFR, deterministic vs. TSSUC

In the next subsection we will analyse the results of the first frequency stability constraint: the RoCoF.

5.4.4 RoCoF, deterministic vs. TSSUC

In the fig. 5.5 we can see average value of the RoCoF of the 5 deterministic cases paired with the stochastic expected value of the RoCoF. The average and the expected value of the RoCoF are calculated as on:

$$avg\ (RoCoF)^t = \frac{1}{J}\sum_{j\in\mathcal{J}}(RoCoF)_j^t \ \text{ for all } t \in \{1,2,\ldots,T\} \tag{5.4.38}$$

$$\mathbf{E}(RoCoF)^t = \sum_{\xi \in \Xi} \pi_\xi (RoCoF)^t_\xi \text{ for all } t \in \{1, 2, \ldots, T\} \tag{5.4.39}$$

And the equation that shows the dynamics of the RoCoF constraint using the auxiliary variables of separable programming is shown in eq. (5.4.40). Again, this is performed for each time step of the scheduling.

$$\frac{x_{1\xi} + x_{2\xi}}{\alpha} \geq \left| \frac{\Delta P_L^{max} f_0}{2RoCoF_{max}} \right| \tag{5.4.40}$$

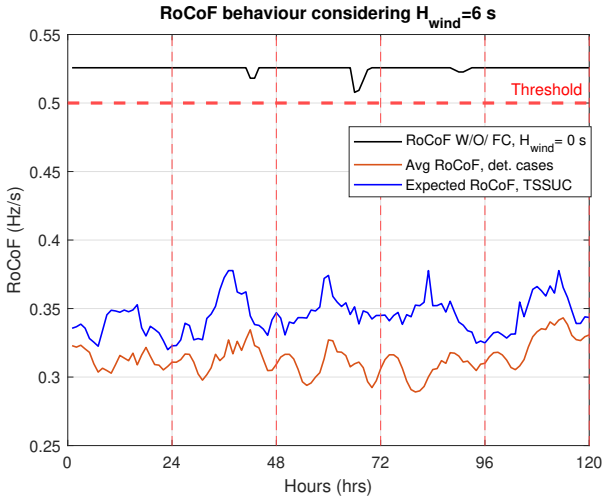

Figure 5.5: RoCoF, deterministic vs. stochastic comparison

It can be seen from the fig. 5.5 that the RoCoF in the average of the deterministic case is located further away from the constraint threshold, whereas the expected RoCoF is closer to the threshold. In the TSSUC case without frequency constraints, the expected value of the RoCoF would be above the threshold against the largest in-feed through the whole scheduling. The solver gives priority to the use of the virtual inertia due to the zero-cost assigned to this provision. This graphic would change when costs are asigned to this response. Now we will observe the Frequency Nadir results under a stochastic approach.

5.4.5 Frequency nadir, deterministic vs TSSUC

For addressing the Frequency Nadir constraint we will be following a similar approach as the one that it was modelled in section 3.3.1, where we will compare the

maximum frequency deviation Δf_{max}, using the average of the deterministic cases, and the expected Δf_{max} of theTSSUC case. As a reminder, the Frequency Nadir is lowest value that the frequency in the power system can reach after the largest in-feed, which was shown in fig. 3.5 as f_{min}, from chapter 3. We are interested in quantifying the maximum deviation from the nominal frequency in the system, which is $\Delta f_{max} = f_0 - f_{min}$. At each time step of the scheduling, we obtain the stochastic expected value of theoretical value of Δf_{max}. This expected value of Δf_{max} is calculated as in eq. (5.4.42) whereas the average value of Δf_{max} of the deterministic cases is obtained with eq. (5.4.41).

$$avg\ (\Delta f_{max})^t = \frac{1}{J}\sum_{j\in\mathcal{J}}(\Delta f_{max})^t_j \text{ for all } t \in \{1, 2, \ldots, T\} \tag{5.4.41}$$

$$\mathbf{E}(\Delta f_{max})^t = \sum_{\xi\in\Xi}\pi_\xi(\Delta f_{max})^t_\xi \text{ for all } t \in \{1, 2, \ldots, T\} \tag{5.4.42}$$

The auxiliary variables x_{ξ_1} and x_{ξ_2} that model the product of inertia and PFR for the Frequency Nadir are calculated according to the proposed modelling of eq. (5.3.22) and eq. (5.3.23). Thus the deterministic modelling of eq. (3.2.33) that dictates the dynamics of the frequency nadir changes for the stochastic case in the form of eq. (5.4.43). We will omit the superscript for the time t, but it is assumed that this applies for all the time points of the scheduling.

$$x^2_{\xi 1} - x^2_{\xi 2} - \frac{f_0\, T_g (\Delta P_L^{max})^2}{4(\Delta f_{max})} + \frac{D\, P_D\, T_g\, \Delta P_L^{max}\, f_0}{4} \geq 0 \tag{5.4.43}$$

The theoretical value of Δf_{max} is shown in fig. 5.6 for both the deterministic UC and the TSSUC schedulings, including the case where no frequency stability constraints are enforced for a TSSUC case, where the theoretical value of Δf_{max} would be above the threshold at all times of the scheduling. It can be seen that for the average Δf_{max} of the deterministic case, the frequency deviation is further away from the threshold. As a similar condition to the RoCoF constraint, on average, there is a larger amount of wind power input in the deterministic case, which considers synthetic inertia provision of $H_{wind} = 6\,\text{s}$, and a larger provision of PFR, as it was seen in the schedulings of both inertia and PFR shown in fig. 5.3a and in

fig. 5.4a, respectively. Let us remember that the dynamics of the Frequency Nadir are controlled by the product of the inertia and PFR. For the expected value of the TSSUC, there are hours of the scheduling that Δf_{max} gets closer to the threshold. These are the moments of expected low wind power input expected in the grid. As an important observation is that the PFR sets a "defence" against the largest in-feed event.

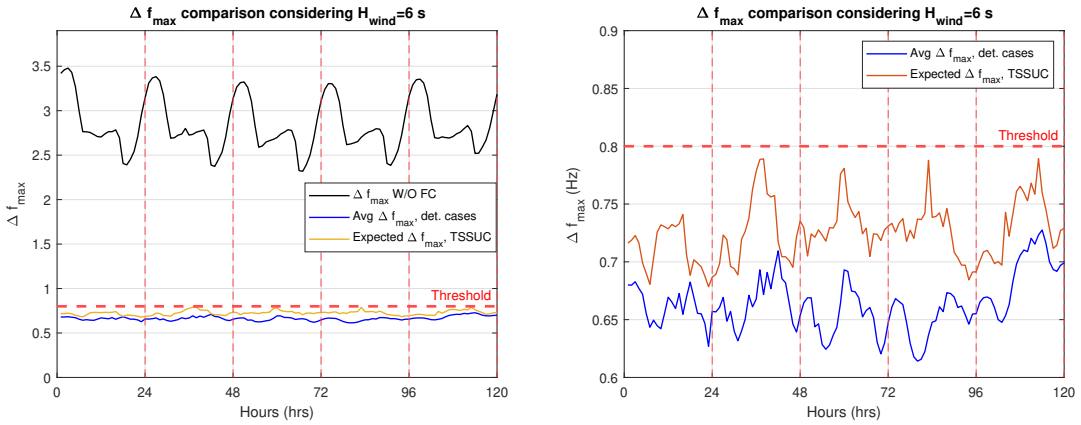

(a) Δf_{max}, W/O FC case included

(b) Δf_{max}, FC cases

Figure 5.6: Frequency Nadir, deterministic vs. stochastic comparison

Now we will consider the minimum frequency recovery in quasi-steady state (QSS) in the next subsection.

5.4.6 QSS, deterministic vs. TSSUC

The last of the frequency constraints, the minimum frequency recovery in quasi-steady state, depends only of the allocated amount of PFR in the system. By recalling on section 3.2.5, we set a minimum value of frequency that theoretically the frequency must reach after the frequency drop has been fully arrested, and the governor responses or storage output that provide PFR have been fully deployed, which is the f_{ss}. In order to define this value, we set a maximum value of frequency deviation in the form of $\Delta f_{ss} = 0.5$ Hz. The average value of Δf_{ss} of the 5 deterministic cases is obtained as in eq. (5.4.44). The expected value of this deviation, as similar with the last two stochastic frequency stability constraints, is obtained as in eq. (5.4.45):

$$avg\ (\Delta f_{ss})^t = \frac{1}{J}\sum_{j\in\mathcal{J}}(\Delta f_{ss})_j^t \ \text{ for all } t \in \{1,2,\ldots,T\} \tag{5.4.44}$$

$$\mathbf{E}(\Delta f_{ss})^t = \sum_{\xi\in\Xi}\pi_\xi(\Delta f_{ss})_\xi^t \ \text{ for all } t \in \{1,2,\ldots,T\} \tag{5.4.45}$$

The dynamics of this constraint are modelled into eq. (5.4.46) with their corresponding auxiliary variables to use the separable programming technique, and assuming this calculation is performed for all the time points of the scheduling.

$$\frac{x_{\xi 1} - x_{\xi 2}}{\beta} \geq \Delta P_L^{max} - D\,P_D\,\Delta f_{ss} \tag{5.4.46}$$

The graphical representation at each time step of the scheduling is shown in fig. 5.7.

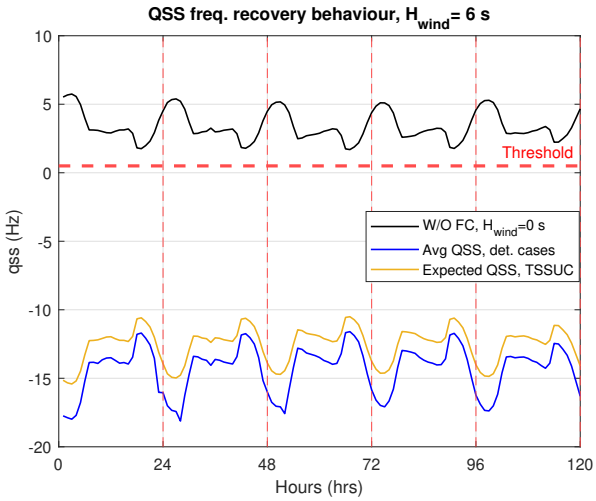

Figure 5.7: QSS, deterministic vs. stochastic comparison

As it can be seen, theoretically the Δf_{ss} threshold would never be violated since there would be enough PFR in the frequency constrained cases, but not in the case without frequency constraints. The inertia does not play a role in the behaviour of this constraint. If we refer to the differences of the PFR scheduling shown in fig. 5.4a and fig. 5.4b, there is a difference of approximately 60 MW between them. This prompts the Δf_{ss} of the average of the deterministic cases to be further away from the threshold, compared to the TSSUC. The theoretical values of Δf_{ss} are only an approximation of the deviation from the nominal frequency. the negative

sign of the value only indicates a recovery of the frequency before the 60 seconds set by the Grid Code recommendations.

5.4.7 Role of solar resource in the scheduling

From the active power scheduling, and specifically the solar power input, we can see that the expected value of the solar resource in the form of active power, is reduced in the TSSUC problem. There are some points to discussed regarding this situation, such as:

- Faster ramping constraints: The gradual increase ofpower output and disconnection from the grid of the solar resource is deemed to be controlled by two factors: the solar resource on the PV panels, and the converter adjustments to accommodate the power injection, gradually. Contrary to a conventional generator that is tied up to physical ramping up and down constraints, there are no moving parts in the PV panels, hence the flexibility and rapidness to adjust for a change of active power. The solver uses this advantage in the solution, by acknowledging this provided flexibility.

- Due to its characteristic zero-cost of the PV resource, there is no penalisations in the form of start up and shut down costs either, hence the flexibility.

- No synthetic inertia provided: For this work, we did not consider a synthetic inertia provision of the solar resources in the problem. Assigning a virtual inertia to this resource would have changed how the solver approaches to utilise this response, in benefit of the first two frequency stabilit constraints.

Now we will discuss on the costs related to the problem in the next subsection.

5.5 The value of information

In this section we are aiming to understand the effect of a concept known as the **value of information**. First, we will compare the costs associated in each one of the deterministic cases where it is included the inclusion of the frequency stability

constraints. This is shown in table 5.3. As it was expected, the higher the share of renewable energy, the less is the cost of the system due to the assumed zero-cost associated to the RESs, but a higher share of PFR is required to handle the the frequency stability constraints. It is worth mentioning that for each one of the cases, we used 10 breaking points if linearisation. The reason to use this number of breaking points stems from the tuning that was previously introduced in section 3.4.3, specifically on the analysis shown in table 3.6. The results of this setting is observed on the convergence time and the duality gap. Further investigation on the deterministic MH case would be required in future works due to the relatively larger convergence time when it is compared with the rest of the cases.

It is also noticeable that the higher the share of average aggregated system inertia H_{agg}, the more the solver is able to use the virtual inertia available to be deployed in the light of the largest generator or interconnector outage. The cost associated with these system could change if we assign a cost to the virtual inertia emulation provision. Let us remember that generally speaking, the conventional generators provide the inertial response to the system with no extra cost associated. Further studies would be required to analyse how this would impact the system costs associated to this response.

Table 5.3: Deterministic cases of UC

Comparison between deterministic cases					
concept	det. LL case	det. LM case	det. MM case	det. MH case	det. HH case
system cost	£8,138,300.00	£7,244,800.00	£6,795,000.00	£6,817,400.00	£6,226,000.00
reserves cost	£251,930.00	£198,910.00	£209,010.00	£189,480.00	£201,030.00
convergence time (s)	207.64	153.00	247.59	1755.20	356.73
duality gap (%)	0.96%	1.39%	0.43%	1.37%	0.22%
mean H_{agg} [min max] (s)	4.3617 [3.7313 4.9507]	4.23 [3.5523 4.8472]	4.58 [3.63 5.02]	4.643 [3.73 4.98]	4.91 [3.80 5.13]
mean R_G^{tot} [min max] (MW)	879.97 [872.36 895.21]	938.86 [921.82 970.10]	959.29 [942.55 984.13]	955.45 [938.04 971.95]	1014.1 [992.7 1213.3]
wind energy (MWh)	22,116	82,862	123,750	140,340	176,140
solar energy (MWh)	48,002	53,338	29,144	19,065	10,536

Next, we will look at the results of the average of these five deterministic cases, against the expected values of the TSSUC approach.

Table 5.4: Comparison table of UC and TSSUC cases

Comparison between the average of det. cases of UC and TSSUC

concept	average of deterministic cases	Expected value, TSSUC
system cost	£7,044,300.00	£8,031,300.00
reserves cost	£210,072.00	£203,490.00
convergence time (s)	544.03	8,378.90
duality gap (%)	0.87%	0.89%
mean H_{agg} [min, max] (s)	4.55 [3.689 4.986]	5.21 [3.60 5.67]
mean R_G^{tot} [min, max] (MW)	949.534 [933.494 1006.938]	883.39 [882.53 884.12]
wind energy (MWh)	109,042	51,299
solar energy (MWh)	32,017	42,028

In table 5.4 we can see the so called value of information. The system cost is higher in the TSSUC case for almost a million pounds. This extra million pounds is the result of the uncertainty handling in the second stage of the TSSUC problem. In a expected value sense, the share of wind and solar resources are lower when they are compared to the average of the deterministic cases, but the TSSUC accounts for the uncertainty of the RESs scenarios. A further explanation of this key finding is mathematically introduced in the next set of equations.

$$\text{one-stage: } \min_{u,r} g(u,r,x) = G_1^*(x) \tag{5.5.47}$$

$$\text{two-stage: } \min_{u} \min_{r:x\to\mathbb{R}} \mathbf{E}[g(u,r(X),X)] = G_2^* \tag{5.5.48}$$

Let us consider the minimisation (it could be maximisation) of the objective function eq. (5.5.47). This modelling represents a single-stage optimisation problem of the equation $g(u,r,x)$, where the terms u and r represent the variables of the problem, and the term x represents the single scenario under analysis. This could represent an analogy with the deterministic and single-stage UC problem, where the variable u represents the start up and shut down events of generators, and r represents the active power dispatch. The single scenario x is understood as an assumed known wind power input from wind generators.

On the other hand, the eq. (5.5.48) represents a two-stage stochastic problem, where we optimise for the first stage using the u variable. Then, the minimisation covers the expected value of the function $g(u,r(X),X)$ where there is a total number of X scenarios, and variable $r(X)$ depends on the $x-th$ scenario under analysis. Again, a similar analology of the UC problem applies here, the difference is that this is done from a stochastic perspective namely the TSSUC problem. Furthermore, The expected value of all the scenarios can the be understood as the weighted sum of the objective function based on its corresponding probabilitiy of scenario x such as:

$$\sum_{x\in X} P(X=x) \min_{r\in R} g(u,r,x) \tag{5.5.49}$$

$$G_2^*(u,x) = \min_{r\in R} g(u,r,x) \tag{5.5.50}$$

$$G_2^*(u,x) \geq G_1^*(x) \tag{5.5.51}$$

The inequality in eq. (5.5.51) can be proven including all the variables u:

$$\sum_{x\in X} P(X=x) G_1^* \leq \sum_{x\in X} P(X=x) G_2^*(u,x) \text{ for all } u = \{1,2,\cdots,U\} \tag{5.5.52}$$

Bearing in mind that the right hand side of the inequality in eq. (5.5.52) still

needs to be optimised for the u variable, we have:

$$\sum_{x \in X} P(X = x) G_1^*(x) \leq \min_u \sum_{x \in X} P(X = x) G_2^*(u, x) \tag{5.5.53}$$

Finally, we will have that the expected value of the two-stage stochastic programming objective function is greater that the average of the single-stage stochastic programming problem, and this is due to the fact that the second stage decisions of the variable r accounts for the variability of the multiple scenarios x. This is shown in eq. (5.5.54)

$$\sum_{x \in X} P(X = x) G_1^*(x) \leq G_2^* \tag{5.5.54}$$

In the further section we will join the reliability and security analysis of the UC.

5.6 Reliability and Security Analysis of UC

Finally in this section of the thesis we will add an schematic representation on how the the works of the UC problem with frequency stability constraints covered initially in chapter 3, and the contingency analysis implemented in chapter 4 are joined together into the whole framework of this thesis. This is shown in fig. 5.8.

A risk analysis with contingency ranking algorithms can be implemented with the UC results. The advantages of proceeding in this way is that we are working with an initial stage of generation that is theoretically secured against the largest in-feed, from the frequency stability constraints perspective. The scheduling results can work as an initial point for studies such as OPF or simple load flow analysis. These generation scheduling points would work to implement dynamic studies as well. Evidently, this is beyond the power systems operations planning problem treated in this thesis.

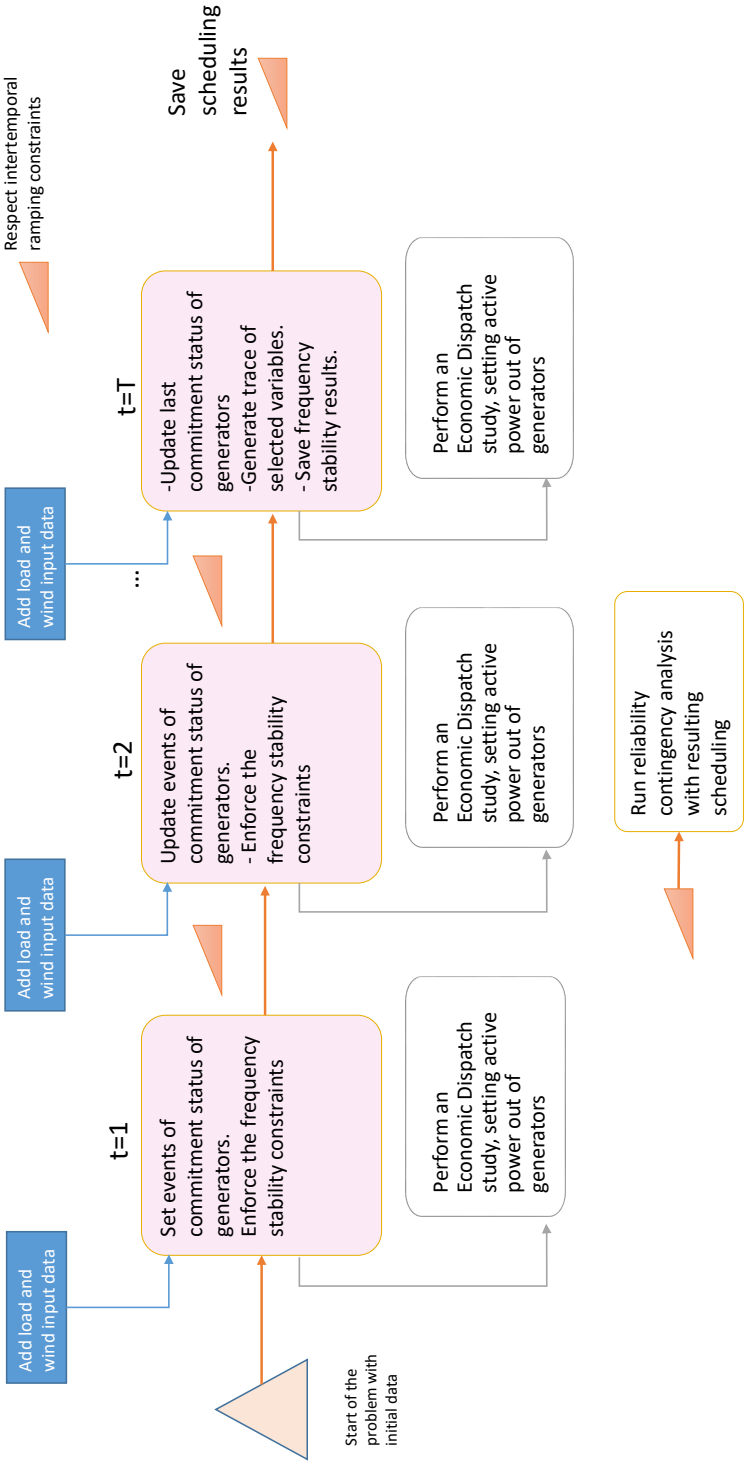

Figure 5.8: Framework of the UC and contingency analysis

5.7 Chapter remarks

In this chapter we were able to add the frequency stability constraints under a stochastic framework, using separable programming for the first time with this problem. The so-called value of information was investigated in this chapter, highlighting the justification to use a stochastic approach when the analysis is run for future energy scenarios, or simply when the uncertainty plays a role into the short-term UC. A stratified sampling technique is used for organising the available time series of data points of the RTS grid, creating the scenarios that would later serve as input data of the TSSUC. Due to the safeguarding against the largest in-feed of this TSSUC, it is fair to acknowledge that this is a secure-stochastic unit commitment problem. The posterior work of including the contingency ranking algorithms with the scheduling results presents another layer of risk and security analysis.

Next, we will elaborate on the conclusions of this thesis work.

Chapter 6

Conclusions and future work

On this final chapter we will review the conclusions of the research that has been carried out and presented in this thesis. We will emphasise on the novelty of the contributions, according to the aims and objectives that were introduced in chapter 1. Moreover, we will use these conclusions to outline potential pathways for future work.

6.1 Key results

We have reviewed the state of the art of one of the most used tools in power systems operations planning namely, the UC problem. This tool allows the entity in charge of generating the day-ahead or week-ahead generation schedules, typically the TSO, to optimally allocate generation capacity based on network's operational constraints. Meanwhile, we have also introduced a method for identifying and filtering network contingencies weighted by their probability of occurrence for a more accurate and risk-informed contingency ranking mechanism which is integral to the problem of UC.

Moreover, to be able to address the challenges of frequency variations in low-rotational inertia systems, in this work, we have opted to include in the UC problem constraints explicitly designed to help operators hedge against the largest loss of in-feed for a more secure operating regime. The addition of the frequency stability constraints into the UC problem which by default does not include such constraints,

means an extra set of constraints that cover the largest generation or interconnector outage. Without this extra set of constraints, low rotational inertia grids are more prone to risks of instability due to frequency excursions and inherently limiting in their hosting capacity of renewable resources which are inherently converter interfaced and normally do not add to the system's inertia. This problem is further exacerbated due to the fact that under a scheme of almost-zero marginal cost from these power inputs, they are scheduled in the UC results for the majority of time. If no restriction of frequency stability is enforced, the system loses the conventional inertia that has been operating naturally in conventional power systems and the loss of the largest in-feed becomes a problem in this case.

With this thesis, the so called frequency stability constraints were modelled and incorporated into the traditional UC formulated as a linear program using a new technique not used before to incorporate linear constraints in this form. In the subsequent sections we will elaborate specifically on how the research challenges were tackled in this thesis.

6.1.1 Research objectives achieved

1. *To determine a secure operating floor of inertia in the power system for the day-ahead planning horizon that includes frequency stability constraints, as well as PFR from the available plants.*

Before working with the UC optimisation problem, certain considerations must be done. The widely used UC is non-linear in its natural form, and solving it using mathematical programming techniques such as mixed-integer linear programming (MILP) we will need to linearise its non-linear constraints first. After this condition has been met, only linear constraints can be added to the UC optimisation problem to solve it using traditional techniques such as MILP.

This thesis includes the addition of the frequency stability constraints one of which is strongly non-linear namely, the Frequency Nadir. It is non-linear since it depends on the product of available inertia and the available PFR in the power system. There has been techniques to add this constraint to the UC problem in

a linearised form, without using the advantages of the actual MILP mathematical programming tool. The contribution of this thesis includes the use of separable programming techniques that tackle this non-linearity by approximating the Frequency Nadir into a linear form, using extra auxiliary variables. Minimum levels of inertia have been established in the problem. This inertia provision is modelled as a natural response from conventional generators, but we have included the synthetic inertia (or virtual inertia) provision from wind CIG sources. It has been shown that using this response from large wind resources helps alleviate the frequency excursions occasioned by a generation and load imbalance. All in all, the strength of the modelling followed in this thesis is that it uses the actual MILP formulation of the UC, and no pre-processing or handling of the constraints are needed.

2. *To quantify a reliability metric index that indicates the severity of a contingency in the power system.*

In the contingency analysis side, the so called RPI has been calculated, for transmission lines thermal limits violations and bus voltage magnitudes violations. This index encapsulates both the severity of a transmission line contingency in the system, and its probability of occurrence. The validity of the probabilistic behaviour was proven using Monte Carlo simulation, validating the use of the reliability rates of transmission lines included in the RTS grid. This index gives a better understanding on the severity of a contingency, accounting as well its probabilistic event. The RPI can be expanded to generation outages using the available reliability data. Thus, this index is of use with the single-hour scheduling results of the UC, adding on a tool that can fast-screen for contingencies in the power system of these results, considering its reliability historic information. The approach can be used into a single-snapshot approximation of a regular load flow study that accounts for the full calculation of the state variables of the problem.

3. *To include the stochasticity of RESs in the day-ahead planning horizon.*

Finally, we acknowledge that if the UC is to be used in future planning scenarios, or simply if there is a need to account for the uncertainty inherent in variability of renewable resources in the problem, a solely deterministic approach might not cover

for the extreme cases of low and high RESs power injections, specifically wind and solar resources. In this thesis we propose the use of historical data to create strata structures that organise a selected number of scenarios of wind and solar resources as the input to be used in the UC problem. After arranging the scenario generation stage, we model the deterministic UC as a two-stage stochastic programming (TSSUC) problem, where in the first stage, also known as the here-and-now phase, we commit the generators that will meet the demand of the UC problem. This is the part where the inertia is tied to the commitment of the generators in the grid.

Next, in the second stage of the problem, also known as wait-and-see phase, we handle the differences between scenarios of RESs, namely wind and solar resources, changing the power generation output of the generators. At each path of the scenario, we look to enforce the physical capabilities of ramping up and down of the generators at all time. Above all these considerations, the separable programming auxiliary variables used in the UC are modelled for each of the scenarios as well, setting different levels of inertia and PFR. The expected value of these two variables is calculated at the end of the simulation, describing their respective trajectories. The results indicate the value of information, when there is uncertainty of the generation scheduling due to the variation between scenarios of RESs namely wind and solar.

The novelty of this work is that a separable programming approach under a stochastic environment have not been implemented before, opening the path for future investigation of this technique applied to non-linearities of the problem. Since with this modelling we are hedging against the largest loss of in-feed in the power system, it is correct to state that this two-stage stochastic unit commitment (TSSUC) approach is a stochastic security-constrained unit commitment (SSCUC) modelling as well.

6.2 Contributions

The main contributions of the thesis will be listed as follows:

1. Separable programming modelling for frequency stability constraints

   Incorporating the frequency stability constraints using separable program-

ming for the first time into the UC problem.

2. Probabilistic and risk-informed contingency ranking algorithms using reliability rates for system components including transmission lines and generators

   Use the available reliability rates in the RTS to propose a Reliability Performance Index (RPI) that captures the severity and the probabilistic behaviour of a contingency in the power system.

3. Inclusion of the frequency stability constraints under the two-stage stochastic unit commitment (TSSUC)

   The frequency stability constraints have been modelled into a TSSUC problem environment using separable programming for the first time, creating an overall SCUC modelling, accounting for the largest loss of in-feed in the power system. The use of stratified sampling is proposed to account for the uncertainty that RESs, namely wind and solar in this thesis, carry into the operations planning analysis.

4. Conference Paper

   A conference paper was submitted, accepted and presented for the IEEE International Conference of Electrical Engineering 2018 for Energy systems in Europe (EEEIC/I&CPS Europe), in Palermo, Italy [62].

5. Journal Paper

   Currently under the last phase of the revision, a paper with the formulation of the deterministic UC with the inclusion of frequency stability constraints using separable programming has been submitted with the assigned Manuscript Number EPSR-D-21-00126R2, to the Electric Power Systems Research journal.

6.3 Future Work

There will be a further research paper based on the works carried out in this thesis. This paper will focus on the stochastic analysis in the UC, namely the TSSUC

formulation and implementation together with the frequency stability constraints. Moreover, the following pathways for future reseearch have been identified whilst carrying out this research. These have been outlined in the next sub-section.

Future Research Topics and Improvements

The list of possible future works that draw from this thesis is listed as follows:

- Investigate the techniques to optimally tuning the number of breaking points used in the linearisation of the Frequency Nadir, improving the convergence time,
- Include other constraints for the transmission grid, specifically the dynamic line rating, due to its non-linearity, into the UC problem,
- Implement the UC problem directly into commercial solvers, such as AIMMS and Gurobi, taking advantage on the recent advances on handling products of two variables in the MILP problem for frequency stability constraints.

Bibliography

[1] The Crownstate, "Off shore wind electricity," 2017, [Online] Available: https://www.thecrownestate.co.uk/energy-minerals-and-infrastructure/offshore-wind-energy/ [Last day accessed: 24/10/2021].

[2] National Grid Electricity System Operator, *National Grid Operability Strategy Report 2020*, National Grid ESO, November 2020, [Online] Available: https://www.nationalgrideso.com/document/159726/download [Last day accessed: 24/10/2021].

[3] United Nations Climate Change. (December 2015) What is the Paris agreement? . United Nations. [Online] Available: https://unfccc.int/process-and-meetings/the-paris-agreement/what-is-the-paris-agreement [Last day accessed: 24/10/2021].

[4] J. Cochran, M. Miller, O. Zinaman, M. Milligan, D. Arent, B. Palmintier, M. O´Malley, S. Mueller, E. Lannoye, A. Tuohy, B. Kujala, H. Holttinen, J. K. M. Sommer, and S. Soonee, "Flexibility in 21st Century Power Systems," *21st Century Power*, May 2014.

[5] N. Hatziargyriou, J. Milanovic, C. Rahmann, V. Ajjarapu, C. Canizares, I. Erlich, D. Hill, I. Hiskens, I. Kamwa, B. Pal, P. Pourbeik, J. Sanchez-Gasca, A. Stankovic, T. Van Cutsem, V. Vittal, and C. Vournas, "Definition and classification of power system stability – revisited amp; extended," *IEEE Transactions on Power Systems*, vol. 36, no. 4, pp. 3271–3281, 2021.

[6] National Grid Electricity System Operator, *System Operability Framework 2019 - Past Frequency Events*, National Grid ESO, November 2019,

[Online] Available: https://www.nationalgrideso.com/document/156761/download [Last day accessed: 24/10/2021].

[7] ——, *System Operability Framework 2019 - Operating a Low Inertia System*, National Grid ESO, February 2020, [Online] Available: https://www.nationalgrideso.com/document/164586/download [Last day accessed: 24/10/2021].

[8] ——, *Operating a Low Inertia System*, National Grid ESO, February 2020, [Online] Available: https://www.nationalgrideso.com/document/164586/download [Last day accessed: 24/10/2021].

[9] Jan Machowski and Janusz W. Bialek and James R. Bumby, *Power System Dynamics, Stability and Control*. John Wiley and Sons, 2008.

[10] P. Tielens and D. Van Hertem, "The relevance of inertia in power systems," *Renewable and Sustainable Energy Reviews*, vol. 55, pp. 999–1009, 2016, [Online] Available: http://dx.doi.org/10.1016/j.rser.2015.11.016 [Last day accessed: 24/10/2021].

[11] Office of Gas and Electricity Markets, *9 August 2019 power outage report*, Ofgem, January 2020, [Online] Available: https://www.ofgem.gov.uk/system/files/docs/2020/01/9_august_2019_power_outage_report.pdf [Last day accessed: 24/10/2021].

[12] National Grid Electricity System Operator, *Mandatory response services*, National Grid ESO, July 2020, [Online] Available: https://www.nationalgrideso.com/balancing-services/frequency-response-services/mandatory-response-services [Last day accessed: 24/10/2021].

[13] European Network of Transmission System Operator, *System Operator Guideline (SOGL)*, ENTSO-E, August 2017, [Online] Available: https://www.entsoe.eu/network_codes/sys-ops/ [Last day accessed: 24/10/2021].

[14] National Grid, *System Operability Framework 2016*.

[15] National Grid Electricity System Operator, *Dynamic Containment Service*, National Grid ESO, January 2021, [Online] Available: https://www.nationalgrideso.com/industry-information/balancing-services/frequency-response-services/dynamic-containment [Last day accessed: 24/10/2021].

[16] F. Milano and O. Manjavacas, *Frequency Variations in Power Systems: Modeling, State Estimation, and Control*, ser. Wiley - IEEE. Wiley, 2020, [Online] Available: https://books.google.co.uk/books?id=Hv2FzQEACAAJ [Last day accessed: 24/10/2021].

[17] Renewable UK, *Wind Energy Statistics*, Renewable UK, March 2021, [Online] Available: https://www.renewableuk.com/page/UKWEDhome/Wind-Energy-Statistics.htm [Last day accessed: 24/10/2021].

[18] GOV.UK, *Solar photovoltaics deployment*, GOV.UK, March 2021, [Online] Available: https://www.gov.uk/government/statistics/solar-photovoltaics-deployment [Last day accessed: 24/10/2021].

[19] R. H. Kerr, J. L. Scheidt, A. J. Fontanna, and J. K. Wiley, "Unit commitment," *IEEE Transactions on Power Apparatus and Systems*, vol. PAS-85, no. 5, pp. 417–421, 1966.

[20] B.M. Gorsten, *Economic Generation Schedulling of Parallel Working Electrical Power Stations*. Book in Russian, 1940.

[21] H. W. Dommel and W. F. Tinney, "Optimal power flow solutions," *IEEE Transactions on Power Apparatus and Systems*, vol. PAS-87, no. 10, pp. 1866–1876, 1968.

[22] J. Carpentier, "Optimal power flows," *International Journal of Electrical Power & Energy Systems*, vol. 1, no. 1, pp. 3–15, 1979, [Online] Available: https://www.sciencedirect.com/science/article/pii/0142061579900267 [Last day accessed: 24/10/2021].

[23] D. Bertsekas, G. Lauer, N. Sandell, and T. Posbergh, "Optimal short-term scheduling of large-scale power systems," *IEEE Transactions on Automatic Control*, vol. 28, no. 1, pp. 1–11, 1983.

[24] P. Bendotti, P. Fouilhoux, and C. Rottner, "On the complexity of the unit commitment problem," *Annals of Operations Research*, vol. 274, pp. 1–12, 04 2018.

[25] C. J. Baldwin, K. M. Dale, and R. F. Dittrich, "A study of the economic shutdown of generating units in daily dispatch," *Transactions of the American Institute of Electrical Engineers. Part III: Power Apparatus and Systems*, vol. 78, no. 4, pp. 1272–1282, 1959.

[26] P. G. Lowery, "Generating unit commitment by dynamic programming," *IEEE Transactions on Power Apparatus and Systems*, vol. PAS-85, no. 5, pp. 422–426, 1966.

[27] K. Hara, M. Kimura, and N. Honda, "A method for planning economic unit commitment and maintenance of thermal power systems," *IEEE Transactions on Power Apparatus and Systems*, vol. PAS-85, no. 5, pp. 427–436, 1966.

[28] R. C. Johnson, H. H. Happ, and W. J. Wright, "Large scale hydro-thermal unit commitment-method and results," *IEEE Transactions on Power Apparatus and Systems*, vol. PAS-90, no. 3, pp. 1373–1384, 1971.

[29] R. Doherty and M. O'Malley, "Quantifying reserve demands due to increasing wind power penetration," in *2003 IEEE Bologna Power Tech Conference Proceedings,*, vol. 2, 2003, pp. 5 pp. Vol.2–.

[30] X. Lei, E. Lerch, and C. Xie, "Frequency security constrained short-term unit commitment," *Electric Power Systems Research*, vol. 60, no. 3, pp. 193–200, 2002, [Online] Available: https://www.sciencedirect.com/science/article/pii/S0378779601001778 [Last day accessed: 24/10/2021].

[31] B. C. Ummels, M. Gibescu, E. Pelgrum, W. L. Kling, and A. J. Brand, "Impacts of wind power on thermal generation unit commitment and dispatch,"

IEEE Transactions on Energy Conversion, vol. 22, no. 1, pp. 44–51, March 2007.

[32] J. Restrepo and F. Galiana, "Unit commitment with primary frequency regulation constraints," in *2006 IEEE Power Engineering Society General Meeting*, 2006, pp. 1 pp.–.

[33] David G. Luenberger and Yinyu Ye, *Linear and non-linear programming*. Springer, 2008.

[34] A. Tuohy, P. Meibom, E. Denny, and M. O'Malley, "Unit commitment for systems with significant wind penetration," *IEEE Transactions on Power Systems*, vol. 24, no. 2, pp. 592–601, May 2009.

[35] EIRGRID plc, *EIRGRID dashboard of wind power*, EIRGRID, 2020, [Online] Available: http://smartgriddashboard.eirgrid.com/#all/wind [Last day accessed: 24/10/2021].

[36] R. Doherty, A. Mullane, G. Nolan, D. J. Burke, A. Bryson, and M. O'Malley, "An assessment of the impact of wind generation on system frequency control," *IEEE Transactions on Power Systems*, vol. 25, no. 1, february 2010.

[37] A. Sturt and G. Strbac, "Efficient stochastic scheduling for simulation of wind-integrated power systems," *IEEE Transactions on Power Systems*, vol. 27, no. 1, pp. 323–334, 2012.

[38] T. Shiina and J. R. Birge, "Stochastic unit commitment problem," *International Transactions in Operational Research*, vol. 11, no. 1, pp. 19–32, 2004, [Online] Available: https://onlinelibrary.wiley.com/doi/abs/10.1111/j.1475-3995.2004.00437.x [Last day accessed: 24/10/2021].

[39] P. Tielens and D. Hertem, "Grid inertia and frequency control in power systems with high penetration of renewables," in *2012 Young Researchers Symposium in Electrical Power Engineering*, no. 2, 2012, pp. 1–6, [Online] Available: https://lirias.kuleuven.be/handle/123456789/345286 [Last day accessed: 24/10/2021].

[40] H. Ahmadi and H. Ghasemi, "Security-constrained unit commitment with linearized system frequency limit constraints," *IEEE Transactions on Power Systems*, vol. 29, no. 4, pp. 1536–1545, 2014.

[41] A. Ulbig, T. S. Borsche, and G. Andersson, "Impact of Low Rotational Inertia on Power System Stability and Operation," *Power Systems Laboratory, ETH Zurich*, december 2014.

[42] Centro Nacional de Control de Energía, *Programa de Desarrollo del Sistema Eléctrico Nacional*, CENACE, 2017, [Online] Available: https://www.gob.mx/sener/acciones-y-programas/programa-de-desarrollo-del-sistema-electrico-nacional-33462 [Last day accessed: 24/10/2021].

[43] R. Castellanos Bustamante, A. Roman Messina, M. Ramirez Gonzalez, and G. Calderon Guizar, "Assessment of frequency performance by wind integration in a large-scale power system," *Wind Energy*, vol. 21, no. 12, pp. 1359–1371, 2018, [Online] Available: https://onlinelibrary.wiley.com/doi/abs/10.1002/we.2259 [Last day accessed: 24/10/2021].

[44] F. Teng, V. Trovato, and G. Strbac, "Stochastic scheduling with inertia-dependent fast frequency response requirements," *IEEE Transactions on Power Systems*, vol. 31, no. 2, pp. 1557–1566, 2016.

[45] L. Badesa, F. Teng, and G. Strbac, "Economic value of inertia in low-carbon power systems," in *2017 IEEE PES Innovative Smart Grid Technologies Conference Europe (ISGT-Europe)*, 2017, pp. 1–6.

[46] S. Naghdalian, T. Amraee, S. Kamali, and F. Capitanescu, "Stochastic network-constrained unit commitment to determine flexible ramp reserve for handling wind power and demand uncertainties," *IEEE Transactions on Industrial Informatics*, vol. 16, no. 7, pp. 4580–4591, 2020.

[47] M. Paturet, U. Markovic, S. Delikaraoglou, E. Vrettos, P. Aristidou, and G. Hug, "Stochastic unit commitment in low-inertia grids," *IEEE Transactions on Power Systems*, vol. 35, no. 5, pp. 3448–3458, Sep. 2020.

[48] F. Capitanescu and J.L. Martinez Ramos and P. Panciatici and D. Kirschen and A. Marano Marcolini and L. Pratbood and L. Wehenkel, "State of the art, challenges and future trends in security constrained optimal power flow," *Electric Power System Research*, vol. 81, no. 8, pp. 1731–1741, ago 2011.

[49] S. C. Savulescu, *Real-Time Stability in Power System Analysis*. Springer, 2006.

[50] N. M. Peterson, W. F. Tinney, and D. W. B. Jr., "Iterative linear ac power flow solution for fast approximate outage studies," *IEEE Winter Meeting, New York*, vol. 25, february 1972.

[51] W. F. Tinney and C. E. Hart, "Power flow solution by newton's method," *IEEE Transactions on Power Apparatus and Systems*, vol. PAS-86, no. 11, pp. 1449–1460, 1967.

[52] G. Irisarri and A. Sasson, "An Automatic Contingency Selection Method for On-Line Security Analysis," *IEEE Transactions on Power Apparatus and Systems*, vol. PAS-100, no. 4, pp. 1838–1844, 1981.

[53] T. Mikolinnas and B. Wollenberg, "An Advanced Contingency Selection Algorithm," *IEEE Transactions on Power Apparatus and Systems*, vol. 2, no. 2, pp. 608–617, 1981.

[54] G. Ejebe and B. Wollenberg, "Automatic Contingency Selection," *IEEE Transactions on Power Apparatus and Systems*, vol. PAS-98, no. 1, pp. 97–109, 1979.

[55] S. Meliopoulos, D. Taylor, C. Singh, F. Yang, S. W. Kang, and G. Stefopoulos, *Comprehensive Power System Reliability Assessment Final Project report*, 2005.

[56] F. Fatehi, M. Rashidinejad, and A. Gharaveisi, *2007 Large Engineering Systems Conference on Power Engineering.*

[57] Ian Dobson and Kevin R. Wierzbicky and Jangoon Kim and Hui Ren, "Towards Quantifying Cascading Blackout Risk," *2017 iREP Symposium - Bulk*

Power System Dynamics and Control - VII, Revitalizing Operational Reliability, August 2007.

[58] Hui Ren and Ian Dobson, "Using Transmission Line Outage Data to Estimate Cascading Failure Propagation in an Electric Power System," *IEEE Transactions on Circuits and Systems -II: Express Briefs*, vol. 55, no. 9, September 2008.

[59] W. S. Tan and M. Shaaban, "Ranking of power system contingencies based on a risk quantification criterion," in *2015 IEEE Student Conference on Research and Development (SCOReD)*, Dec 2015, pp. 356–361.

[60] GRID Modernization Laboratory Consortium - US Department of Energy, *Updated IEEE Reliability Test System*, 2017, [Online] Available: https://github.com/GridMod/RTS-GMLC [Last day accessed: 24/10/2021].

[61] S. C. Savulescu, *Real-Time Stability Assessment in Modern Power System Control Centers*. IEEE Press - Wiley, 2009.

[62] C. J. F. Cervantes, B. Kazemtabrizi, and M. C. M. Troffaes, "Contingency ranking in power systems via reliability rates," in *2018 IEEE International Conference on Environment and Electrical Engineering and 2018 IEEE Industrial and Commercial Power Systems Europe (EEEIC / I CPS Europe)*, June 2018, pp. 1–6.

[63] G. B. Dantzig, *Linear Programming and Extensions*. Princeton University Press, 1991, [Online] Available: http://www.jstor.org/stable/j.ctt1cx3tvg [Last day accessed: 24/10/2021].

[64] R. Bosch, *Opt Art: From Mathematical Optimization to Visual Design*. Princeton University Press, 2019, [Online] Available: http://www.jstor.org/stable/j.ctvh8qxtt [Last day accessed: 24/10/2021].

[65] Igor Griva and Stephen G. Nash and Ariela Sofer, *Linear and nonlinear optimisation*. SIAM, 2009.

[66] A. J. Wood, B. F. Wollenberg, and G. B. Sheble, *Power generation, operation, and control, 3rd Edition.* Wiley, 2014.

[67] R. Billinton and L. Wenyuan, *Reliability Assessment of Electric Power Systems Using Monte Carlo Methods*, ser. Wiley - IEEE. Springer, 1994, [Online] Available: https://www.springer.com/gp/book/9780306447815 [Last day accessed: 24/10/2021].

[68] Gurobi Optimization, *Gurobi solver manual*, Gurobi, June 2021, [Online] Available: https:/www.https://www.gurobi.com/resource/mip-basics/ [Last day accessed: 24/10/2021].

[69] P. H. Kumar and R. Mageshvaran, "Methods and solvers used for solving mixed integer linear programming and mixed nonlinear programming problems: A review," *International Journal of Scientific & Technology Research*, vol. 9, pp. 1872–1882, 2020.

[70] H. P. Williams, *Model building in mathematical programming / H.P. Williams.*, 5th ed. Chichester [England] ;: Wiley, 2013.

[71] D. De Wolf and Y. Smeers, *The Simplex Algorithm Extended to Piecewise-Linearly Constrained Problems*, 01 1998.

[72] Miller, C. E., "The simplex method for local separable programming," *Recent advances in mathematical programming*, pp. 89–100, 1963, [Online] Available: "https://ci.nii.ac.jp/naid/10012745123/en/" [Last day accessed: 24/10/2021].

[73] S. P. Bradley, *Applied mathematical programming / Stephen P. Bradley, Arnoldo C. Hax, Thomas L. Magnanti.* Reading, Massachusetts ;: Addison-Wesley Publishing Company, 1977.

[74] H. A. Taha, *Operations Research: An Introduction (8th Edition).* USA: Prentice-Hall, Inc., 2006.

[75] S. Boyd and L. Vandenberghe, *Convex Optimization*, C. U. Press, Ed. Cambridge University Press, 2004, [Online] Available: https://web.stanford.edu/~boyd/cvxbook/ [Last day accessed: 24/10/2021].

[76] M.-H. Lin, J. Carlsson, D. Ge, J. Shi, and J.-F. Tsai, "A review of piecewise linearization methods," *Mathematical Problems in Engineering*, vol. 2013, pp. 1–8, 11 2013.

[77] H. D. Sherali, "On mixed-integer zero-one representations for separable lower-semicontinuous piecewise-linear functions," *Operations Research Letters*, vol. 28, no. 4, pp. 155–160, 2001, [Online] Available: https://www.sciencedirect.com/science/article/pii/S0167637701000633 [Last day accessed: 24/10/2021].

[78] G. Cooper and C. McGillem, *Probabilistic methods of signal and system analysis*. Oxford University Press, 1997.

[79] F. H. Mahmood, A. K. Resen, and A. B. Khamees, "Wind characteristic analysis based on weibull distribution of al-salman site, iraq," *Energy Reports*, vol. 6, pp. 79–87, 2020, [Online] Available: https://www.sciencedirect.com/science/article/pii/S2352484719308716 [Last day accessed: 24/10/2021].

[80] A. Shapiro and A. Philpott, *A Tutorial on Stochastic Programming*, 2007.

[81] UK TECHNICAL COMMITTEE REPORT FOR 2020, *Power System Development and Economics*, CIGRE, 2020, [Online] Available: www.https://cigre.org.uk/uk-technical-committee/ [Last day accessed: 24/10/2021].

[82] S. K. Thompson, *Stratified Sampling*, Wiley, Ed. John Wiley & Sons, Ltd, 2012, [Online] Available: https://onlinelibrary.wiley.com/doi/abs/10.1002/9781118162934.ch11 [Last day accessed: 24/10/2021].

[83] G. B. Dantzig, "Linear programming under uncertainty," *Management Science*, vol. 1, no. 3/4, pp. 197–206, 1955, [Online] Available: http://www.jstor.org/stable/2627159 [Last day accessed: 24/10/2021].

[84] J. R. Birge and F. Louveaux, *Introduction to Stochastic Programming*. New York, NY, USA: Springer-Verlag, 2011.

[85] C. Grigg, P. Wong, P. Albrecht, R. Allan, M. Bhavaraju, R. Billinton, Q. Chen, C. Fong, S. Haddad, S. Kuruganty, W. Li, R. Mukerji, D. Patton, N. Rau,

D. Reppen, A. Schneider, M. Shahidehpour, and C. Singh, "The IEEE Reliability Test System-1996. A report prepared by the Reliability Test System Task Force of the Application of Probability Methods Subcommittee," *IEEE Transactions on Power Systems*, vol. 14, no. 3, pp. 1010–1020, Aug 1999.

[86] Z. Chu, U. Markovic, G. Hug, and F. Teng, "Towards optimal system scheduling with synthetic inertia provision from wind turbines," *IEEE Transactions on Power Systems*, vol. 35, no. 5, pp. 4056–4066, 2020.

[87] J. Restrepo and F. Galiana, "Unit commitment with primary frequency regulation constraints," in *2006 IEEE Power Engineering Society General Meeting*, June 2006, pp. 1 pp.–.

[88] F. Teng, V. Trovato, and G. Strbac, "Stochastic scheduling with inertia-dependent fast frequency response requirements," in *2016 IEEE Power and Energy Society General Meeting (PESGM)*, July 2016, pp. 1–1.

[89] M. Paturet, U. Markovic, S. Delikaraoglou, E. Vrettos, P. Aristidou, and G. Hug, "Stochastic unit commitment in low-inertia grids," *IEEE Transactions on Power Systems*, pp. 1–1, 2020.

[90] L. Badesa, F. Teng, and G. Strbac, "Simultaneous scheduling of multiple frequency services in stochastic unit commitment," *IEEE Transactions on Power Systems*, vol. 34, no. 5, pp. 3858–3868, 2019.

[91] ——, "Optimal portfolio of distinct frequency response services in low-inertia systems," *IEEE Transactions on Power Systems*, vol. 35, no. 6, pp. 4459–4469, 2020.

[92] Benson, Hande and Sağlam, Ümit, "Mixed-integer second-order cone programming: A survey," *INFORMS, Tutorials in Operations Research*, pp. 13–36, 10 2014.

[93] M. Malekpour, M. Zare, R. Azizipanah-Abarghooee, and V. Terzija, "Stochastic frequency constrained unit commitment incorporating virtual inertial re-

sponse from variable speed wind turbines," *IET Generation, Transmission & Distribution*, vol. 14, no. 22, pp. 5193–5201, 2020.

[94] Z. Zhang, E. Du, F. Teng, N. Zhang, and C. Kang, "Modeling frequency dynamics in unit commitment with a high share of renewable energy," *IEEE Transactions on Power Systems*, vol. 35, no. 6, pp. 4383–4395, 2020.

[95] Y. Yin, T. Liu, L. Wu, C. He, and Y. Liu, "Frequency-constrained multi-source power system scheduling against N-1 contingency and renewable uncertainty," *Energy*, vol. 216, p. 119296, 2021.

[96] National Grid, "THE GRID CODE," 2020, [Online] Available: https://www.nationalgrideso.com/industry-information/codes/grid-code [Last day accessed: 24/10/2021].

[97] F. Gonzalez-Longatt, "Impact of synthetic inertia from wind power on the protection/control schemes of future power systems: Simulation study," in *11th IET International Conference on Developments in Power Systems Protection (DPSP 2012)*, 2012, pp. 1–6.

[98] C. E. Murillo-Sánchez, R. D. Zimmerman, C. L. Anderson, and R. J. Thomas, "Secure planning and operations of systems with stochastic sources, energy storage, and active demand," *IEEE Transactions on Smart Grid*, vol. 4, no. 4, pp. 2220–2229, Dec 2013.

[99] R. D. Zimmerman, C. E. Murillo-Sanchez, and R. J. Thomas, "Matpower: Steady-state operations, planning, and analysis tools for power systems research and education," *IEEE Transactions on Power Systems*, vol. 26, no. 1, pp. 12–19, Feb 2011.

[100] Yuping Huang and Panos M. Pardalos and Qipeng P. Zheng, *Electrical Power Unit Commitment - Deterministic and Two-Stage Stochastic Programming Models and Algorithms*. Springer, 2014.

[101] D. A. Tejada-Arango, S. Wogrin, P. Sánchez-Martın, and A. Ramos, "Unit

commitment with acopf constraints: Practical experience with solution techniques," in *2019 IEEE Milan PowerTech*, 2019, pp. 1–6.

[102] M. Hildmann, A. Ulbig, and G. Andersson, "Empirical analysis of the merit-order effect and the missing money problem in power markets with high res shares," *IEEE Transactions on Power Systems*, vol. 30, no. 3, pp. 1560–1570, 2015.

[103] E. Vaahedi, *Power System Operation Optimization.* John Wiley & Sons, Ltd, 2014, ch. 8, pp. 119–150, [Online] Available: https://onlinelibrary.wiley.com/doi/abs/10.1002/9781118915110.ch8 [Last day accessed: 24/10/2021].

[104] Secretaría de Energia, *Código de Red*, Gobierno de México, 2016, [Online] Available: https://www.cenace.gob.mx [Last day accessed: 24/10/2021].

[105] Xi-Fang Wang and Yonghua Song and Malcolm Irving, *Modern Power System Analysis.* Springer, 2008.

[106] P. Kundur, *Power System Stability and Control.* McGRaw-Hill, 1993.

[107] Roy Billinton and Ronald N. Allan, *Reliability Evaluation of Engineering Systems.* Springer, 1992.

[108] Athanasios Papoulis and S. Unnikrishna Pillai, *Probability, Random Variables and Stochastic Processes.* McGraw Hill Series in Electrical and Computer Engineering, 2002.

[109] Wenyuan Li, *Risk Assessment of Power Systems.* IEEE Press-Wiley, 2014.

[110] Ebrahim Vaahedi, *Practical Power System Operation.* IEEE Press-Wiley, 2014.

[111] J. McCalley, S. Asgarpoor, L. Bertling, R. Billinton, H. Chao, J. Chen, J. Endrenyi, R. Fletcher, A. Ford, C. Grigg, G. Hamoud, D. Logan, A. P. Meliopoulos, M. Ni, N. Rau, L. Salvaderi, M. Schilling, Y. Schlumberger, A. Schneider, and C. Singh, "Probabilistic security assessment for power system operations,"

in *IEEE Power Engineering Society General Meeting, 2004.*, June 2004, pp. 212–220 Vol.1.

[112] S. Meliopoulos, D. Taylor, C. Singh, F. Yang, S. W. Kang, and G. Stefopoulos, *Comprehensive Power System Reliability Assessment Final Project report*, Power Systems Engineering Research Center, 2005.

[113] U.G. Knight, *Power Systems in Emergencies*. John Wiley and Sons LTD, 2001.

[114] Comisión Reguladora de Energía, *Código de Red*, CENACE, 2016.

[115] Geoffrey Grimmett and David Stirzaker, *Probability and Random Processes*. OXFORD University Press, 2001.

[116] Q. P. Z. Yuping Huang, Panos Pardalos, "Deterministic and two-stage stochastic programming models and algorithmss," in *Electrical Power Unit Commitment*. Springer International Publishing, 2017.

[117] G. B. Dantzig and M. N. Thapa, *Linear programming 2: theory and extensions*. Springer Science & Business Media, 2006.

[118] P. Carpentier, G. Gohen, J.-C. Culioli, and A. Renaud, "Stochastic optimization of unit commitment: a new decomposition framework," *IEEE Transactions on Power Systems*, vol. 11, no. 2, pp. 1067–1073, 1996.

[119] G. Strbac, R. Moreno, D. Pudjianto, and M. Castro, "Towards a risk-based network operation and design standards," *IEEE Power and Energy Society General Meeting*, pp. 1–4, 2011.

[120] F. Teng and G. Strbac, "Evaluation of synthetic inertia provision from wind plants," *2015 Power and Energy Society General Meeting*, 2015.

[121] J. Zou, S. Ahmed, and X. A. Sun, "Multistage stochastic unit commitment using stochastic dual dynamic integer programming," *IEEE Transactions on Power Systems*, vol. 34, no. 3, pp. 1814–1823, 2019.

[122] X. Wang, Z. Hu, M. Zhang, and M. Hu, "Two-stage stochastic optimization for unit commitment considering wind power based on scenario analysis," in *2016 China International Conference on Electricity Distribution (CICED)*, 2016, pp. 1–5.

[123] I. Blanco and J. M. Morales, "An efficient robust solution to the two-stage stochastic unit commitment problem," *IEEE Transactions on Power Systems*, vol. 32, no. 6, pp. 4477–4488, 2017.

[124] M. Håberg, "Fundamentals and recent developments in stochastic unit commitment," *International Journal of Electrical Power & Energy Systems*, vol. 109, pp. 38–48, 2019, [Online] Available: https://www.sciencedirect.com/science/article/pii/S014206151832547X [Last day accessed: 24/10/2021].

[125] r-project, "sample_n function," 2021, [Online] Available: https://search.r-project.org/CRAN/refmans/dplyr/html/sample_n.html [Last day accessed: 24/10/2021].

[126] ——, "group_by function," 2021, [Online] Available: https://search.r-project.org/CRAN/refmans/dplyr/html/group_by.html [Last day accessed: 24/10/2021].

Appendix A

Separable Programming

A.1 Frequency nadir linearisation

Next, x_1 and x_2 are modelled using λ_{1r} and λ_{2r} operators to obtain the linearised form as in:

$$x_1 = \sum_{r=0}^{R} a_{1r}\lambda_{1r} \quad \text{and} \quad \phi_1(x_1) = x_1^2 \approx \sum_{r=0}^{R} a_{1r}^2\lambda_{1r} \tag{B.1}$$

$$x_2 = \sum_{r=0}^{R} a_{2r}\lambda_{2r} \quad \text{and} \quad \phi_2(x_2) = x_2^2 \approx \sum_{r=0}^{R} a_{2r}^2\lambda_{2r} \tag{B.2}$$

$$a_{1r} \coloneqq \frac{r}{2R}(\alpha H_{max} + \beta R_{Gmax}), \quad \text{for} \quad r \in \{0, 1, \ldots, R\} \tag{B.3}$$

$$a_{2r} \coloneqq \frac{r}{2R}(\alpha H_{max} - \beta R_{Gmax}), \quad \text{for} \quad r \in \{0, 1, \ldots, R\} \tag{B.4}$$

$$\lambda_{10} \leq y_{11}, \quad \lambda_{1r} \leq y_{1r} + y_{1,r+1}, \quad \text{for} \quad r = 1, \ldots, R-1, \quad \lambda_{1R} \leq y_{1R} \tag{B.5}$$

$$\lambda_{20} \leq y_{21}, \quad \lambda_{2r} \leq y_{2r} + y_{2,r+1}, \quad \text{for} \quad r = 1, \ldots, R-1, \quad \lambda_{2R} \leq y_{2R} \tag{B.6}$$

$$\sum_{r=0}^{R} \lambda_{1r} = 1, \quad \sum_{r=0}^{R} \lambda_{2r} = 1, \quad \sum_{r=1}^{R} y_{1r} = 1, \quad \sum_{r=1}^{R} y_{2r} = 1 \tag{B.7}$$

and

$$\lambda_{1r} \geq 0, \quad \lambda_{2r} \geq 0, \quad y_{1r} \in \{0, 1\}, \quad y_{2r} \in \{0, 1\}, \quad \text{for all } r \in \{0, 1, \ldots, R\};$$

where:

- a_{1r} and a_{2r} are the breaking points in point r of the variables x_1 and x_2, respectively,
- λ_{1r} and λ_{2r} are the weights associated with each transition between breaking points a_{1r} and a_{2r} for breaking point r,
- y_{1r} and y_{2r} are the binary operators that select the affin segment of the linearisation,

and finally, the updated set of variables to optimise in the problem will be:

$$\Phi^{'} \coloneqq (S^{+}_{gt}, S^{-}_{gt}, P^{t}_{g}, f^{t}_{g}, R^{t}_{g}, u^{t}_{g}, \delta^{+}_{gt}, \delta^{-}_{gt}, \theta^{t}_{v}, \lambda_{1r}, \lambda_{2r}, y_{1r}, y_{2r})_{g\in\mathcal{G},\, t\in\mathcal{T},\, v\in\mathcal{M},\, r\in R} \tag{B.8}$$